

DEVELOPMENT OF THE TIMING SYSTEM FOR THE BUNCH-TO-BUCKET TRANSFER BETWEEN THE FAIR ACCELERATORS

Vom Fachbereich
Institut für Angewandte Physik
der Goethe-Universität, Frankfurt am Main
zur Erlangung des akademischen Grades
eines Doktor der Naturwissenschaften
genehmigte Dissertation

Von
Jiaoni Bai
geboren am 9. November 1986 in Taiyuan, Shanxi Province, China

Referent: Prof. Dr.
Korreferent: Prof. Dr.
Tag der Einreichung: Date. Month Year
Tag der mündlichen Prüfung: Date. Month Year

Darmstadt 2016

I would like to dedicate this dissertation to my dear parents,
loving husband and good friends ...

Acknowledgement

First and foremost, I would like to thank my professor Prof. Dr. Oliver Kester. It is a great honour for me to be his Ph.D. student. He gave me the chance to study at Goethe Universität, Frankfurt am Main and work in GSI for this interesting Ph.D. topic. I appreciate all his contributions of time and ideas to make my Ph.D. successful. I was deeply influenced by his enthusiasm for his research and his selfless support for his students. I was thankful for his support, that I participated many international conferences, schools and workshops. This experience enriched my life and broadened my horizons.

I wish to express my sincere gratitude to Dr. David Ondreka and Dr. Dietrich Beck for their supervision, valuable guidance and helpful suggestions throughout my Ph.D. study. I have been greatly lucky to have so good supervisors, who cared much about my work and who answered my doubts patiently. They were like a lighthouse in the ocean, which guides me in the right direction. They are not only my scientific supervisors, but also my mentors. They encouraged and motivated me during tough time of my Ph.D. Hence, I will keep a positive attitude and keep moving forward when I face with challenges, difficulties and temporary setbacks in the future.

I would like to acknowledge all colleagues in the timing group, CSCO department, GSI, Mathias Kreider, Stefan Rauch, Marcus Zweig, Alexander Hahn and former employee Dr. Wesley Terpstra, who provided me much technical support. I would like to extend my appreciation to department leader Dr. Ralph Bär, who gave much support for my Ph.D. topic. Thanks for their friendship and collaboration. I am especially grateful for the group member Cesar Prados, by whom I learned not only technical knowledge, but also how to work efficiently and how to become a good engineer. I would also like to thank Matthias Thieme, who provided me the devices for the test setup and Marko Stanislav Mandakovic for the discussion about the MPS. I would like to extend gratitude to Dr. Udo Krause and Peter Kainberger for the information about the GSI control system.

I am also thankful for the good cooperation with Thibault Ferrand, who studies at Technische Universität Darmstadt and works in PBRF department, GSI. Thanks for his valuable contribution of the development of the LLRF system for the B2B transfer system for FAIR. I would like to extend my sincerest thanks and appreciation to PBRF department leader Prof. Dr. Ing. Harald Klingbeil for his support. In addition, a special thanks is also extended to Dr. Dieter Lens and Stefan Schäfer for their technical support. Thanks for Dr. Bernhard Zipfel to give me support about BuTiS.

I wish to express my sincere gratitude to SBES department leader Dr. Markus Steck for his technical support of ESR and CRYRING, Dr. Udo Blell in PBHV department for the technical support of kicker and Dr. Michael Block in SHE-P department for the supply of two SRS function generators.

I must express my gratitude to GSI and also HGS-HiRe, who provided the scholarship which allowed me to undertake this research.

Lastly, I would like to thank my family for all their love and encouragement. My parents always support me to pursuing my dreams. Most of all, my loving husband Zigao Li is so appreciated, who always encourages me to realize my dreams. Thank you.

Jiaoni Bai
Darmstadt, September 2016

Abstract

This dissertation contributes to the conceptual development, the systematic investigation and the timing system realization of the FAIR Bunch-to-Bucket (B2B) transfer system.

The FAIR B2B transfer system plays an important role for the FAIR project, which will achieve various complex bunch-to-bucket transfer for FAIR accelerators in the future. It focuses first of all on the transfer from the SIS18 to the SIS100, but it will be firstly tested for the transfer from the SIS18 to the ESR and from the ESR to the CRYRING. The system is developed based on the FAIR existing infrastructures, the Low Level Radio Frequency system and the FAIR control system. It coordinates with the Machine Protection System, which protects SIS100/SIS300 from fatal errors and considerable damage and indicates beam status for Beam Instrumentation.

The FAIR B2B transfer system obtains the radio frequency (rf) phase difference between two synchrotrons by means of a campus wide distributed reference signal with picosecond precision, which is provided by the Bunchphase Timing System (BuTiS). The part of the B2B electronic is located in the source synchrotron supply room and serves as the “B2B transfer master”. The most important tasks of B2B transfer master are:

- The data collection (e.g. the rf phase).
- The data calculation (e.g. the start of the synchronization window, the required phase shift for the phase match between two rf systems, the phase correction for the bucket indication, the B2B transfer status check and etc.).
- The data redistribution (e.g. the start of the synchronization window).

The synchronization window is a coarse time frame for the transfer (coarse synchronization) and the bucket indication signal is used to indicate a specified bucket to be injected within the window, which is called the “fine synchronization”. This system is applied to all FAIR B2B transfer use cases and most transfers achieve the bunch-to-bucket injection center mismatch within the tolerate limits.

This dissertation presents the basic idea of the FAIR B2B transfer system, the basic procedure of the FAIR B2B transfer and the realization of each function. Because the system focuses first of all on the transfer from the SIS18 to the SIS100, the beam dynamic of the B2B transfer from the SIS18 to the SIS100 is simulated for two synchronization methods, the phase shift and the frequency beating method. In addition, the SIS18 extraction and SIS100 injection kickers are analyzed for different triggering strategies. This dissertation also explains the timing constraints of the system, the calculation of the synchronization window and presents the usage of the WR network for the B2B transfer system.

A test setup of the FAIR B2B transfer system focusing mainly on the timing aspects is presented and the test result is analyzed in this dissertation.

Kurzfassung

Contents

Abstract	v
1 Introduction	1
1.1 Bunch-to-Bucket Transfer worldwide	4
1.2 Objectives, Contribution and Structure of the Dissertation	5
2 Theoretical Background	8
2.1 Bunch and Bucket	8
2.2 Phase Difference	14
2.2.1 Circumference Ratio is an Integral	15
2.2.2 Circumference Ratio is close to an Integer	17
2.2.3 Circumference Ratio is far away from an Integer	18
2.3 Phase Match of two Rf Systems	20
2.3.1 Phase Shift Method	20
2.3.2 Frequency Beating Method	24
2.4 Synchronization of Extraction and Injection Kicker Magnets	25
3 Technical Basis for FAIR B2B Transfer System	29
3.1 FAIR Control System	29
3.1.1 Bunch Phase Timing System	29
3.1.2 General Machine Timing System	30
3.1.3 Settings Management	30
3.1.4 FESA	31
3.2 Low-Level RF System	31
3.2.1 Local Cavity Synchronization	32
3.2.2 Longitudinal Feedback System	33
3.3 Machine Protection System	33
4 Concept of FAIR B2B Transfer System	35
4.1 Basic Idea	35
4.1.1 Phase Alignment	35
4.1.2 Trigger of Extraction and Injection Kickers	37
4.1.2.1 Bucket Indication Signal	38
4.1.2.2 Extraction and Injection Kicker Delay Compensation	38
4.2 Basic Procedure	40
4.3 Realization	40
4.3.1 Phase Measurement and corresponding Timestamp of each Rf System	43
4.3.1.1 Measurement of Actual Phase Values of each Rf System	43

CONTENTS

4.3.1.2	Phase Extrapolation of each Rf System	44
4.3.1.3	Timestamp of Extrapolated Phase	44
4.3.2	Exchange of Measured Data	46
4.3.3	Rf Synchronization	46
4.3.4	Coarse Synchronization	49
4.3.5	Bucket Label	50
4.3.6	Fine Synchronization of Extraction and Injection Kickers	53
4.3.7	B2B Transfer Status Check	54
4.4	Data Flow	55
4.5	Comparison between FAIR B2B Transfer System and current B2B Transfer	56
5	Realization and systematic Investigation of FAIR B2B Transfer System	60
5.1	Beam Dynamic Analysis of two Synchronization Methods for B2B Transfer from SIS18 to SIS100	60
5.1.1	Beam Dynamics of Phase Shift Method for U^{28+}	60
5.1.1.1	Longitudinal Dynamic Analysis for Frequency Modulation	63
5.1.1.2	Transverse Dynamics Analysis	68
5.1.2	Beam Dynamics of Frequency Beating Method for U^{28+}	68
5.1.2.1	Longitudinal Dynamics Analysis	68
5.1.3	Beam Dynamics of Phase Shift Method for H^+	69
5.1.3.1	Longitudinal Dynamics Analysis	69
5.1.3.2	Transverse Dynamics Analysis	70
5.1.4	Beam Dynamics of Frequency Beating Method for H^+	70
5.1.4.1	Longitudinal Dynamics Analysis	70
5.2	GMT systematic Investigation	71
5.2.1	Calculation of the Start of the Synchronization Window	71
5.2.1.1	Uncertainty of Phase Alignment	71
5.2.1.2	Uncertainty of the Start of the Synchronization Window	73
5.2.1.3	Accuracy of the Start of the Synchronization Window	75
5.2.2	Characterization of WR Network	75
5.2.2.1	WR Network Test Setup	77
5.2.2.2	Test Result of Frame Loss Rate	77
5.2.2.3	Test Result of Latency and Jitter	78
5.2.2.4	Conclusion	81
5.3	Kicker systematic Investigation	82
5.3.1	SIS18 Extraction Kicker	83
5.3.2	SIS100 Injection Kicker	85
5.4	Test Setup for Data Collection, Merging and Redistribution	86
5.4.1	Functionality of the Test Setup	86
5.4.2	Test Setup	87
5.4.3	Firmware	88
5.4.4	Time Constraints	91
5.4.5	Test Result	94

CONTENTS

6 Application of FAIR B2B Transfer System for FAIR Accelerators	95
6.1 Circumference Ratio is an Integer	96
6.1.1 Use Case of U^{28+} B2B Transfer from SIS18 to SIS100	97
6.1.2 Use Case of H^+ B2B Transfer from SIS18 to SIS100	99
6.2 Circumference Ratio is close to an Integer	100
6.2.1 Use Case of h=4 B2B Transfer from SIS18 to ESR	100
6.2.2 Use Case of h=1 B2B Transfer from SIS18 to ESR	102
6.2.3 Use Case of B2B transfer from ESR to CRYRING	103
6.3 Circumference Ratio is far away from an Integer	103
6.3.1 Use Case of H^+ B2B Transfer from SIS100 to CR	105
6.3.2 Use Case of RIB B2B Transfer from SIS100 to CR	105
6.3.3 Use Case of B2B Transfer from CR to HESR	107
6.3.4 Use Case of B2B Transfer from SIS18 to ESR via a FRS . . .	108
6.4 Summary of Formulas related to B2B Transfer	108
7 Conclusion and Outlook	113
A FAIR B2B Transfer related Timing Frames	115
B Timing Frames Transfer for FAIR B2B Transfer System	117
C Parameters of FAIR Use Cases	119
C.1 Parameters related to the B2B transfer from SIS18 to SIS100	119
C.2 Parameters related to the B2B transfer from SIS18 to ESR	120
C.3 Parameters related to the B2B transfer from SIS18 to ESR via FRS .	121
C.4 Parameters related to the B2B transfer from ESR to CRYRING . . .	122
C.5 Parameters related to the B2B transfer from CR to HESR	123
C.6 Parameters related to the B2B transfer from SIS100 to CR	124
D Parameters of FAIR B2B Transfer System from Settings Management	125
E Parameters of kicker magnets	127
Bibliography	127
Glossary	133
Abbreviations	137
Symbols	141
List of Figures	147
List of Tables	151
Publications	152

Chapter 1

Introduction

Beam of high energy particles is useful for both fundamental and applied research in the sciences, and also in many technical and industrial fields unrelated to fundamental research. It has been estimated that there are approximately 30000 accelerators worldwide. Only about 1% of them are research machines with energies above 1 GeV [1]. As we all known, particles are accelerated by the electric field. The radio frequency (rf) system is devoted to generate the electric field at rf cavities around the ring. Particles are accelerated when they pass through rf cavities. Every rf cavity has a limited frequency range, so particles at rest could not be accelerated to several tens of GeV energy in one ring accelerator. Hence, the acceleration must be divided into several energy stages: the first energy stage is achieved usually by a small ring, which is called “booster” and the second stage by a large ring, which is usually called “main ring”. The energy of a beam is related to the ‘magnetic rigidity’ of the dipole magnet, which is the multiplication of the magnetic field and the bending radius of a particle immersed in the magnetic field. At the time of the beam transfer, the magnetic rigidity of the booster must be equal to that of the main ring. Since the bending radius of the main ring is generally larger than that of the booster, the magnetic field in the main ring starts the further acceleration at a lower level. This allows a continuous increasing of the particle energy until the limits of the dipole magnets of the main ring. The usage of the booster and the main ring works faster to reach the required beam energy, because the booster can be filled and accelerated, when the main ring accelerates particles. The faster acceleration has the advantage to reduce the interaction time between the accelerated particles and the residual-gas atoms in the vacuum chamber, achieving a better beam quality [2]. Furthermore, the particle beam transfer among different rings is also used for the production of high intensity beam, e.g. the beam is transferred to a storage ring for the beam accumulation and the beam compression. Hence, the transfer of beam between rings is of great importance for high energy, high intensity and high quality beam.

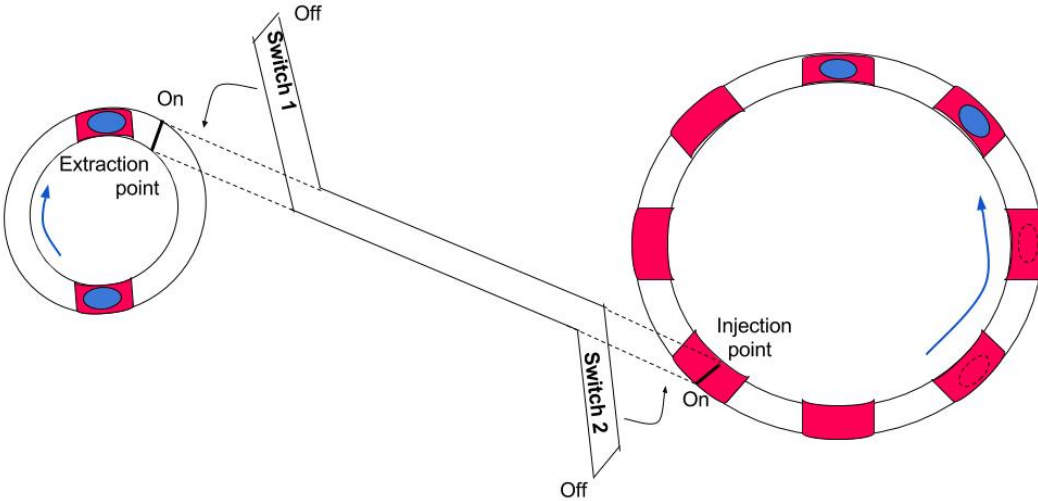


Figure 1.1: Illustration of a bunch-to-bucket transfer.

Red rectangles represent buckets and blue dots bunches.

ESR

The beam transfer is not arbitrary. A bunch of particles running in a ring should be transferred into the correct position of another ring. Fig. 1.1 illustrates the transfer of a bunch of particles between two rings. The example in Fig. 1.1 is with the circumference ratio between the right and left rings of four. Bunches of particles are transferred from the left ring to the right one. The blue ellipse represents a bunch of particles and the red rectangle represents the allowable area for particles to be injected. The red rectangles are equally spaced around the ring and determined by the rf frequency. The white space between two red rectangles is forbidden for particles. The allowable area (red rectangle) for particles is termed as a “bucket” and a bunch of particles (blue ellipse) as a “bunch”. The definition of a bunch and a bucket from the accelerator physics perspective, please see Chap. 2. There are two buckets at the left ring and every bucket keeps a bunch. There are eight buckets in the right ring and two of them are filled with bunches. The left ring is connected to a track by a switch, which is called a “switch 1”. When the switch 1 is off, bunches circulate around the ring. When it is on, bunches will be guided from the ring to the track at a specific position around the ring, which is called the “extraction point” (represented as a black short bar on the left ring). The track is connected to the right ring by another switch, called a “switch 2”. When the switch 2 is on, bunches will be guided from the track to the right ring at a specific position around the ring, which is called the “injection point” (represented as a black short bar on the right ring). Generally both switches are off. The bunch-to-bucket (B2B) transfer is defined as that bunches of the left ring are transferred to the correct buckets at the right ring. For the B2B transfer, bunches at the left ring and buckets at the right ring must have not only a constant but same velocity. Because the circumference of the right ring is four times longer than that of the left ring, bunches run four cycles of the left ring when buckets run one cycle of the right ring. The distance between two bunches of the left ring is equal to the distance between two continuous buckets of the right ring. Besides, the relative position between bunches and buckets must match. Bunches of the left ring are guided to the track and transferred to the right

CHAPTER 1. INTRODUCTION

ring. They are guided exactly to two empty buckets of the right ring. Every time when a bunch of the left ring passes by the extraction point, a bucket of the right ring will pass by the injection point after a specific time delay, which equals to the time-of-flight of a bunch on the track. What's more, the time for the track switch-on is of great importance, determining which buckets to be filled. In Fig. 1.1, two empty buckets closely following the filled buckets of the right ring need to be filled (represented as the dotted ellipse). The switch 2 must be switched on when the first empty bucket following two filled buckets passes the injection point and the switch 1 must be switched on a specific time earlier, when a bunch passes by the extraction point.

The ring is called a “source ring”, from which the beam is extracted. The ring is called a “target ring”, into which the beam is injected. From the above illustration, several preconditions are compulsory for the B2B transfer. The first precondition is that bunches of the source ring and buckets of the target ring have a constant speed, namely the revolution frequency of two rf systems of the source and target rings must be constant. Beam feedback loops on the rf system are usually implemented in order to keep the stability of the beam. The constant revolution frequency requires that the beam feedback loop must be switched off before the B2B transfer. The second precondition is that bunches and buckets are with a same speed, which requires that the revolution frequency ratio between two rings is equal to the reciprocal of the circumference ratio. When the circumference ratio between two rings is an integer, the phase difference between two revolution frequencies is constant. It means that bunches always pass the extraction position a constant time earlier/later before/after buckets pass the injection position. But the constant phase difference is not correct for the transfer. In order to get the correct phase difference, an azimuthal positioning of bunches in the source ring or buckets in the target ring must be adjusted. This is called “phase shift method”. After the phase shift, the phase difference of two revolution frequencies is correct and the correct phase difference keeps infinite theoretically. Because beam feedback loops are switched off, the beam is stable only for a period of time. So the beam must be transferred as soon as possible. When the circumference ratio is not an integer, the phase difference between two revolution frequencies varies periodically. Within one period, there must be one time point when the phase difference between two rf systems is correct. Before and after this time point, there exists the mismatch between bunches and buckets. The earlier and later than this time point within a period, the larger the mismatch. This is called ”frequency beating method”. For both the phase shift and frequency beating methods, the transfer can only happen when the mismatch is smaller than a tolerate limit, introducing a time frame. The time frame is called the “synchronization window”, which achieves the “coarse synchronization”.

Bunches are switched from one path to another path by kicker magnets (short: kicker). The extraction kicker kicks bunches out of the source ring to the track and the injection kicker kicks them from the track into buckets of the target ring. They are located at the extraction position and injection position in Fig. 1.1. When the phase difference between two rf systems is correct, the extraction kicker could kick bunches of the source ring at the exact time-of-flight to the track before empty buckets pass the injection kicker. With the synchronization window, the extraction and injection kickers must be fired at the correct time in order to transfer bunches into correct empty buckets. The process of the kicker firing at the correct time is

1.1. Bunch-to-Bucket Transfer worldwide

termed as the “fine synchronization”.

1.1 Bunch-to-Bucket Transfer worldwide

Nowadays, there are several accelerator institutes in the world, who operate the B2B transfer among rings for specific purposes. CERN, the European Organization for Nuclear Research, is one of the world’s largest and most respected center for scientific research. The Large Hadron Collider (LHC) beam injection chain achieves the proton beam with the energy of 7 TeV. After accelerated by a linear accelerator, bunches are injected into buckets of the Proton Synchrotron Booster (PSB) and further into the Proton Synchrotron (PS), the Super Proton Synchrotron (SPS) and LHC [3]. For the LHC heavy ion beam injection chain with the achievement of the energy of 2.76 TeV/u, bunches are first of all injected into the Low Energy Ion Ring (LEIR) and the following transfer from PSB to LHC is same as the proton beam chain [3]. For Japan Proton Accelerator Complex (J-PARC), bunches are transferred from the Rapid Cycle Synchrotron (RCS) to buckets of the Main Ring (MR) [4]. The Booster of Brookhaven National Laboratory (BNL) transfers bunches to buckets of the Alternating Gradient Synchrotron (AGS) and bunches of AGS are transferred further into the Relativistic Heavy Ion Collider (RHIC) [5]. Fermi National Accelerator Laboratory (Fermilab)’s accelerator complex provides high energy proton beams for a broad range of experiments. Proton beams are injected into the Recycler from the Fermi National Accelerator Laboratory (Fermilab) Booster. Then the proton beam enters the Main Injector from the Recycler. The beam is accelerated to the energy of 120 GeV. Some of the proton beam from the Booster will be used to produce a beam of special particles for Muon Delivery Ring. The Muon Delivery Ring delivers the beam into a muon storage ring for further study [6]. Institute of Modern Physics of the Chinese Academy of Sciences (IMP) operates the Heavy Ion Research Facility (HIRFL) in Lanzhou. Two existing cyclotrons, the Sector Focusing Cyclotron (SFC) and the Separated Sector Cyclotron (SSC), are used as an injector system for the Cooler Storage Ring main ring (CSRm) for the accumulation, cooling and acceleration. Then the beam is extracted from CSRm to produce radioactive ion beams or highly-charged heavy ions, which can be transferred to the Cooler Storage Ring experimental ring (CSRe) for many experiments [7, 8].

FAIR, Facility for Antiproton and Ion Research, is a new international accelerator facility under construction at GSI Helmholtz center for Heavy Ion Research GmbH (short: GSI)¹ [9, 10]. It is aiming at providing high-energy beams of ions from antiproton to uranium with high intensities. The new FAIR accelerator complex with storage rings consists of the SIS100², the SIS300³, the Collector Ring (CR), the Recycled Experimental Storage Ring (RESR), the New Experimental Storage Ring (NESR) and the High Energy Storage Ring (HESR) [11, 12]. FAIR has so many rings, so the B2B transfer among FAIR ring accelerators is of great importance to accelerate beams to higher energy with high intensity and achieve beams for various experiments. Based on the existing GSI UNILAC and SIS18 serving as

¹Planckstrasse 1, 64291 Darmstadt, www.gsi.de

²SIS18 stands for SchwerIonen Synchrotron (100 Tm magnetic rigidity).

³SIS300 stands for SchwerIonen Synchrotron (300 Tm magnetic rigidity).

1.2. Objectives, Contribution and Structure of the Dissertation

injectors, high intensity ion beams over the whole range of stable isotopes will be accelerated in the new heavy ion machine SIS100/SIS300 to higher energy. The beam from the SIS100 will be transferred to the CR via the proton bar (Pbar)⁴ or the Superconducting Fragment Separator (Super-FRS)⁵. The CR has the purpose of stochastic cooling of both secondary rare isotope and antiproton beams and of measuring nuclear masses [13, 14]. The CR transfers the beam to the HESR and further to the RESR for the accumulation. The HESR serves experiments with high energy antiproton and rare isotope beams [15]. The proton and heavy ion beam could also be transported from the SIS18 to the existing GSI Experimental Storage Ring (ESR) and further to the first FAIR-storage ring CRYRING@ESR (short: CRYRING) for the atomic and nuclear physics experiment [16, 17]. The proton and heavy ion could also be transferred from SIS18 to ESR via the Fragment Separator (FRS)⁶.

For many FAIR accelerator pairs, the circumference ratio between the large and small rings is an integer, e.g. the SIS100 and the SIS18, so the phase difference between two revolution frequencies of rings is constant. The frequency is in the MHz range. In this scenario, the phase shift method must be used for the match of the phase difference between two rf systems. When the circumference ratio between FAIR accelerator pairs is not an integer, e.g. the SIS18 and the ESR⁷, the phase difference between two revolution frequencies shifts automatically. The frequency of the phase difference variability is in the kHz range. The synchronization window for the FAIR B2B transfer is in the μ s range. The beams of ion species, from hydrogen to uranium as well as antiprotons, should be transferred among all rings. And every transfer must be achieved within the upper bound 10 ms and the B2B injection mismatch in the range between -1° and $+1^\circ$. Both the phase shift and the frequency beating method should be applicable in the upcoming FAIR facilities. The B2B transfer system is designed to work in a parallel operation, e.g. the transfer from SIS18 to SIS100 and the transfer from ESR to CRYRING can be performed at the same time. It is cable to transfer the beam between two rings via a FRS or a Super FRS. The B2B transfer system must coordinate with the SIS100 emergency dump for all unacceptable failure or situation.

1.2 Objectives, Contribution and Structure of the Dissertation

This dissertation contributes to the development of the FAIR B2B transfer system from the timing perspective. It concentrates on the introduction of the concept of the FAIR B2B transfer system and its application for FAIR accelerators. In addition, it explains the systematic investigation for the FAIR B2B transfer system in details.

The dissertation is structured as follows and as depicted in Fig. 1.2.

⁴Pbar is used to produce antiprotons in inelastic collisions of high energy protons with nucleons of a target nucleus.

⁵Super-FRS is used to produce rare isotopes of all elements up to uranium at relativistic energies and spatially separate them within a few hundred nanoseconds.

⁶An ion-optical device used to focus and separate products from the collision of relativistic ion beams with thin targets.

⁷ESR has an injection/extraction orbit, which is 15 cm longer than the design orbit. The orbit of ESR in this dissertation means the injection/extraction orbit.

1.2. Objectives, Contribution and Structure of the Dissertation

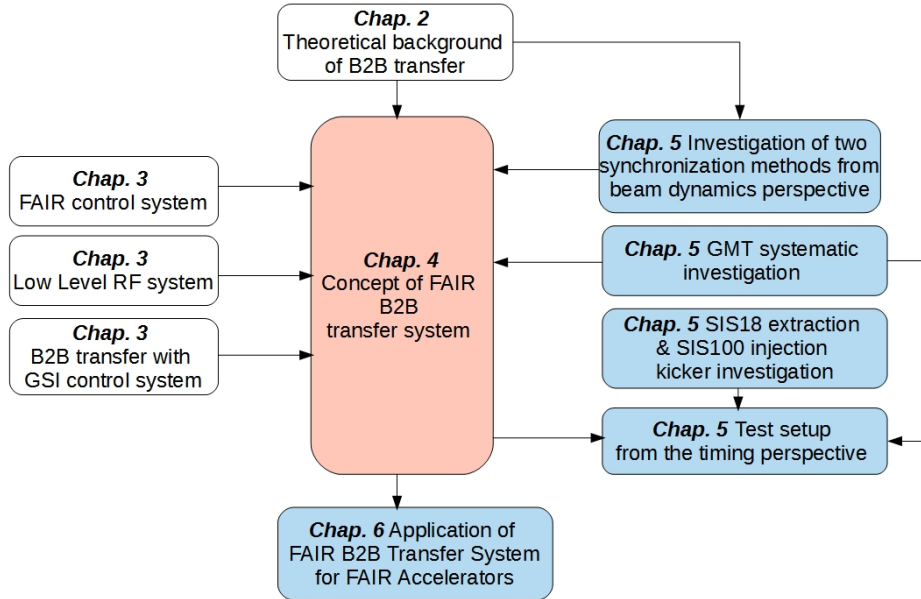


Figure 1.2: The structure of the dissertation.

Contributions are marked blue and red is team work, existing systems or theory are not colored.

In Chap.2, the theoretical background for the B2B transfer are reviewed. First of all, the energy, phase and voltage match between the source and target synchrotrons are introduced. Secondly, two rf synchronization methods are discussed from the perspective of beam dynamics in order for the phase alignment. At the end of this chapter, the synchronization of the extraction and injection kicker magnets are discussed.

Chap.3 is concerned with the existing FAIR technical basis for the development of the FAIR B2B transfer system and the uniqueness of the system. The B2B transfer system is realized based on the FAIR control system and low-level rf system, so these two systems are introduced. In addition, the comparison between the FAIR B2B transfer system and the current B2B transfer with the GSI control system is discussed before the chapter ends.

In Chap.4, a brief overview on the basic idea of the B2B transfer system is presented. After that the basic procedure of the FAIR B2B transfer is introduced and the realization of each step of the procedure is explained. In addition, the FAIR B2B transfer system is explained from the data flow perspective.

Chap.5 presents the systematic investigation for the B2B transfer system, mainly focusing on the timing aspect. The calculation of the synchronization window is explained and the transfer of the B2B messages via the WR network is tested. In addition, for the B2B transfer from the SIS18 to the SIS100, two synchronization methods are analyzed from the perspective of the beam dynamics. The SIS18 extraction and the SIS100 injection kicker are systematically investigated. Finally, the test setup is presented and the result is analyzed.

The application of the FAIR B2B transfer system for FAIR accelerator pairs are outlined in Chap.6. The applications are classified into three categories according to the feature of the circumference ratio. Many FAIR use cases are with an integral

1.2. Objectives, Contribution and Structure of the Dissertation

circumference ratio, e.g. the SIS18 and the SIS100, there is a constant phase difference between two rf system. Although the phase shift can be used for the phase match, the frequency beating method is preferred via the detune of one rf system. Because the phase shift must be executed slowly enough to guarantee the beam quality, which needs much longer time than the frequency beating method. The ratio of the circumference between many pair of machines in FAIR is close to an integer or far away from an integer, e.g. the SIS18 and the ESR, the SIS100 and the CR, the CR and the HESR. the phase match is achieved by the frequency beating. For each category, the corresponding FAIR use cases are presented.

Chapter 2

Theoretical Background

In Chap. 1, the bunch and bucket are introduced with simplified definition. In this chapter, the bunch and bucket are first of all defined from the accelerator physics perspective in Sec. 2.1. Transferring bunches from a synchrotron into specific buckets of another synchrotron has several underlying basic principles. The energy of the beam is same before and after the B2B transfer, so the energy of the source synchrotron must match that of the target synchrotron. The amplitude of the accelerating voltage match of two rf systems is needed to ensure that buckets capture bunches efficiently. Principally speaking, every synchrotron has its independent rf system. The phase difference between bunches and buckets must be precisely controlled before the transfer. The energy and voltage match will be done by machine physicists, which are out of the scope of this dissertation, so only the phase match is explained in detail in Sec. 2.2. Two methods for the phase alignment between two rf systems are discussed in Sec. 2.3. For the correct bucket injection, the bunch extraction must happen exactly the time-of-flight before the required bucket of the target synchrotron passes the injection kicker. The synchronization of extraction and injection kicker magnets are presented in Sec. 2.4.

2.1 Bunch and Bucket

For a ring accelerator, particles gain energy from electric field in longitudinal direction and are deflected by magnetic field to a particle orbit. A rf cavity operating at a resonance condition is used to provide a longitudinal accelerating voltage¹ u in the vacuum chamber.

$$u(t) = V_0 \sin(\phi_s + 2\pi f_{rf} t) \quad (2.1)$$

where V_0 is the amplitude of the rf voltage, ϕ_s is an initial phase, and f_{rf} is the frequency of the accelerating voltage. In order to accelerate particles with an accelerating voltage at the rf cavity, the cavity rf frequency must always be an integer multiple of the revolution frequency of particles.

$$f_{rf} = h f_{rev} \quad (2.2)$$

where the integer multiple h is called the “harmonic number”.

A particle who always sees the rf phase ϕ_s at the rf cavity with the revolution frequency f_{rev} and the momentum p is called a “synchronous particle”. For circular

¹Rf voltage with a single harmonic operation is considered in this dissertation.

2.1. Bunch and Bucket

accelerators, the revolution frequency is decided by the machine circumference and the particle velocity.

$$f_{rev} = \frac{\beta c}{2\pi R} \quad (2.3)$$

where R is the radius of the orbit, β the relative velocity to the speed of light and c the speed of light. The differential of eq. 2.3 is

$$\frac{\Delta f_{rev}}{f_{rev}} = \frac{\Delta\beta}{\beta} - \frac{\Delta R}{R} \quad (2.4)$$

Because of the relation $\Delta f_{rf}/f_{rf} = \Delta f_{rev}/f_{rev}$, so eq. 2.4 can be written as

$$\frac{\Delta f_{rf}}{f_{rf}} = \frac{\Delta\beta}{\beta} - \frac{\Delta R}{R} \quad (2.5)$$

The momentum of the synchronous particle p is related to the particle energy and its velocity.

$$p = \gamma\beta m_0 c \quad (2.6)$$

where m_0 is the rest mass and $\gamma = (1 - \beta^2)^{-\frac{1}{2}}$. γ is the relativistic factor, which measures the total particle energy, $E = pc/\beta$, in units of the particle rest energy, $E_0 = m_0 c^2$.

The fractional change in β is related to the fractional change in p .

$$\frac{\Delta p}{p} = \gamma^2 \frac{\Delta\beta}{\beta} \quad (2.7)$$

Substituting $\Delta\beta/\beta$ into eq. 2.5, we get

$$\frac{\Delta f_{rf}}{f_{rf}} = \frac{1}{\gamma^2} \frac{\Delta p}{p} - \frac{\Delta R}{R} \quad (2.8)$$

For the constant magnetic field, a particle will have a different orbit, if it is slightly shifted in momentum. The “momentum compaction factor” α_p^2 is defined as:

$$\frac{\Delta R}{R} = \alpha_p \frac{\Delta p}{p} \quad (2.9)$$

Substituting eq. 2.9 into eq. 2.8, we finally obtain the required relation between the frequency offset and the momentum error.

$$\frac{\Delta f_{rf}}{f_{rf}} = \left(\frac{1}{\gamma^2} - \alpha_p \right) \frac{\Delta p}{p} \quad (2.10)$$

The phase-slip factor η is defined as

$$\eta = \frac{1}{\gamma^2} - \alpha_p \quad (2.11)$$

which gives the relationship between the revolution frequency and the momentum for a given accelerator. When particles are at low energy ($\eta > 0$), they run faster and arrive earlier at the rf cavity. When they are at high energy close to the speed of light ($\eta < 0$), they cannot run faster, but rather obtain more mass and are pushed to a dispersive orbit, resulting a late arrival at the rf cavity [18].

2.1. Bunch and Bucket

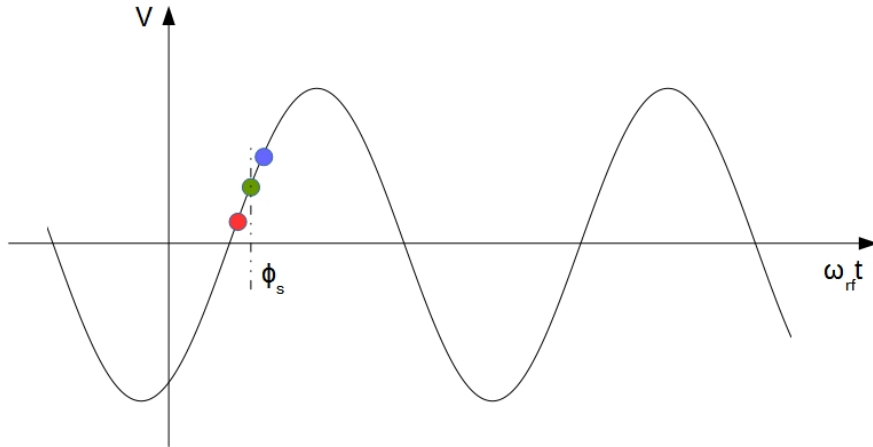


Figure 2.1: The longitudinal focusing of particles by a rf voltage ($\eta > 0$).

The red spot represents a particle with a higher energy, the blue spot a particle with a lower energy and the green dot the synchronous particle.

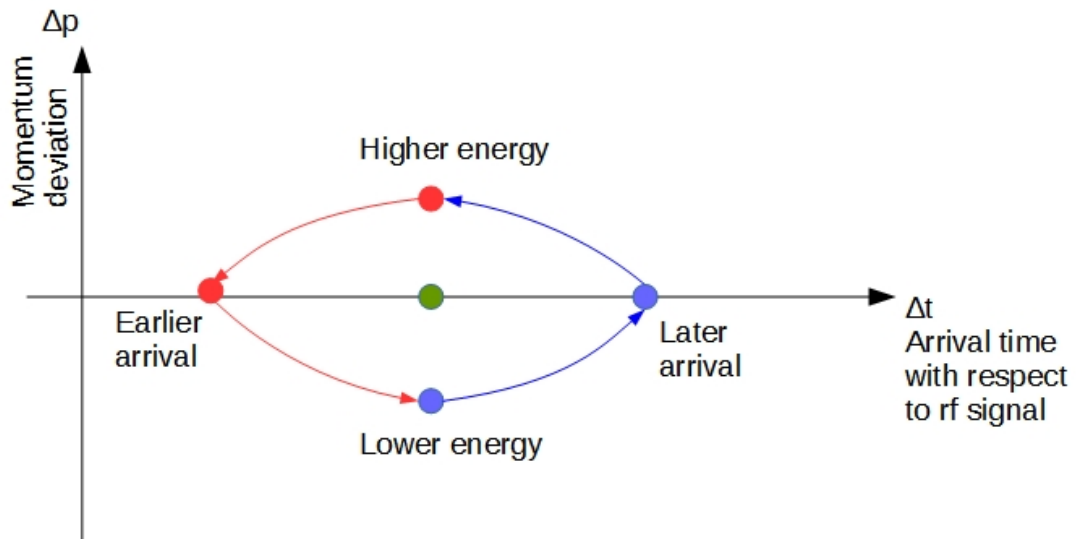


Figure 2.2: The longitudinal motion of asynchronous particles in the longitudinal phase space plane ($\eta > 0$).

The red spot represents a particle with a higher energy, the blue spot a particle with a lower energy and the green dot the synchronous particle. The red arrow shows the trend of a particle with a higher energy and the blue arrow the trend of a particle with a lower energy.

A bunch of particles consists of particles with slightly different momentum as the synchronous particle, which are called “asynchronous particles”. When $\eta > 0$, the longitudinal focusing of particles is explained in Fig. 2.1.

The synchronous particle is indicated by the green spot in Fig. 2.1. It will

²FAIR complex is with $\alpha_p > 0$.

2.1. Bunch and Bucket

gain the energy of $qV_0 \sin \phi_s$ per passage through a rf cavity, where q is the charge of a particle. When $\eta > 0$, a particle with a smaller energy (blue spot) than the synchronous particle will run slower and have a longer revolution period, arriving the same rf cavity later and seeing a higher accelerating voltage. This particle has a decreasing revolution period to the revolution period of the synchronous particle. During the decreasing process, the lack of energy is compensated step-by-step approaching to the energy of the synchronous particle. Oppositely for a particle with a higher energy. As it is faster than the synchronous particle and has a shorter revolution period, it will arrive at the rf cavity earlier, seeing a smaller accelerating voltage. This particle has an increasing revolution period to the revolution period of the synchronous particle. During the increasing process, the excess energy will be reduced step-by-step approaching to the synchronous particle. Asynchronous particles will oscillate longitudinally around the synchronous particle. This longitudinal motion is plotted in the longitudinal phase space plane, See Fig. 2.2.

All particles oscillate around the synchronous particle and stay together, forming a “bunch”. The “bunch gap” is the area without any particles. The area occupied by a bunch in the longitudinal phase space plane is called the “longitudinal emittance”. First of all, we consider the synchronous particle with the synchronous phase 0° . In this scenario, particles with a small energy deviation follow an elliptical path inside the bunch. For a given rf system with a specific rf voltage and harmonic number, there exists a maximum energy deviation. For particles with energy deviations larger than the maximum energy deviation, they cannot be trapped around the synchronous particle. The trajectory of a particle with the maximum energy deviation in longitudinal phase space plane defines a region with a specific size and form. This region is called the “rf bucket” or “stationary rf bucket”, see Fig. 2.3. The maximum momentum deviation of the rf bucket is called the “bucket height”. These buckets will exist as soon as the rf voltage is switched on and the number of circulating buckets is determined by the harmonic number and the bucket area and height are proportional to the square root of the rf voltage [18]. The order of buckets to be filled is called the “bucket pattern”.

So far we give the definition of the bucket, when the synchronous particle sees no accelerating rf voltage. When the synchronous particle is accelerated, seeing the synchronous phase ϕ_s per passage through an rf cavity, it will gain the energy of $qV_0 \sin \phi_s$. Particles oscillate around the synchronous particle at ϕ_s with an elliptical orbit. The particle at $\pi - \phi_s$ traces a closed fish-shaped orbit, which defines a “running rf bucket”, see Fig. 2.4. Particles at bigger phase than $\pi - \phi_s$ cannot be captured by the bucket.

The “bucket size” is defined as the area of the longitudinal phase space plane enclosed by the bucket [18]. For a same rf voltage, the bucket size of a running bucket is always smaller than that of a stationary bucket. The ratio of the bucket size of a running bucket to that of a stationary bucket is called the “bucket area factor”, α_b . The bucket area factor can be calculated by [18].

$$\alpha_b(\phi_s) \approx \frac{1 - \sin \phi_s}{1 + \sin \phi_s} \quad (2.12)$$

The oscillation of asynchronous particles is called the “synchrotron motion”. The

2.1. Bunch and Bucket

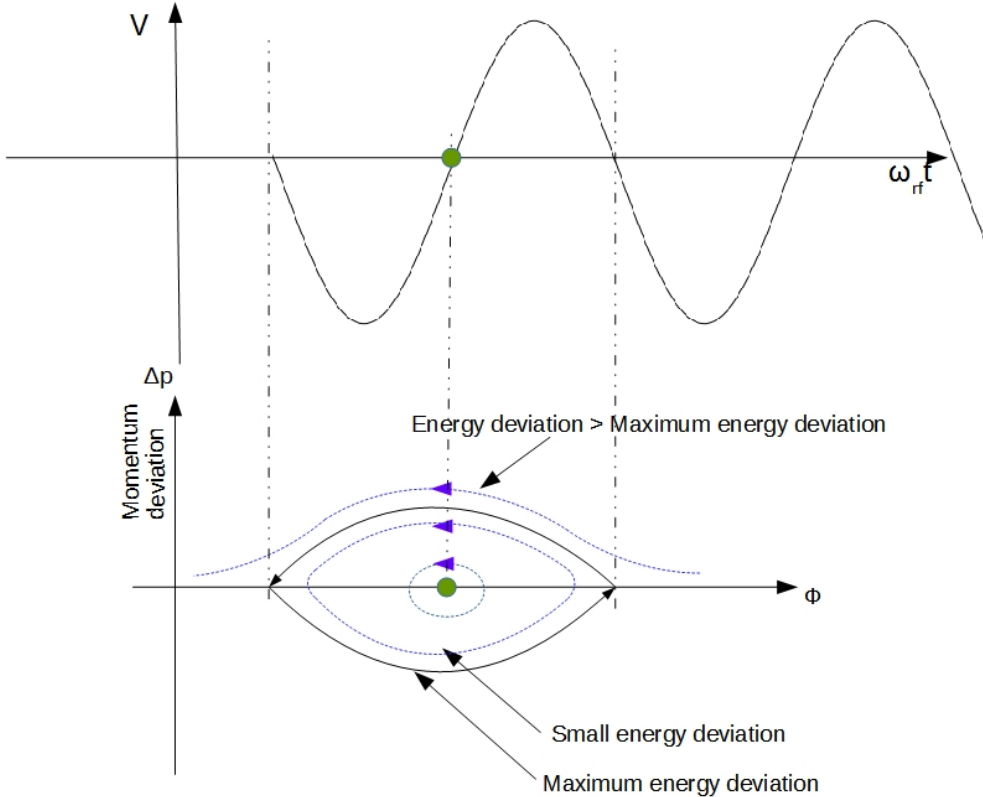


Figure 2.3: A stationary rf bucket.

The green dot represents the synchronous particle (top), the blue path orbits of asynchronous particles and the black path the boundary of a stationary rf bucket (bottom).

angular synchrotron frequency ³ ω_s is [18]

$$\omega_s = 2\pi f_{rev} \sqrt{\frac{hqV_0|\eta \cos \phi_s|}{2\pi\beta^2 E_0}} \quad (2.13)$$

Bunches are always captured in buckets. A synchrotron can have same amount of bunches as buckets. It is also possible for a synchrotron to have less amount of bunches than buckets, e.g. only a part of buckets are filled by bunches. A train of bunches circulating along a synchrotron to be transferred to buckets is defined as a “batch”.

The energy of a beam is related to the ‘magnetic rigidity’, which is defined as the following:

$$B\rho = \frac{p}{q} \quad (2.14)$$

where B is magnetic field, and ρ is the bending radius of a particle immersed in a magnetic field B . The ratio of p to q describes the “stiffness” of a beam, it can be considered as a measure of how much angular deflection results when a particle travels through a given magnetic field [19]. The relation between a rf cavity and the beam acceleration rate is

$$V_0 \sin \phi_s = 2\pi R\rho \dot{B} \quad (2.15)$$

³For the small-amplitude synchrotron motion.

2.1. Bunch and Bucket

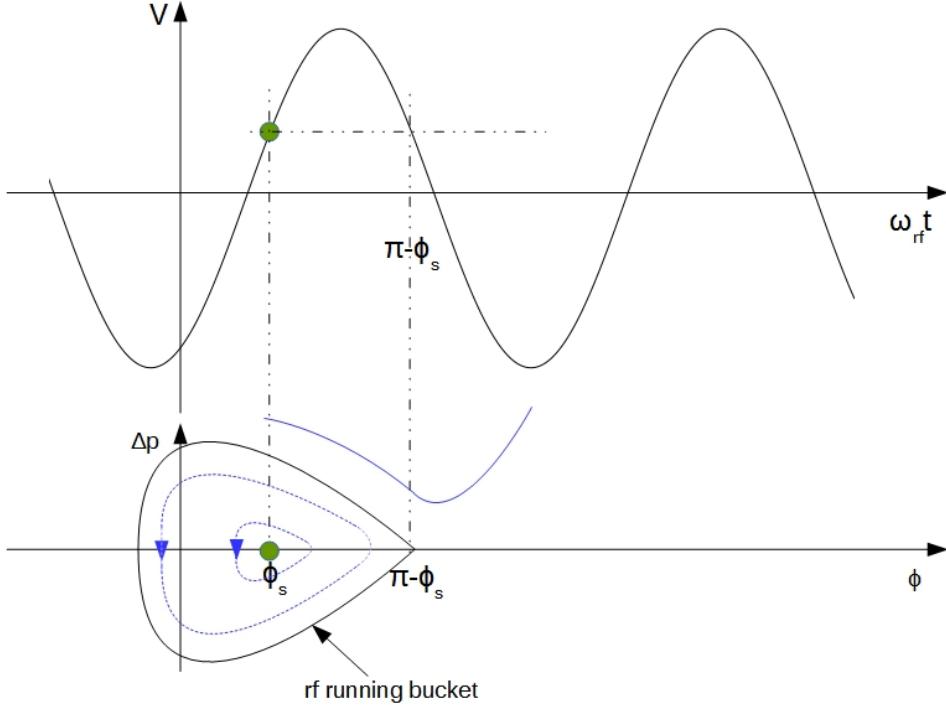


Figure 2.4: A running rf bucket.

The green dot represents the synchronous particle (top), the blue path orbits of asynchronous particles and the black path the boundary of a running rf bucket (bottom).

Bunches must be injected exactly in the center of buckets for the preservation of the longitudinal emittance, which requires the energy and phase match between bunches and buckets. Besides, the shape of bunches to be transferred must match the shape of buckets to be injected in the longitudinal phase space plane. If the source and target synchrotrons have same cavity rf frequency, buckets of the source synchrotron must have same size and height as that of the target synchrotron. The voltage mismatch between bunches and buckets will cause an emittance blow-up. Fig. 2.5 illustrates a bunch-to-bucket injection with an energy, a phase or a voltage error.

The bunch coordinates in the longitudinal phase space plane of the source synchrotron, just before transfer, must be accurately controlled, according to the bucket to be filled [20]. The bunch is transferred from the source to the target synchrotron with the same energy. So the beam has the same momentum for both synchrotrons. According to eq. 2.14, the magnetic rigidity of two synchrotrons must be same.

$$(B\rho)^{src} = \frac{p}{q} = (B\rho)^{trg} \quad (2.16)$$

Where the superscript of the symbol denotes the synchrotron, *src* represents the source synchrotron and *trg* the target synchrotron.

Before the B2B transfer, the revolution frequency of two synchrotrons must meet the following relation based on eq. 2.3.

$$C^{src} f_{rev}^{src} = \beta c = C^{trg} f_{rev}^{trg} \quad (2.17)$$

2.2. Phase Difference

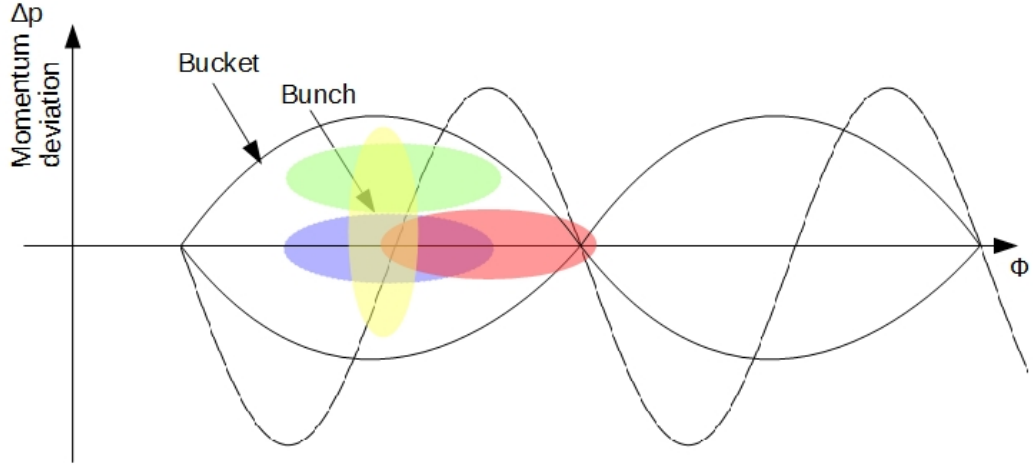


Figure 2.5: The bunch-to-bucket injection with a phase, energy or voltage error.

The blue area represents an injection without any error, the red area an injection with a phase error, the green an injection with a energy error and the yellow an injection with a voltage error (e.g. the rf voltage in the target Synchrotron is too high).

where C^X represents the circumference of a specific synchrotron. A group of new symbols are necessary to be defined. The revolution frequency and cavity rf frequency are denoted by f_{rev}^X and f_{rf}^X , the harmonic number by h^X . The superscript X can be either *src* or *trg* denoting the source or target synchrotron.

Due to the relation between the revolution frequency and cavity rf frequency, eq. 2.2, the ratio between cavity rf frequencies of two rf systems is

$$\frac{f_{rf}^{src}}{f_{rf}^{trg}} = \frac{h^{src}}{h^{trg}} \cdot \frac{f_{rev}^{src}}{f_{rev}^{trg}} = \frac{h^{src}}{h^{trg}} \cdot \frac{C^{trg}}{C^{src}} \quad (2.18)$$

The energy and voltage match will be done by machine physicists, which are out of the scope of this dissertation. The dissertation concentrates on the phase match.

2.2 Phase Difference

The rf voltage of two rf systems are $u_1(t)$ and $u_2(t)$.

$$u_1(t) = V_1 \sin(2\pi f_1 t + \phi_1) \quad (2.19)$$

$$u_2(t) = V_2 \sin(2\pi f_2 t + \phi_2) \quad (2.20)$$

where V_1 and V_2 are the amplitude, ϕ_1 and ϕ_2 the initial phases and f_1 and f_2 are the frequencies of two rf voltages.

The phase difference between u_1 and u_2 is

$$\Delta\phi = [2\pi(f_1 - f_2)t + \phi_1 - \phi_2] \mod 2\pi \quad (2.21)$$

The phase difference $\Delta\phi$ is constant when two frequencies are same ($f_1 = f_2$). In order to change the phase difference for the phase match between two rf voltages, the phase of either (or both) rf system can be shifted backward or forward by means of the rf frequency modulation. The frequency of one (or both) rf voltage is modulated

2.2. Phase Difference

away from the nominal value for a specified period of time and then modulated back. This is the so-called phase shift. Eq. 2.22 gives the relation between the required phase shift $\Delta\phi$ and the frequency modulation.

$$\Delta\phi = 2\pi \int_{t_0}^{t_0+T} \Delta f_{rf}(t) dt \quad (2.22)$$

The phase shift process starts at t_0 . The obtainable phase shift is determined by the frequency offset Δf_{rf} and the duration of the frequency modulation T .

When two frequencies are slightly different, the phase difference $\Delta\phi$ is a periodic function whose rate is the difference between two frequencies. This is the so-called frequency beating. The periodically variable rate is called the “beating frequency”, $\Delta f = |f_1 - f_2|$. The beating period is defined as a period of time for the periodical variation, namely $1/\Delta f$. Within one beating period, there exists a time point, which corresponds to a correct phase difference between two rf systems, namely the phase alignment.

The phase alignment is realized based on two same or two slightly different frequencies. These two frequencies are called “synchronization frequencies”, denoted as f_{syn}^X . Some FAIR use cases are with an identical cavity rf frequency or slightly different cavity rf frequencies of two rf systems, so two cavity rf frequencies are chosen as the synchronization frequencies. There exists many FAIR use cases with big different cavity rf frequencies as well. In this scenario, two synchronization frequencies are an integral multiple of the same or slightly different derived rf frequencies, which are the division of the revolution frequencies. e.g. the division of the revolution frequency is f_{rev}^X/m and the synchronization frequency is $Y \cdot f_{rev}^X/m$, both m and Y are positive integers. The division of the revolution frequency and the integral multiple are determined by the circumference ratio and the harmonic number of two synchrotron. Because of the technical requirement (see Chap. 4), the synchronization frequencies are impossible to have higher frequencies than cavity rf frequencies, namely $Y/m \leq h^X$. Besides, either m/Y or Y/m must be an integer for FAIR use cases, namely the revolution frequency is an integral multiple of the synchronization frequency or the synchronization frequency is an integral multiple of the revolution frequency, so the occurrence of positive zero-crossings of the synchronization frequencies and the positive zero-crossing of the revolution frequencies at the same time always indicates a specified bunch and bucket.

The calculation of the synchronization frequencies are explained for the different scenarios of the circumference ratio between two synchrotrons. For simplicity’s sake, the following analysis is from the perspective of the large and small synchrotrons instead of the source and target synchrotrons. The superscript X of C^X , f_{rev}^X , f_{rf}^X and h^X will be either l or s denoting the large or small synchrotron. Δf represents the beating frequency, κ , m , n and Y are used to represent positive integers and λ a decimal number. The following analysis is based on the energy match between two synchrotrons.

2.2.1 Circumference Ratio is an Integral

If the ratio of the circumference of the injection/extraction orbit of the large synchrotron to that of the small synchrotron is an integer, we have the following relation.

$$\frac{C^l}{C^s} = \kappa \quad (2.23)$$

2.2. Phase Difference

From the circumference ratio, the revolution frequency ratio of two synchrotrons can be calculated.

$$\frac{f_{rev}^l}{f_{rev}^s} = \frac{1}{\kappa} \quad (2.24)$$

Based on eq. 2.24 and the harmonic number, the cavity rf frequency f_{rf}^X is calculated by eq. 2.25 and eq. 2.26

$$f_{rf}^s = h^s \cdot f_{rev}^s = h^s \cdot \kappa \cdot f_{rev}^l \quad (2.25)$$

$$f_{rf}^l = h^l \cdot f_{rev}^l \quad (2.26)$$

Dividing eq. 2.26 by eq. 2.25, we get

$$\frac{f_{rf}^l}{f_{rf}^s} = \frac{h^l}{h^s \cdot \kappa} \quad (2.27)$$

In this scenario, the obvious choice of two same synchronization frequencies are f_{rf}^l/h^l and $f_{rf}^s/(h^s\kappa)$. The synchronization frequencies must be less than or equal to the cavity rf frequencies, otherwise they can not indicate the actual location of bunches and buckets. Generally, the rf frequency of $h=1$ is used as the revolution frequency, so the integral multiple of the revolution frequency is a preferable choice for the synchronization frequency. Hence, the best choice of two synchronization frequencies are

$$f_{syn}^l = \frac{f_{rf}^l}{h^l/Y} = Y f_{rev}^l \quad (2.28)$$

$$f_{syn}^s = \frac{f_{rf}^s}{h^s\kappa/Y} = \frac{Y}{\kappa} f_{rev}^s \quad (2.29)$$

where Y is defined as the Greatest Common Divisor (GCD) of h^l and $h^s \cdot \kappa$.

In eq. 2.21, the phase difference between f_1 and f_2 equals to $\phi_1 - \phi_2$ when $f_1 = f_2$. The value of the initial phase is related to the choice of the rf frequency. e.g. when the phase of rf frequency f_1 is ϕ_1 , the phase of the rf frequency Nf_1 is $(N\phi_1 \bmod 2\pi)$. Hence, the phase difference must be defined with regard to the dedicated rf frequencies. The phase difference between two synchronization frequencies f_{syn}^l and f_{syn}^s is denoted as $\Delta\phi_{syn}$. ϕ_{syn}^X denotes the initial phase of the synchronization frequency. The phase difference $\Delta\phi_{syn}$ calculated as

$$\Delta\phi_{syn} = (\phi_{syn}^l - \phi_{syn}^s) \bmod 2\pi \quad (2.30)$$

The cavity rf frequency of a synchrotron is f_{rf}^X/f_{syn}^X times as large as its synchronization frequency, so the phase difference between the cavity rf frequencies $\Delta\phi_{rf}$ is also f_{rf}^X/f_{syn}^X times as large as the phase difference between two synchronization frequencies $\Delta\phi_{syn}$. $\Delta\phi_{rf}$ is the bunch-to-bucket injection center mismatch, so $\Delta\phi_{rf}$ is always with regard to the target synchrotron, namely $X = trg$.

$$\Delta\phi_{rf} = \frac{f_{rf}^{trg}}{f_{syn}^{trg}} \Delta\phi_{syn} \bmod 2\pi \quad (2.31)$$

Fig. 2.6 illustrates two synchronization frequencies f_{syn}^l and f_{syn}^s , when $\kappa = 5$, $h^s = 1$ and $h^l = 10$. The GCD of h^l and $h^s \cdot \kappa$ is 5, namely $Y = 5$, $f_{rf}^l/f_{rf}^s = 2$, $f_{syn}^l = f_{rf}^l/2 = 5f_{rev}^l$, $f_{syn}^s = f_{rf}^s/1 = f_{rev}^s$ and $\Delta\phi_{rf} = 2\Delta\phi_{syn}$. The parameters are from the FAIR use case of the H^+ B2B transfer from the SIS18 to the SIS100, which will be explained in Sec. 6.1.2.

2.2. Phase Difference

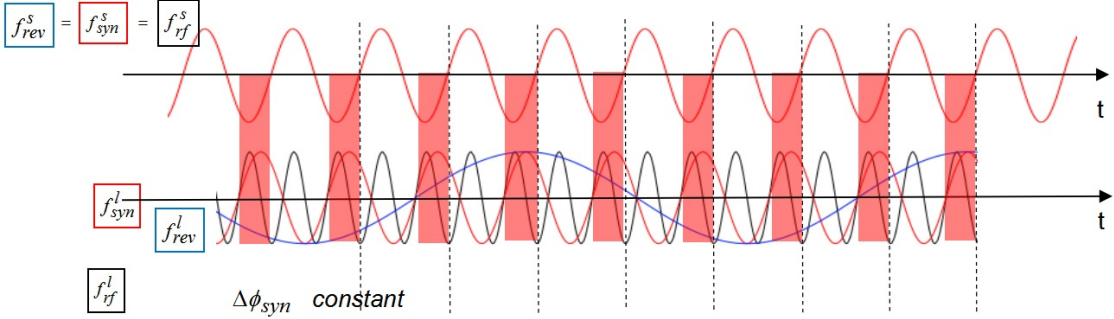


Figure 2.6: The constant phase difference between two synchronization frequencies f_{syn}^l and f_{syn}^s when $\kappa = 5$, $h^s = 1$ and $h^l = 10$.

Red planes represent the constant phase difference between two synchronization frequencies and red sinusoidal waves the individual synchronization frequencies. Black sinusoidal waves represent the individual cavity rf frequencies and the blue sinusoidal wave the revolution frequency. The red sinusoidal wave at the top time axis represents the synchronization frequency, the cavity rf frequency and the revolution frequency.

2.2.2 Circumference Ratio is close to an Integer

If the ratio of the circumference of the injection/extraction orbit of the large synchrotron to that of the small synchrotron is a decimal number close to an integer. Eq. 2.23 changes to

$$\frac{C^l}{C^s} = \kappa + \lambda \quad (2.32)$$

where κ is the integer part and λ is the decimal part of the decimal number and the absolute value of λ is smaller than 0.005 for FAIR use cases. The bound of λ is shown in Chap. 6. From the circumference ratio, the revolution frequency ratio of two synchrotrons can be calculated.

$$\frac{f_{rev}^l}{f_{rev}^s} = \frac{1}{\kappa + \lambda} \quad (2.33)$$

Based on eq. 2.33 and harmonic number, the f_{rf}^X are calculated by eq. 2.34 and eq. 2.35

$$f_{rf}^s = h^s \cdot f_{rev}^s = h^s \cdot (\kappa + \lambda) \cdot f_{rev}^l \quad (2.34)$$

$$f_{rf}^l = h^l \cdot f_{rev}^l \quad (2.35)$$

We get the relation between f_{rf}^s and f_{rf}^l by dividing eq. 2.35 by eq. 2.34.

$$\frac{f_{rf}^l}{f_{rf}^s} = \frac{h^l}{h^s \cdot (\kappa + \lambda)} = \frac{h^l}{h^s \cdot \kappa + h^s \cdot \lambda} \quad (2.36)$$

In eq. 2.36, $h^s \lambda$ is much smaller than $h^s \kappa$, therefore $h^s \lambda$ can be neglected for the calculation of the synchronization frequencies. Apart from the similar reasons mentioned in the scenario of the integral circumference ratio in Sec. 2.2.1, the synchronization frequencies with the integral multiple of f_{rf}^l/h^l and $f_{rf}^s/(h^s \kappa)$ achieve a

2.2. Phase Difference

more precise phase difference. Two best slightly different synchronization frequencies are

$$f_{syn}^l = \frac{f_{rf}^l}{h^l/Y} = Y f_{rev}^l \quad (2.37)$$

$$f_{syn}^s = \frac{f_{rf}^s}{h^s \kappa / Y} = \frac{Y}{\kappa} f_{rev}^s \quad (2.38)$$

Y is the GCD of h^l and $h^s \cdot \kappa$. Substituting two synchronization frequencies into eq. 2.21, we get the periodically variable phase difference between two synchronization frequencies $\Delta\phi_{syn}$.

$$\Delta\phi_{syn}(t) = [2\pi(f_{syn}^l - f_{syn}^s)t + \phi_{syn}^l - \phi_{syn}^s] \mod 2\pi \quad (2.39)$$

Substituting f_{rf}^l in eq. 2.36 into eq. 2.39, we get

$$\Delta\phi_{syn}(t) = [2\pi Y \frac{-\lambda f_{rf}^s}{(\kappa + \lambda) h^s \kappa} t + \phi_{syn}^l - \phi_{syn}^s] \mod 2\pi \quad (2.40)$$

Eq. 2.40 shows that the phase difference is a periodic function. The beating frequency between two synchronization frequency is $\Delta f = |f_{syn}^l - f_{syn}^s|$. The beating frequency must not be too large in order to guarantee the precision, but also not too small to satisfy the time constraint for the phase match. The phase difference between two cavity rf frequencies is

$$\Delta\phi_{rf} = (\frac{f_{rf}^{trg}}{f_{syn}^{trg}} \Delta\phi_{syn}) \mod 2\pi \quad (2.41)$$

Fig. 2.7 shows the periodically variable phase difference between two slightly different synchronization frequencies f_{syn}^l and f_{syn}^s when $\kappa = 2$, $\lambda = -0.003$, $h^s = 2$ and $h^l = 4$. The GCD of h^l and $h^s \cdot \kappa$ is 4, namely $Y = 4$. Hence, according to eq. 2.37 and eq. 2.38, two synchronization frequencies are $f_{syn}^l = f_{rf}^l = 4f_{rev}^l$, $f_{syn}^s = f_{rf}^s = 2f_{rev}^s$ and $\Delta\phi_{rf} = \Delta\phi_{syn}$. The parameters are from the FAIR use case of the h=4 B2B transfer from the SIS18 to the ESR, which will be explained in Sec. 6.2.1.

2.2.3 Circumference Ratio is far away from an Integer

When the circumference ratio of the large synchrotron to that of the small synchrotron is far away from an integer, the circumference ratio is a decimal number and eq. 2.23 can be expressed as a rational number plus a small remainder of the decimal number.

$$\frac{C^l}{C^s} = \frac{m}{n} + \lambda \quad (2.42)$$

where m/n represents a quotient of two integers, m is a numerator and n is a non-zero denominator. λ represents the remainder of the decimal part and the absolute value of λ is smaller than 0.05 for FAIR use cases.

Substituting κ by m/n into eq. 2.36, we get the relation between f_{rf}^s and f_{rf}^l .

$$\frac{f_{rf}^l}{f_{rf}^s} = \frac{h^l \cdot n}{h^s \cdot m + h^s \cdot \lambda \cdot n} \quad (2.43)$$

2.2. Phase Difference

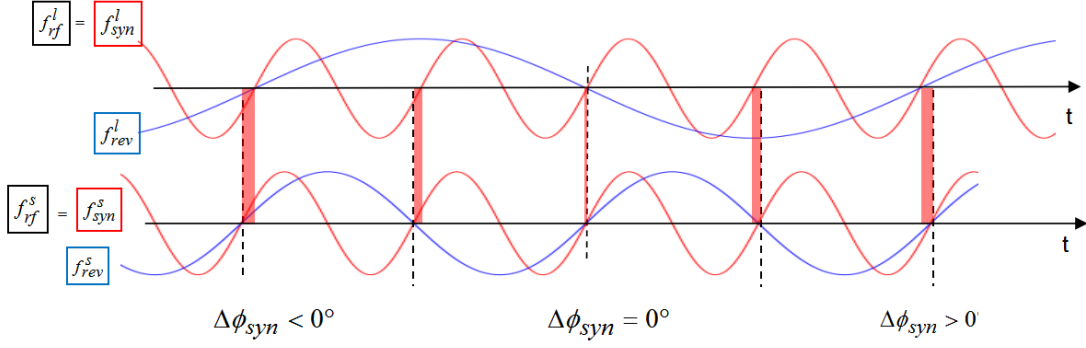


Figure 2.7: The periodically variable phase difference between two slightly different synchronization frequencies f_{syn}^l and f_{syn}^s when $\kappa = 2$, $\lambda = -0.003$, $h^s = 2$ and $h^l = 4$.

Red planes represent the periodical variable phase difference and red sinusoidal waves the synchronization frequencies and cavity rf frequencies and blue sinusoidal waves the revolution frequencies.

In eq. 2.43, $h^s \lambda n$ is much smaller than $h^s m$. Similarly as the scenario of the close to an integral circumference ratio in Sec. 2.2.2, two slightly different synchronization frequencies are

$$f_{syn}^l = \frac{f_{rf}^l}{h^l n / Y} = \frac{Y}{n} f_{rev}^l \quad (2.44)$$

$$f_{syn}^s = \frac{f_{rf}^s}{h^s m / Y} = \frac{Y}{m} f_{rev}^s \quad (2.45)$$

Y is the GCD of $h^l n$ and $h^s m$. Substituting two synchronization frequencies into eq. 2.21, we get the periodical phase difference $\Delta\phi_{syn}$.

$$\Delta\phi_{syn}(t) = [2\pi(f_{syn}^l - f_{syn}^s)t + \phi_{syn}^l - \phi_{syn}^s] \mod 2\pi \quad (2.46)$$

Substituting f_{rf}^l in eq. 2.43 into eq. 2.46, we get

$$\Delta\phi_{syn}(t) = [2\pi Y \frac{-\lambda f_{rf}^s}{(m/n + \lambda) h^s m} t + \phi_{syn}^l - \phi_{syn}^s] \mod 2\pi \quad (2.47)$$

Eq. 2.47 shows that the phase difference is a periodic function. The beating frequency is $\Delta f = |f_{syn}^l - f_{syn}^s|$. It is possible to have various combination of m/n and λ . λ determines the beating frequency. The smaller, the more precise the phase match between two synchronization frequencies. Y/n and Y/m determines two synchronization frequencies. For FAIR use cases, n/Y and m/Y are always integer. So the synchronization frequencies are the division of the revolution frequencies ($h=1$), which is called the “subharmonic“. Hence, we have to find a proper combination of m/n and λ . The phase difference between two cavity rf frequencies is

$$\Delta\phi_{rf} = (\frac{f_{rf}^{trg}}{f_{syn}^{trg}} \Delta\phi_{syn}) \mod 2\pi \quad (2.48)$$

2.3. Phase Match of two Rf Systems

Fig. 2.8 shows the periodically variable phase difference between two slightly different synchronization frequencies f_{syn}^l and f_{syn}^s when $m = 26$, $n = 10$, $\lambda = -0.003$, $h^s = 1$ and $h^l = 1$. $f_{rf}^l/f_{rf}^s = 1 \cdot 10/(1 \cdot 26 - 1 \cdot 10 \cdot 0.003)$. The GCD of $h^l n = 1 \cdot 10$ and $h^s m = 1 \cdot 26$ is 2, namely $Y = 2$. Hence, according to eq. 2.44 and eq. 2.45, two synchronization frequencies are $f_{syn}^l = f_{rf}^l/5 = f_{rev}/5$, $f_{syn}^s = f_{rf}^s/13 = f_{rev}/13$ and $\Delta\phi_{rf} = 5\Delta\phi_{syn}$. The parameters are from the FAIR use case of the B2B transfer from the CR to the HESR, which will be explained in Sec. 6.3.3.

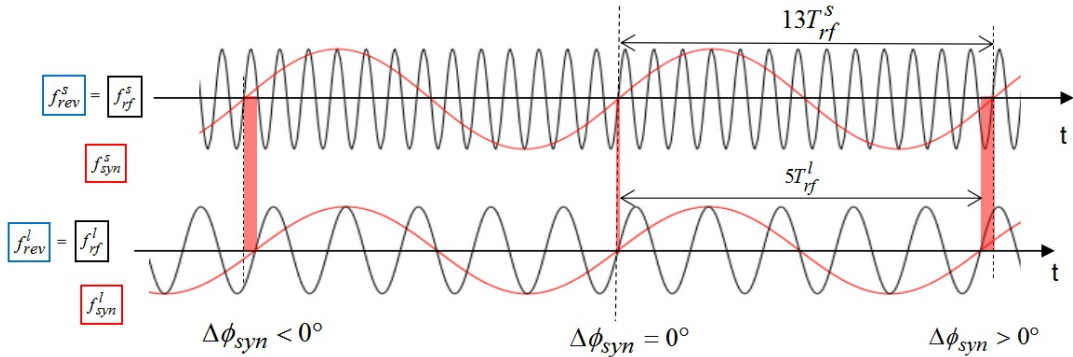


Figure 2.8: The periodically variable phase difference between two synchronization frequencies f_{syn}^l and f_{syn}^s when $m = 26$, $n = 10$, $\lambda = -0.003$, $h^s = 1$ and $h^l = 1$.

Red planes represent the periodical variable phase difference and red sinusoidal waves the synchronization frequencies. Black sinusoidal waves represent the cavity rf frequencies and the revolution frequencies.

2.3 Phase Match of two Rf Systems

For the different scenarios mentioned in Sec. 2.2, two methods are available for the phase alignment of two rf systems, the phase shift and the frequency beating methods. Both methods provide a time frame for the B2B transfer, within which bunches are transferred into buckets with the bunch-to-bucket injection center mismatch smaller than a given upper bound. This time frame is called the “synchronization window”. Both methods are based on the prerequisite that the phase difference between two rf systems is predictable, so the LLRF feedback loops used for phase corrections must be switched off before the B2B transfer starts. e.g. beam phase feedback loop [21] and bunch-by-bunch longitudinal rf feedback loop [22].

2.3.1 Phase Shift Method

In order to change the constant phase difference between two synchronization frequencies, the phase of either (or both) rf system can be shifted backward or forward by means of the rf frequency modulation. The frequency of one (or both) rf system is modulated away from the nominal value for a specified period of time and then modulated back, see Sec. 2.3.

The phase shift process must be performed slowly enough for the preservation of the longitudinal emittance. After the phase shift, bunches of the source synchrotron

2.3. Phase Match of two Rf Systems

are phase aligned with buckets of the target synchrotron. Theoretically the synchronization window is infinitely long. In fact, the beam feedback loops on the rf system are switched off before the B2B starts, so the beam maybe stable for a short period of time only, e.g. 10 ms. Hence, bunches must be transferred as soon as possible, introducing a synchronization window with a limited length.

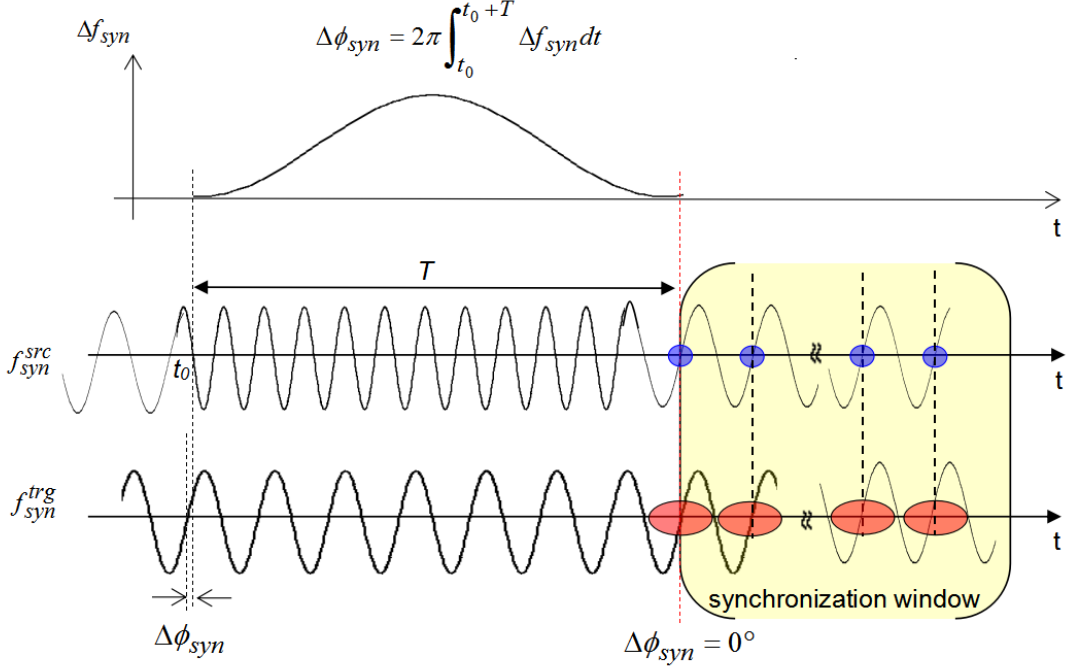


Figure 2.9: An example for the phase shift method with a sinusoidal rf frequency modulation.

Blue dots represent bunches of the source synchrotron and red dots buckets of the target synchrotron.

Fig. 2.9 illustrates an example for the phase shift method with a sinusoidal rf frequency modulation. The f_{syn}^l and f_{syn}^s are the synchronization frequencies respectively from the large and small synchrotrons. The time-of-flight between bunches and buckets is compensated here. The phase shift is done for the small synchrotron in this example. The red dashed line shows the end of the phase shift process ($\Delta\phi_{syn} = 0^\circ$) and the beginning of the synchronization window, drawn in yellow. After the phase shift, bunches match with buckets. A sinusoidal frequency modulation Δf_{syn} with a fixed duration time T is used for the rf frequency modulation on f_{syn}^s .

$$\Delta f_{syn}(t) = A[1 - \cos \frac{2\pi}{T}(t - t_0)] \quad (2.49)$$

where A is the amplitude of the sinusoidal wave. Based on eq. 2.22, the area of the sinusoidal wave equals to $\Delta\phi_{syn}/2\pi$. We can calculate the amplitude A

$$A = \frac{\Delta\phi_{syn}}{2\pi} \cdot \frac{1}{T} \quad (2.50)$$

When the rf frequency modulation on the synchronization frequency f_{syn}^X is Δf_{syn} , the rf frequency modulation on the cavity rf frequency Δf_{rf} and the phase

2.3. Phase Match of two Rf Systems

shift for the cavity rf frequency $\Delta\phi_{rf}$ are

$$\Delta f_{rf} = \frac{f_{rf}^X}{f_{syn}^X} \Delta f_{syn} \quad (2.51)$$

$$\Delta\phi_{rf} = \left(\frac{f_{rf}^{trg}}{f_{syn}^{trg}} \Delta\phi_{syn} \right) \bmod 2\pi \quad (2.52)$$

A particular case of the B2B synchronization occurs, when the target synchrotron is empty, i.e. it did not capture any bunches yet, the phase jump can be done for the target synchrotron.

Now we analyze the rf frequency modulation of the phase shift from the beam dynamics perspective.

- Momentum shift and radial excursion

A rf frequency modulation introduces a momentum shift.

$$\frac{\Delta p}{p} = \frac{1}{\frac{1}{\gamma^2} - \alpha_p} \cdot \frac{\Delta f_{rf}}{f_{rf}} \quad (2.53)$$

Substituting $\Delta R/R$ in eq. 2.9 into eq. 2.53, we get the radial excursion due to the rf frequency modulation.

$$\frac{\Delta R}{R} = \frac{1}{\frac{1}{\alpha_p \gamma^2} - 1} \cdot \frac{\Delta f_{rf}}{f_{rf}} \quad (2.54)$$

The rf frequency modulation causes a radial excursion. The maximum allowed radial excursion is a design parameter, which is given for a synchrotron lattice. Thus, a maximum frequency offset for the rf frequency modulation also exists.

- Shift of the synchronous phase

The rf frequency modulation is accompanied with a beam acceleration or deceleration, so the synchronous phase deviates from 0° . Based on eq. 2.14, we can get the first derivative of the magnetic rigidity

$$\dot{B}\rho = \frac{1}{q} \frac{d\Delta p}{dt} = \frac{B\rho}{p} \frac{d\Delta p}{dt} \quad (2.55)$$

Substituting $\dot{B}\rho$ in eq. 2.55 into eq. 2.15, we get the relation between the change in the synchronous phase ϕ_s and the momentum shift rate based on the prerequisite that $\Delta R/R$ and ϕ_s is very small. The maximum radial excursion of FAIR synchrotrons $\Delta R/R$ is on the order of 10^{-4} and the synchronous phase is less than 10° .

$$V_0 \sin \phi_s \approx V_0 \phi_s = \frac{2\pi R B \rho}{p} \frac{d\Delta p}{dt} \quad (2.56)$$

It is clear from eq. 2.56 that when the rf frequency is modulated, ϕ_s is only determined by $\frac{d\Delta p}{dt}$, since the change of other parameters are very small and negligible. ϕ_s is proportional to the momentum shift rate $\frac{d\Delta p}{dt}$. In eq. 2.53, γ change very slowly as compared to Δp during the rf frequency modulation.

2.3. Phase Match of two Rf Systems

So we can get the relation between $\frac{d\Delta p}{dt}$ and the rf frequency modulation rate $\frac{d\Delta f_{rf}}{dt}$ by the first derivative of eq. 2.53.

$$\frac{1}{p} \frac{d\Delta p}{dt} = \frac{1}{(1/\gamma^2 - \alpha_p)f_{rf}} \frac{d\Delta f_{rf}}{dt} \quad (2.57)$$

Substituting $\frac{d\Delta p}{dt}$ in eq. 2.57 into eq. 2.56, we get the relation between the change in the synchronous phase ϕ_s and the change rate of the rf frequency modulation.

$$V_0 \phi_s = \frac{2\pi RB\rho}{(1/\gamma^2 - \alpha_p)f_{rf}} \frac{d\Delta f_{rf}}{dt} \quad (2.58)$$

Hence, the synchronous phase is proportional to $\frac{d\Delta f_{rf}}{dt}$.

- Bucket size

At the flattop, the bucket is a stationary bucket. During the frequency modulation process, the bucket becomes a running bucket with $\phi_s \neq 0^\circ$. When the synchronous phase is very small, we get the bucket area factor from eq. 2.12.

$$\alpha_b(\phi_s) \approx \frac{1 - \phi_s}{1 + \phi_s} \quad (2.59)$$

Substituting ϕ_s in eq. 2.58 into eq. 2.59, we get

$$\alpha_b(\phi_s) \approx \frac{(1/\gamma^2 - \alpha_p)f_{rf}V_0 - 2\pi RB\rho \frac{d\Delta f_{rf}}{dt}}{(1/\gamma^2 - \alpha_p)f_{rf}V_0 + 2\pi RB\rho \frac{d\Delta f_{rf}}{dt}} \quad (2.60)$$

Buckets must be big enough to capture bunches. Eq. 2.60 shows that the bucket area factor is in inverse proportion to $\frac{d\Delta f_{rf}}{dt}$. Hence, $\frac{d\Delta f_{rf}}{dt}$ must be small enough to guarantee the bucket size, namely the change of the rf frequency modulation must be slow enough.

- Adiabaticity

A process is called “adiabatic” when the rf frequency is changed slowly enough for the beam to follow. The condition that the rf frequency varies slowly can be expressed by

$$\varepsilon = \frac{1}{\omega_s^2} \left| \frac{d\omega_s}{dt} \right| \quad (2.61)$$

where ε is the adiabaticity parameter. For the angular synchrotron frequency, eq. 2.13, all of the other variables change very slowly compared with ϕ_s . From eq. (2.61) and eq. (2.13), the adiabaticity can be written as follows [23]:

$$\varepsilon \approx \frac{1}{2\omega_s} |\dot{\phi}_s \phi_s| \quad (2.62)$$

Substituting ϕ_s and $\dot{\phi}_s$ in eq. 2.58 into eq. 2.62, we get

$$\varepsilon \approx \frac{1}{2\omega_s} \left[\frac{2\pi RB\rho}{(1/\gamma^2 - \alpha_p)f_{rf}V_0} \right]^2 \left| \frac{d\Delta f_{rf}}{dt} \frac{d^2 \Delta f_{rf}}{dt^2} \right| \quad (2.63)$$

2.3. Phase Match of two Rf Systems

where ω_s is the angular synchrotron frequency with no frequency modulation. Form the adiabaticity eq. 2.63, $\frac{d\Delta f_{rf}}{dt}$ and $\frac{d^2\Delta f_{rf}}{dt^2}$ must exist and must be small enough to guarantee the adiabaticity. Namely, $\frac{d\Delta f_{rf}}{dt}$ must be continuous and the change of $\frac{d\Delta f_{rf}}{dt}$ must be slow enough.

- Tune shift

So far the rf frequency modulation is analyzed from the longitudinal beam dynamics perspective. Because of the momentum shift, the rf frequency modulation has an influence on the transverse beam dynamics as well. The beam particle's tune $Q_{x/y}$ is defined as the frequency of the horizontal/vertical oscillations and chromaticity $Q'_{x/y}$ is defined as their horizontal/vertical dependence on particle momentum [24]. The momentum spread $\Delta p/p \neq 0$ during the phase shift process causes horizontal/vertical tune shifts $\Delta Q_{x/y}$ [25].

$$\Delta Q_{x/y} = Q'_{x/y} \frac{\Delta p}{p} \quad (2.64)$$

The momentum shift of FAIR synchrotrons $\Delta p/p$ is in the 10^{-4} range and the chromaticity is on the order of 10. So the tune shift is relative small and has almost no influence on the transverse motion.

According to the beam dynamics analysis, there are several requirements for the rf frequency modulation:

- There exists a maximum rf frequency offset Δf_{rf_max} .
- $\frac{d\Delta f_{rf}}{dt}$ must be continuous and small enough.
- $\frac{d^2\Delta f_{rf}}{dt^2}$ must be small enough.

Application of these criterion to FAIR use cases, please see Chap. 5.

2.3.2 Frequency Beating Method

The frequency beating method uses two slightly different synchronization frequencies. When two synchronization frequencies are slightly different, two rf systems are beating automatically. When they are identical, either the rf system of the source or that of the target is detuned to achieve the beating. The frequency is detuned at constant energy by changing the frequency and magnetic field. This will be done by operators and is out of the scope of this dissertation. The frequency detuning for the synchronization frequency is denoted as Δf_{syn} and that for the cavity rf frequency is denoted as Δf_{rf} , $\Delta f_{rf} = \frac{f_{rf}}{f_{syn}^X} \Delta f_{syn}$. The synchronization window has a certain length, which is denoted as T_w . The synchronization window brings a symmetric time frame with respect to the time, when the phase difference between two synchronization frequencies is closest to the required phase difference, see yellow region in Fig. 2.10. The red dashed line shows the time of the closest to the required phase difference. The bunch-to-bucket injection center mismatch $\Delta\phi_{rf}$ within the synchronization window is related to the length of the synchronization window, see eq. 2.65.

$$\Delta\phi_{rf} = \pm \frac{1}{2} \cdot 2\pi |f_{syn}^{src} - f_{syn}^{trg}| \cdot T_w \cdot \frac{f_{rf}^{trg}}{f_{syn}^{trg}} \quad (2.65)$$

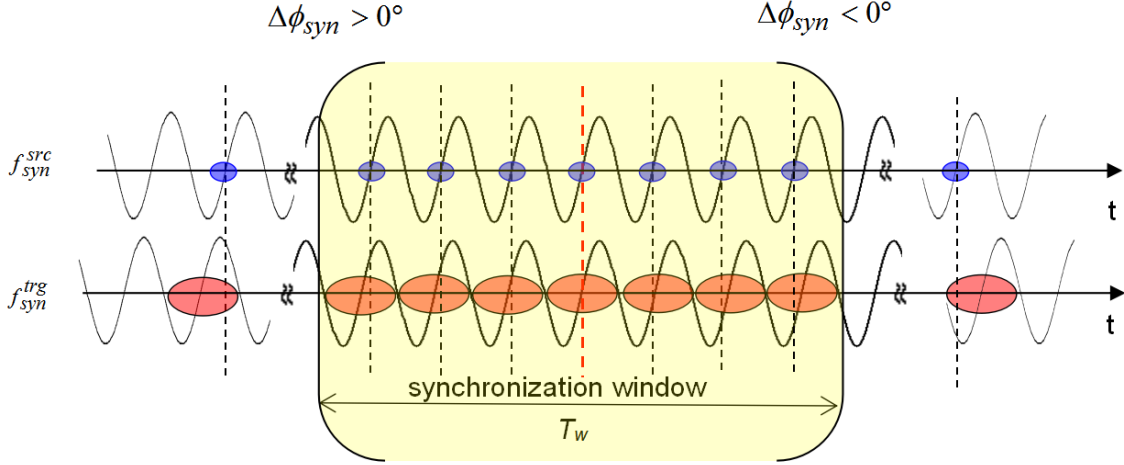


Figure 2.10: The illustration of the frequency beating method.

Blue dots represent bunches of the source synchrotron and red dots buckets of the target synchrotron.

In reality, all B2B transfer have a tolerant upper bound for the bunch-to-bucket center mismatch $\Delta\phi_{rf_max}$ (e.g. $\Delta\phi_{rf_max} = \pm 1^\circ$ for FAIR use cases). The upper bound brings a maximum synchronization window T_{w_max} . The maximum synchronization window is

$$T_{w_max} = \frac{2|\Delta\phi_{rf_max}| \cdot \frac{f_{syn}^{trg}}{f_{rf}^{trg}}}{2\pi} \cdot \frac{1}{|f_{syn}^{src} - f_{syn}^{trg}|} \quad (2.66)$$

The rf frequency is detuned at the end of the acceleration ramp. The rf frequency detuning is accompanied with the magnetic field and orbit change.

- Radial excursion

Because the momentum should not be affected by the frequency detuning for the energy match, namely $\Delta p=0$, we can get the general relation between the radial excursion and the rf frequency change by substituting $\Delta p=0$ into eq. 2.8.

$$\frac{\Delta R}{R} = -\frac{\Delta f_{rf}}{f_{rf}} \quad (2.67)$$

$\frac{\Delta R}{R}$ constrained by the synchrotron lattice is used to check the acceptance.

2.4 Synchronization of Extraction and Injection Kicker Magnets

The proper bunch-to-bucket transfer requires not only that two rf systems are synchronized with each other, but also that the extraction and injection kicker magnets are synchronized with beam.

2.4. Synchronization of Extraction and Injection Kicker Magnets

A kicker magnet (or kicker) is a dipole magnet, which is used to rapidly switch particles between two paths. An injection kicker merges one beam into a circulating beam in a synchrotron and an extraction kicker diverts a circulating beam to leave a synchrotron. Generally, the extraction or injection kicker is consisted of a certain number of kicker magnets instead of a solo one. The B2B transfer needs a fast beam extraction and injection, which extracts and injects beam in a single-turn. Hence, a pulsed kicker magnet must be used with rapid rise time and fall time and the variable pulse flat-top [26]. Fig. 2.11 shows the schematic diagram of a kicker magnet. The energy storage module is charged with a high voltage power supply. It will be discharged via the transmission cable and the kicker magnet by switching on the pulse start switch. Before the increase of the magnetic field, there exist a preparation time for the kicker magnet. The magnet needs a certain period of time to increase from zero to a stable magnetic field, which is so-called a “kicker rise time” (short: rise time). The length of the “kicker flat-top” can be modified by switching on the stop switch in correlation with the pulse start switch. When the pulse stop switch is switched off, the magnet needs a certain period of time to reduce to zero magnetic field. This period is so-called a “kicker fall time” (short: fall time) [27]. For the proper B2B transfer, the extraction and injection kickers must be synchronized with the synchrotron rf signal. The start switch must be switched on the preparation time earlier before the tail of the circulating bunch passes the kicker, so that the transition of the kicker (the rise-up of the magnetic field) will be carried out during bunch gaps. The pulse stop switch must be switched off in time so that the transition of the kicker (the fall-down of the magnetic field) will not affect the head of the next coming bunch in the synchrotron. The kicker control electronic produces the ignition signal to switch on/off two switches. Generally a preparation time of FAIR kickers is within the $5\text{--}10\ \mu\text{s}$ range. Compared with the FAIR rf frequency in the MHz range, a preparation time is not negligible, which can cause an increase of the bunch-to-bucket injection center mismatch especially for the frequency beating method. The kicker control electronic must take the preparation time into consideration, igniting kickers in advance of the preparation time.

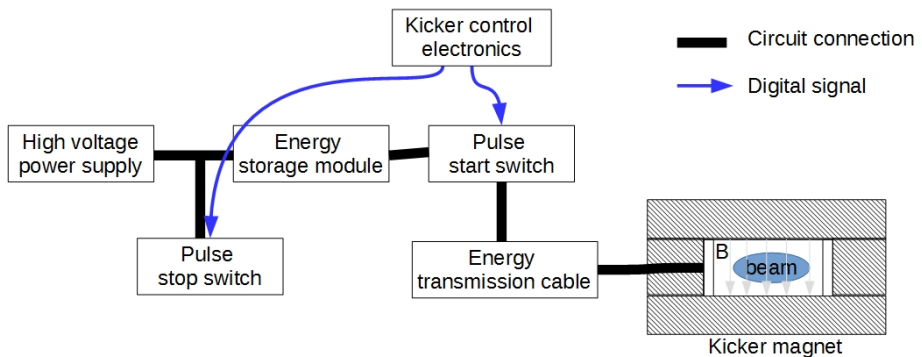


Figure 2.11: The schematic diagram of a kicker magnet.

Most commonly, an extraction kicker is used to eject all bunches. Fig. 2.12 illustrates the rise time, kicker flat-top and fall time of an extraction kicker. The tail of the circulating bunch passes the kicker at t_0 . The start switch is switched on the preparation time earlier than t_0 . The rise time starts at t_0 . The kicker flat-top of the magnetic field must be achieved before the head of the next circulating bunch passes the kicker at t_1 . So the rise time of the extraction kicker must be shorter than

2.4. Synchronization of Extraction and Injection Kicker Magnets

the bunch gap. The kicker flat-top has at least the length of bunches to be extracted. The stop switch is switched on earliest at t_2 , when all bunches are extracted. Then there is no more bunch left in the synchrotron, so there is no constraint for the fall time.

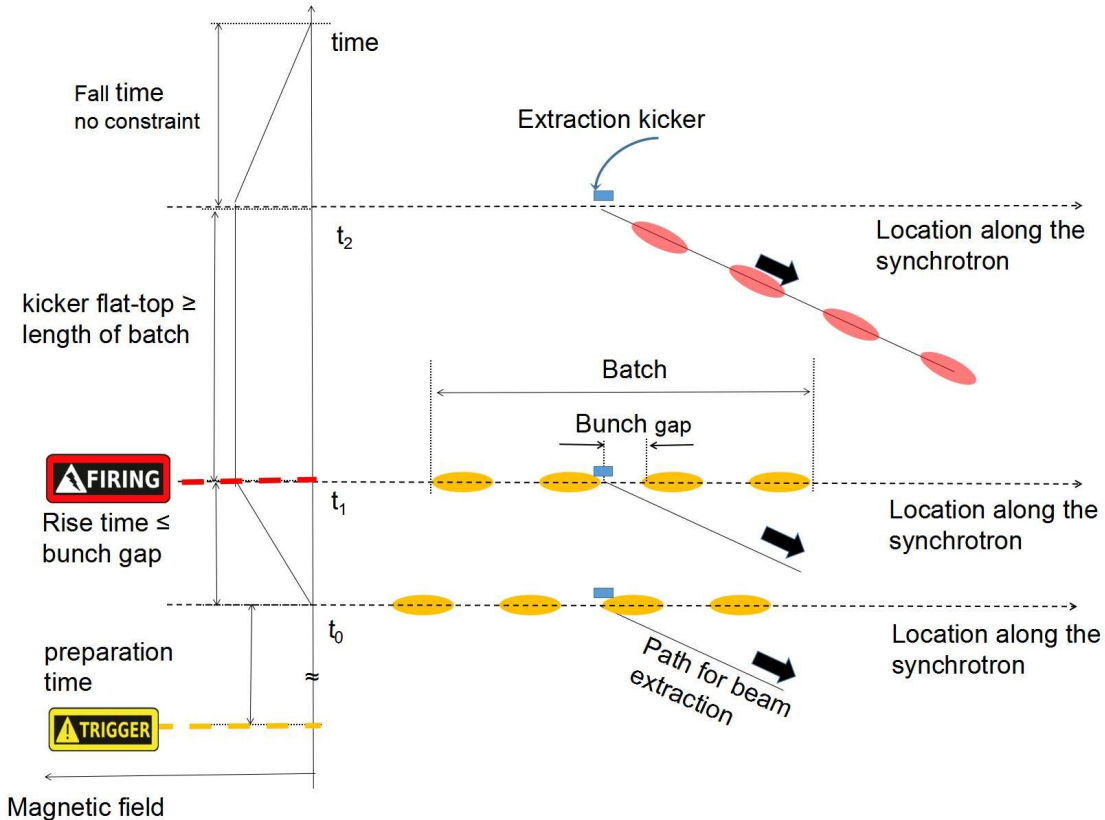


Figure 2.12: The rise time, kicker flat-top and fall time of an extraction kicker.

Yellow ellipses represent circulating bunches in the synchrotron, red ones extracted bunches. The warning sign indicates the kicker trigger and the flash sign indicates the kicker firing.

For multiple batches injection, see Fig. 2.13, the tail of the circulating bunch passes the kicker at t_0 . The start switch is switched on the preparation time earlier than t_0 . The rise time starts at t_0 . The kicker flat-top of the magnetic field must be achieved before bunches are injected at t_1 . So the rise time of the injection kicker must be shorter than the bunch gap. The length of the kicker flat-top is determined by the length of bunches to be injected. The stop switch is switched on as soon as the tail of the last injected bunch passes the kicker at t_2 . The magnetic field must be reduced to zero before the head of the circulating bunch passes the kicker at t_3 . So the fall time must be shorter than $t_3 - t_2$.

2.4. Synchronization of Extraction and Injection Kicker Magnets

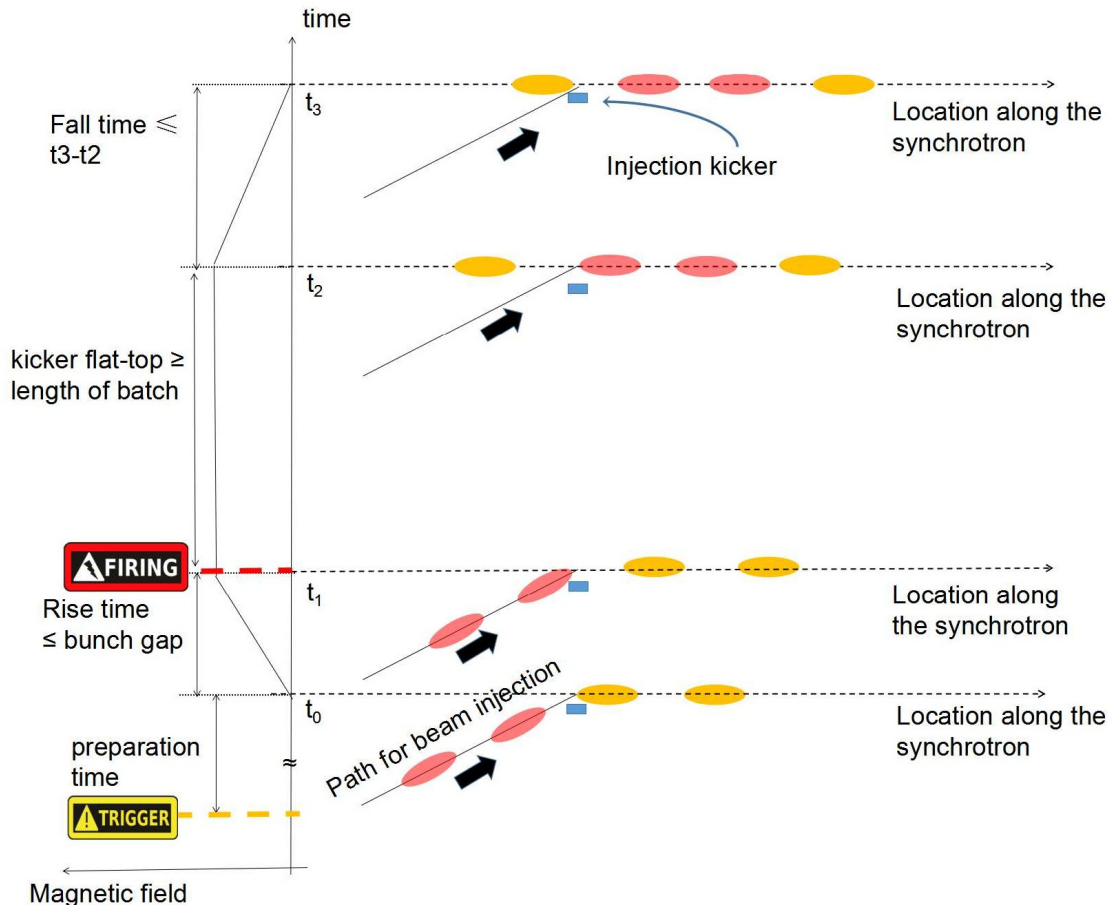


Figure 2.13: The rise time, kicker flat-top and fall time of an injection kicker for multiple batches injection.

Yellow ellipses represent circulating bunches in the synchrotron, red ones bunches to be injected.

Chapter 3

Technical Basis for FAIR B2B Transfer System

For the FAIR accelerator complex, synchronization of the B2B transfer will be realized by the FAIR control system and the Low-Level RF (LLRF) system. For the synchronization of LLRF system, the General Machine Timing (GMT) system is complemented and linked to the Bunchphase Timing System (BuTiS). Machine Protection System (MPS) protects SIS100 and subsequent accelerators or experiments from damage. Hence, the B2B transfer system for FAIR coordinates with the MPS system.

3.1 FAIR Control System

The FAIR control system takes advantage of collaborations with CERN in using framework solutions like Front-End System Architecture (FESA) [28], LHC Software Architecture (LSA), White Rabbit (WR) [29]. It consists of the equipment layer, middle layer and application layer. The equipment layer consists of equipment interfaces, GMT and software representations of the equipment FESA. The middle layer provides service functionality both to the equipment layer and the application layer through the IP control system network. LSA is used for the Settings Management (SM). The application layer combines the applications for operators as GUI applications or command line tools. The application layer and the middle layer only request what the FAIR accelerator complex should do and transmit set values to the equipment layer. Before an accelerator cycle is started, the setting properties of FESA are pre-supplied by LSA from SM for all scheduled beams with specific settings accordingly. At run time, FESA real time software actions are triggered by timing message, the actual beam specific data is then selected based on information carried by the timing message and send to the equipment [29].

3.1.1 Bunch Phase Timing System

Bunch Phase Timing System (BuTiS) serves as a campus-wide clocks distribution system with sub nanosecond resolution and stability over distances of several hundred meters while maintaining 100 ps per km timing stability [30]. Two BuTiS reference clocks 100 kHz P0 pulse and 10 MHz S1 phase reference signal are generated centrally in the BuTiS center. A star-shaped optical fiber BuTiS distribution

3.1. FAIR Control System

system transfers these two reference clocks to the BuTiS local reference synthesizer all over the FAIR campus. The optical signal transmission delay between the BuTiS center and the different BuTiS local reference synthesizer is measured by a measurement setup in the BuTiS center. This measurement information is used to correct the phases of the signals generated in each BuTiS local reference synthesizer for the delay compensation. So at each BuTiS reference synthesizer, two delay compensated clock signals, 200 MHz C2 sine and 100 kHz T0 ident clocks, are generated from 100 kHz P0 and 10 MHz S1 reference clocks [30, 31]. The main task of BuTiS is the supply of the reference clock signals for phase measurement signal rf systems, see Sec. 3.2.

3.1.2 General Machine Timing System

The GMT system is contained in the equipment layer. It synchronizes all FECs (FEC) with nanosecond accuracy over the whole FAIR campus and distributes timing messages to all FECs and controls all FECs to execute real-time actions at a designated time [32]. The GMT system is a time based system. The GMT consists of the Timing Master (TM), the White Rabbit (WR) timing network and FECs. The timing master is a logical device, containing the data master (DM), the clock master (CM) and the management master (MM). The data master receives a schedule for the operation of the FAIR accelerator complex from the Settings Management and provides the real-time schedule by broadcasting timing messages to the WR timing network, which will be received and executed by the corresponding equipment connected to the FECs at the designated time. The clock master is a dedicated WR switch. It is the topmost switch layer of the WR timing network and provides the grandmaster clock and timestamps which are distributed to all other FECs in the timing network. The clock master derives its clock from BuTiS 200 MHz C2 and 100 kHz T0 clocks and timestamps distributed are phase locked to BuTiS clocks. The GMT system could generate BuTiS T0 and C2 with any FECs and FECs are capable to timestamp clock edges. All active components including FECs and WR switches are registered to the MM. The MM monitors and manages the active components of the GMT system [33, 34]. The SCU (SCU) is a new generation of the standard FEC for the FAIR control system, which provides a compact and flexible solution for controlling all types of accelerator equipment.

A timing message is sent across the WR network, so it must be contained in the Ethernet frame. An Ethernet frame including one timing message has a length of 110 byte, which is called “timing frame” in this dissertation. A Virtual LAN (VLAN)¹ is a group of FECs in the WR network that is logically segmented by function or application, without regard to the physical locations of the FECs. All FECs in the WR network are assigned to the DM VLAN, within which the DM forwards broadcast timing telegrams downwards to all FECs.

3.1.3 Settings Management

The Settings Management (SM) is based on a physics model for accelerator optics, parameter space and overall relations between parameters and between accelerators. It supports off-line generation of accelerator settings, sending these settings to all

¹https://en.wikipedia.org/wiki/Virtual_LAN

3.2. Low-Level RF System

involved devices, and programming the schedule for the GMT system [29]. The core component of SM is the LSA framework. A standardized LSA-API allows accessing data in a common way as basis for generic client applications for all accelerators. Using the LSA-API, applications can coherently modify settings [29]. E.g. the LSA generates timing constraints (e.g. ramp curve) as well as the equipment's data settings (e.g. the current) for all devices derived from physics parameters (e.g. beam energy). For FAIR, LSA is extended to model the overall schedule of all accelerators. Beams are described as “Beam Production Chains“ to allow a description from beam source to beam target for settings organization and data correlation.

3.1.4 FESA

The FESA² is a framework used to fully integrate the large amount of front-end equipment into the accelerator control system. FESA was developed by CERN and has already been implemented into the CERN control system. Now it is developed further in collaboration with GSI for the FAIR project. For the FAIR project the necessary interaction with the FECs is realized by FESA. For a specific type of equipment, a FESA implementation accesses to the control interface of the equipment. The FESA class models the equipment as device, so the FESA output is called device class. The FEC use FESA to implement generic and equipment specific functions in form of the device classes. FESA provides JAVA based graphical user interfaces (GUI) to design, deploy, instantiate and test the device classes. Interaction with the equipment is synchronized with the GMT system [28].

3.2 Low-Level RF System

The FAIR low-level rf (LLRF) system will be used in the existing synchrotrons SIS18 and ESR, as well as in the FAIR synchrotrons SIS100 and SIS300 and in CR, NESR, and RESR. It supports fast ramp rates and large frequency span for the acceleration of a variety of ion species. It supports different rf manipulations, including operation at different harmonic numbers, barrier bucket generation, bunch compression and longitudinal feedback. [35].

Each rf supply room has a phase measurement signal distribution system shown in Fig. 3.1. The phase measurement signals in different supply rooms are synchronized by BuTiS. BuTiS 200MHz C2 and 100kHz T0 clock signals are generated by BuTiS receivers in different supply rooms in phase. In Fig. 3.1, a number of Group Direct Digital Synthesizer (DDS) units are located in each supply room, which are synchronized by BuTiS local reference. The Group DDS signals can be routed to the different cavity systems by a Switch Matrix. All cavities in a synchrotron could be providing with the same Group DDS signal. The cavities at different harmonic numbers could be realized by using Group DDS signals with different harmonic numbers and by adjusting the harmonic number at the Cavity DDS accordingly. The Group DDS concept allows to synchronize a variety of cavities in a very flexible way [35].

All the cavities of the SIS18 are driven from one supply room. The SIS100 cavities will be gathered in five acceleration sections, each of them is driven by a dedicated supply room.

²<https://www-acc.gsi.de/wiki/FESA/WhatIsFESA>

3.2. Low-Level RF System

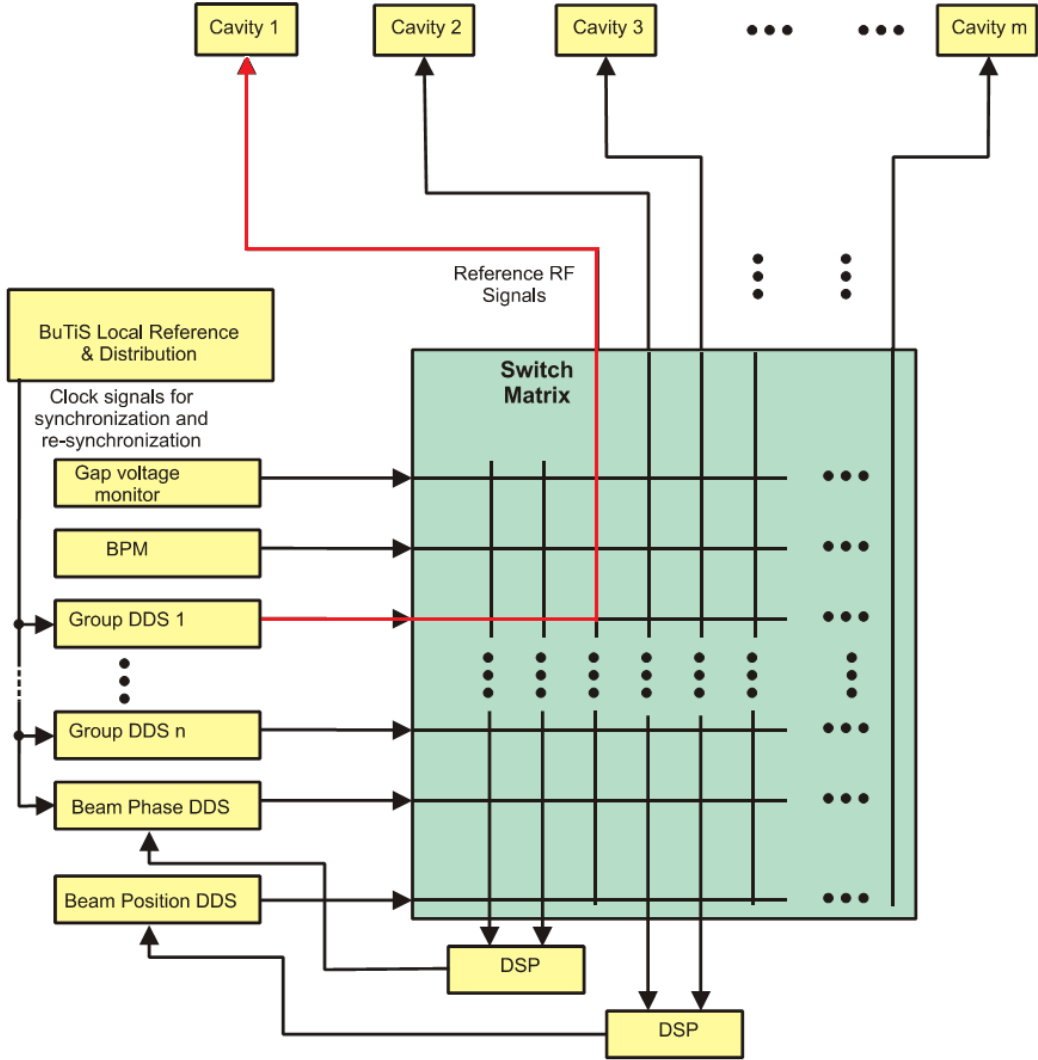


Figure 3.1: phase measurement signal distribution system
[35]

3.2.1 Local Cavity Synchronization

All rf cavities are driven by one of phase measurement signals, which are generated in each supply room . Fig. 3.2 shows the local cavity synchronization system, which synchronizes the local Cavity DDS unit to the phase measurement signal with a specified phase offset. The cavity gets the rf signal from a local Cavity DDS unit, which receives rf frequency ramps from the Central Control System (CCS). A Digital Signal Processor (DSP)-System measures the phase difference between the phase measurement signal and the gap voltage of the cavity. In the DSP system, a closed-loop control algorithm is implemented, which generates frequency corrections for the local Cavity DDS unit. This process is called local synchronization loop, which ensures that the phase of the gap voltage follows the phase of the Reference RF signal [35]. The path from the Group DDS 1 to Cavity 1 marked with the red line in Fig. 3.1 is realized by the local cavity synchronization in Fig. 3.2. The virtual rf cavity is a virtual position around the ring, to which the phase measurement signal corresponds.

3.3. Machine Protection System

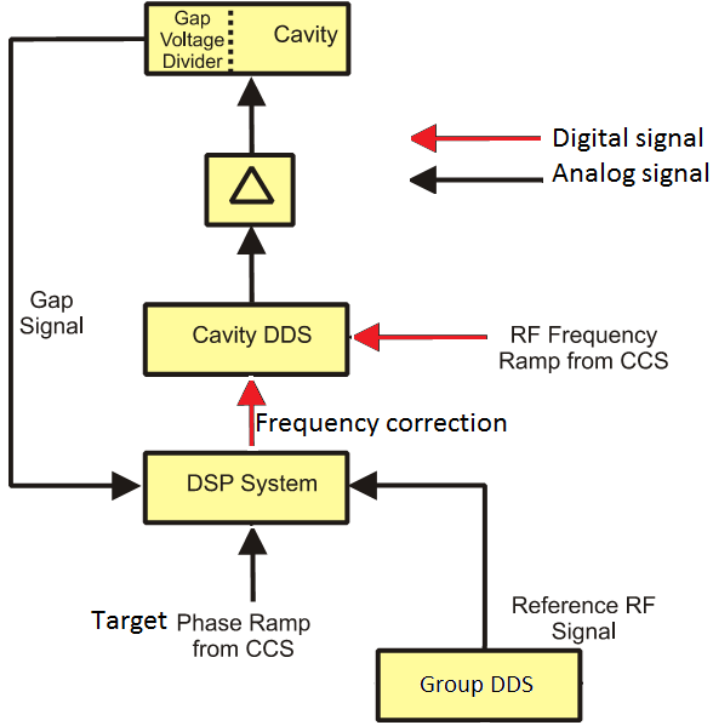


Figure 3.2: Local Cavity Synchronization
[35]

3.2.2 Longitudinal Feedback System

In order to damp coherent longitudinal dipole oscillations, the beam phase control loop is used. The phase difference between the beam signal and the phase measurement signal is fed back via an FIR filter. The beam signal is obtained by a fast current transformer or a beam position monitor. The filter output is converted in a phase-correction and forwarded to the Group DDS. The corrections are added to the phase of the frequency ramp in the Cavity DDS, which results in a change of the phase of the gap voltage and thus a feedback to the beam [36]. Unfortunately, the actual beam phase control loop in SIS18 is not able to damp incoherent longitudinal dipole oscillations. For SIS100, a bunch-by-bunch longitudinal feedback system will be developed. The bunch-by-bunch longitudinal feedback system generates a correction voltage in dedicated feedback cavities for a specified bunch [22].

3.3 Machine Protection System

A MPS protects current accelerator and subsequent accelerators or experiments from damage or unacceptable failure, e.g. the beam position is out of tolerance, the rf cavity failure and so on. Thereby, the individual equipment is assumed self-protecting, which could trigger accelerator safety critical actions, such as an emergency beam dump ³, a shutdown of magnets or a beam injection inhibit. In case of relevant

³A beam dump is a device designed to absorb the beam.

3.3. Machine Protection System

equipment failures or other inappropriate equipment states, a MPS signal is generated from this equipment [37]. The FAIR B2B transfer must coordinate with the SIS100 emergency dump signal and the beam injection inhibit signal from the MPS.

The SIS100 emergency dump signal indicates that the beam should be transferred to the emergency dump as soon as possible. If the beam injection inhibit signal is off, the B2B transfer extraction and injection kickers are allowed to be fired. If the beam injection inhibit signal is on, the injection and extraction kickers will be blocked for firing.

Chapter 4

Concept of FAIR B2B Transfer System

In this Chapter, the basic idea of the FAIR B2B transfer system is presented in Sec. 4.1. The standard procedure of the system is defined and described in Sec. 4.2. Sec. 4.3 illustrates how the basic functionality of the system are realized. In Sec. 4.4, the data flow of the system is described. In Sec. 4.5 the FAIR B2B transfer system is compared with the current B2B transfer.

4.1 Basic Idea

The basic idea of the B2B transfer is simple. First of all, two rf systems of the source and target synchrotrons must be correct phase aligned. Secondly, the trigger for the extraction and injection kickers must be synchronized with beam. In the end, the actual beam injection point must be indicated, which qualifies the beam instrumentation (BI) to measure the properties and the behavior of the beam directly after the injection.

4.1.1 Phase Alignment

The phase alignment is one of the most important prerequisites for the B2B transfer. It guarantees that extracted bunches will hit the dedicated empty buckets at the correct time. The phase alignment is based on the synchronization frequencies, see Sec. 2.2. When two rf systems have an identical cavity rf frequency or slightly different cavity rf frequencies, two cavity rf frequencies are chosen as the synchronization frequencies. When two rf systems have hugely different cavity rf frequencies, two synchronization frequencies are an integral multiple of the same or slightly different derived rf frequencies, which are a division of the revolution frequencies. More details about the calculation of the synchronization frequencies, see Sec. 2.2. If two synchronization frequencies of two rf systems are same, the phase difference between two rf systems is constant. The phase difference can be adjusted by the phase shift method or the frequency beating method with the frequency detuning on one (or both) rf system. If two synchronization frequencies of two rf systems are slight different, the phase difference is adjusted automatically because of the beating frequency.

4.1. Basic Idea

Before the basic steps for the achievement of the phase alignment, some basic concepts and their symbols are introduced, see Fig. 4.1.

- The bucket delay t_{bucket} , which specifies a certain bucket to be injected by delaying a certain number of the rf period to a marker.
- The Time-Of-Flight (TOF) between two synchrotrons t_{TOF} .
- The Time-Of-Flight between the virtual rf cavity and the extraction/injection kicker, t_{v_ext} and t_{v_inj} .
- The sum of the kicker preparation time, the rise time and the propagation delay of the kicker trigger signal in the cable of an extraction kicker and that of an injection kicker, t_{ext} and t_{inj} .

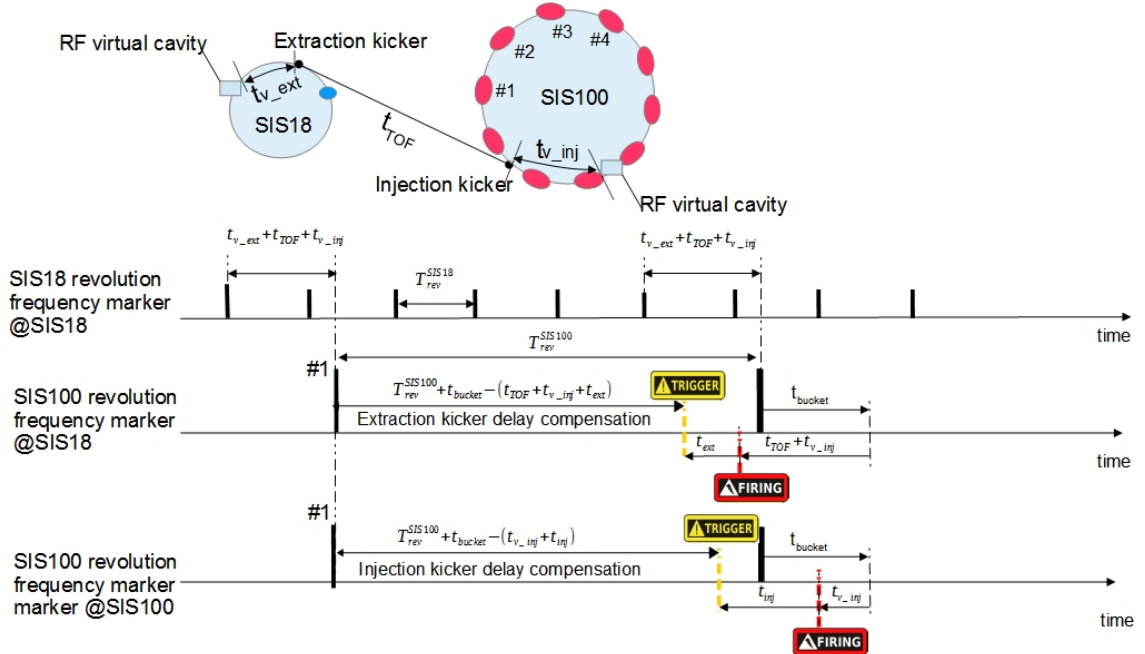


Figure 4.1: The illustration of the B2B transfer from the SIS18 to the SIS100.

The blue dot represents a bunch, red ones buckets.

Fig. 4.1 illustrates the B2B transfer from the SIS18 to the SIS100. The SIS18 U^{28+} super cycle consists of four SIS18 cycles. Each cycle produces two U^{28+} bunches. From the SIS18, four batches, each of two bunches, are injected into eight out of ten buckets of the SIS100. The SIS18 H^+ super cycle consists of four SIS18 cycles. Each cycle produces one H^+ bunch. From the SIS18, four batches, each of one bunch, are injected into four out of ten buckets of the SIS100 [38, 39]. The SIS18 and SIS100 revolution frequency markers (black bars on the first time axis and bars on the second/third time axis in Fig. 4.1) indicate the time when a bunch or the first bucket (#1) pass by the virtual rf cavity. The extraction and injection kicker trigger have a delay with respect to the first bars of the SIS100 revolution frequency marker at the SIS18 and at the SIS100. This delay is called the “extraction/injection kicker delay compensation”. The mentioned four instances of time are related to the second

4.1. Basic Idea

bars of the SIS100 revolution frequency marker. T_{rev}^X represents the revolution period of the synchrotron X, e.g. the SIS18 revolution period is T_{rev}^{SIS18} . T_{rf}^X represents the period of the cavity rf frequency of the synchrotron X, e.g. the SIS18 rf period of the cavity rf frequency is T_{rf}^{SIS18} . After the rf phase alignment, the time difference between the SIS18 and SIS100 synchronization frequency (denoted as t_{diff_sync}) for the U^{28+} and H^+ odd bucket injection is

$$t_{diff_sync} = (t_{v_ext} + t_{TOF} + t_{v_inj}) \bmod 1/f_{syn}^{trg} \quad (4.1)$$

For the H^+ even bucket injection t_{diff_sync} is

$$t_{diff_sync} = (t_{v_ext} + t_{TOF} + t_{v_inj} - T_{rf}^{SIS100}) \bmod 1/f_{syn}^{trg} \quad (4.2)$$

The phase alignment for the odd or even bucket injection is informed by the “extra phase shift“ from the SM. More details about the use cases of the B2B transfer from the SIS18 to the SIS100, please see Sec. 6.1.1 and Sec. 6.1.2. More details about the parameters of the B2B transfer system from the SM, please see Appendix D.

For the phase alignment, the steps below must be carried out.

1. The measurement of the phase of the rf system and the corresponding timestamp in each synchrotron.
2. The exchange of the measured phase and the timestamp.
3. The phase comparison between two rf systems.
4. The adjustment of the phase on one (or both) rf system, when the phase shift method is used.
5. The calculation of the time duration for the required phase alignment of two rf systems.

4.1.2 Trigger of Extraction and Injection Kickers

For the proper B2B transfer, not only the relative position of bunches and buckets, but also the firing of the extraction and injection kickers must be precisely controlled. The extraction kicker must kick the bunch exactly the time-of-flight earlier before a specific bucket passes the injection kicker and the transition of the magnetic field must be carried out during the bunch gap. For the calculation of the trigger time for the extraction and injection kickers, the following steps must be processed.

1. The kicker firing requires the bunch-to-bucket injection center phase mismatch within a upper bound, which defines a “coarse synchronization“.
2. The bucket label requires the kicker firing based on a bucket indication signal for the first bucket (e.g. the SIS100 revolution frequency markers in Fig. 4.1) plus a fixed delay (the extraction/injection kicker delay compensation), for more details please see Sec. 4.3.5. With the help of the bucket label, bunches are injected into correct buckets. This process is called the “fine synchronization“.

4.1. Basic Idea

4.1.2.1 Bucket Indication Signal

The bucket indication signal of the phase shift method or the frequency beating method indicates the passing time of the first bucket of the target synchrotron, when the first bucket is correct or periodical phase aligned with a bunch of the source synchrotron for the bunch-to-bucket injection. For FAIR use cases, we have $f_{syn}^X = Y \cdot f_{rev}^X / m$ and either m/Y or Y/m must be an integer, see Sec. 2.2. There exist either that the revolution period is the integer times of the period of the synchronization frequency or that the period of the synchronization frequency is the integer times of the revolution period. The first bucket of the target synchrotron is indicated by f_{rev}^{trg} . The correct or periodical phase alignment of the rf system of the target synchrotron with the rf system of the source synchrotron is indicated by f_{syn}^{trg} . Hence, the bucket indication signal (denoted as “ f_{bucket} “) is either with the revolution frequency or the synchronization frequency of the target synchrotron. It depends on the relation between the revolution frequency and the synchronization frequency of the target synchrotron. When the synchronization frequency of the target synchrotron is greater than or equal to the revolution frequency of the target synchrotron, namely the period of the synchronization frequency is equal to or less than the revolution period, the period of the synchronization frequency is not long enough to include all buckets. In this case, the frequency of the bucket indication signal equals to the revolution frequency of the target synchrotron and the length of the synchronization window equals to one revolution period. On the contrary, the frequency of the bucket indication signal equals to the synchronization frequency of the target synchrotron and the length of the synchronization window equals to the period of the synchronization frequency. The frequency of the bucket indication signal is expressed as

$$f_{bucket} = \begin{cases} f_{rev}^{trg} & f_{syn}^{trg} \geq f_{rev}^{trg} \\ f_{syn}^{trg} & f_{syn}^{trg} < f_{rev}^{trg} \end{cases} \quad (4.3)$$

The corresponding length of the synchronization window is expressed as

$$T_w = \frac{1}{f_{bucket}} \begin{cases} T_{rev}^{trg} & f_{syn}^{trg} \geq f_{rev}^{trg} \\ T_{syn}^{trg} & f_{syn}^{trg} < f_{rev}^{trg} \end{cases} \quad (4.4)$$

Fig. 4.2 shows one example when the frequency of the bucket indication signal equals to the revolution frequency of the target synchrotron. Fig. 4.3 shows one example when the frequency of the bucket indication signal equals to the synchronization frequency of the target synchrotron.

4.1.2.2 Extraction and Injection Kicker Delay Compensation

The calculation of the extraction and injection kicker delay compensation is explained in this section.

- Extraction kick

In order to inject into specific buckets, the extraction kicker delay compensation for the first bar of the SIS100 revolution frequency marker is $T_{rev}^{SIS100} + t_{bucket}$, see Fig. 4.1. For example, when two U^{28+} bunches of the SIS18 are

4.1. Basic Idea

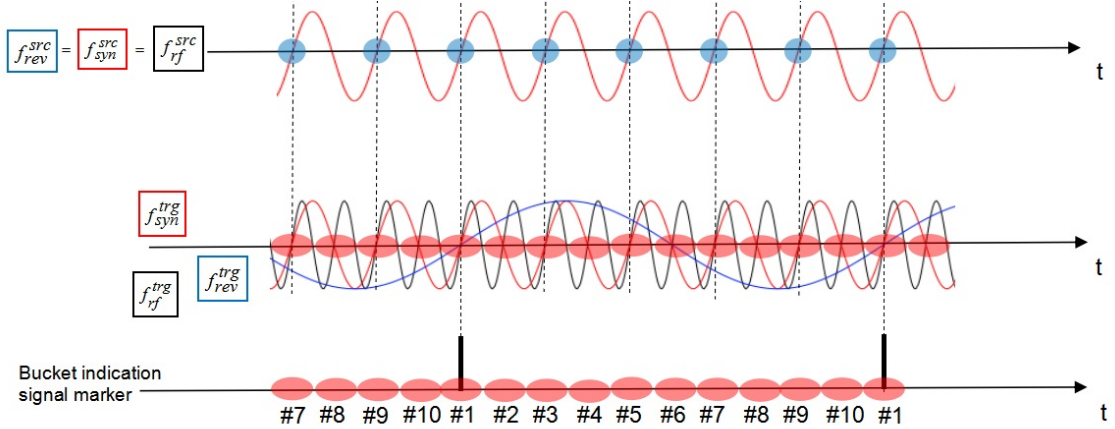


Figure 4.2: The frequency of the bucket indication signal equals to the revolution frequency of the target synchrotron.

Red dots represent buckets of the target synchrotron and blue ones represent bunches of the source synchrotron. This example is the FAIR use case of the H^+ B2B transfer from the SIS18 to the SIS100. The correct phase alignment of two rf systems is assumed with $\Delta\phi_{syn} = 0^\circ$ and only the buckets with the odd number (e.g. #1, #3) are to be filled in this example.

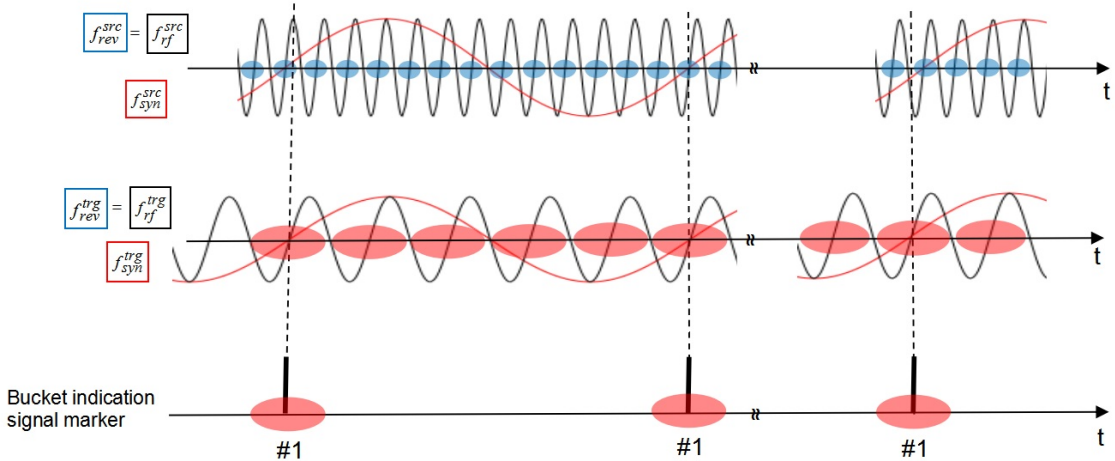


Figure 4.3: The frequency of the bucket indication signal equals to the synchronization frequency of the target synchrotron.

Red dots represent buckets of the target synchrotron and blue ones represent bunches of the source synchrotron. This example is the FAIR use case of the B2B transfer from the CR to the HESR.

to be injected into buckets #3 and #4 of the SIS100, $t_{bucket} = 1 \cdot T_{rev}^{SIS18}$. The extraction kicker must be fired $t_{v,inj} + t_{TOF} + t_{ext}$ earlier as the bucket passes the virtual rf cavity, so the extraction kicker delay compensation is $T_{rev}^{SIS100} + t_{bucket} - (t_{TOF} + t_{v,inj} + t_{ext})$.

- Injection kick

With the consideration of the bucket pattern, the injection kicker delay com-

4.3. Realization

pensation for the first bar of the SIS100 revolution frequency marker is $T_{rev}^{SIS100} + t_{bucket}$, see Fig. 4.1. The injection kicker must be fired $t_{v_inj} + t_{inj}$ time earlier as the bucket passes the virtual rf cavity, so the injection kicker delay compensation is $T_{rev}^{SIS100} + t_{bucket} - (t_{v_inj} + t_{inj})$.

4.2 Basic Procedure

Fig. 4.4 illustrates the basic procedure of the B2B transfer with two different synchronization scenarios. The yellow region shows the synchronization window. The purple region shows the valid time for the emergency kicker.

The B2B transfer process basically needs to follow the six steps [40]:

1. The DM announces the B2B transfer and requests the switch off of the beam feedback loops on the rf system, when required.
2. Two synchrotrons measure the rf phase locally.
3. The source synchrotron receives the measured rf phase from the target synchrotron.
4. The source synchrotron does the B2B related calculation.
 - The source synchrotron calculates the synchronization window and sends it to the target synchrotron and to the DM.

The source synchrotron generally accomplishes the phase alignment in case of the phase shift method. A particular case is the empty target synchrotron. The phase alignment can be achieved very fast and simple by the phase jump at the target synchrotron. Although the synchronization window is theoretically infinite for the phase shift method, bunches should be transferred as soon as the phase shift is done, in order to guarantee the stability of the beam. For both synchronization methods, the synchronization window has a certain length.
 - Besides, the bucket indication signal is reproduced at the source synchrotron for the indication of the 1st bucket.
5. The trigger signals with the delay compensation are generated for the kickers.
6. The kicker electronic fire the kickers. The extraction and injection kicker trigger and firing timestamp are sent to the source synchrotron for the B2B status check. The actual beam injection timestamp and the B2B transfer status are send from the source synchrotron to the DM and the DM sends them further to the BI.

4.3 Realization

This section describes the realization of the FAIR B2B transfer system based on the FAIR control system and LLRF system introduced in Chap. 3.

The phase alignment is based on the phase difference between two synchronization frequencies. Because it is impossible to have a direct connection between

4.3. Realization

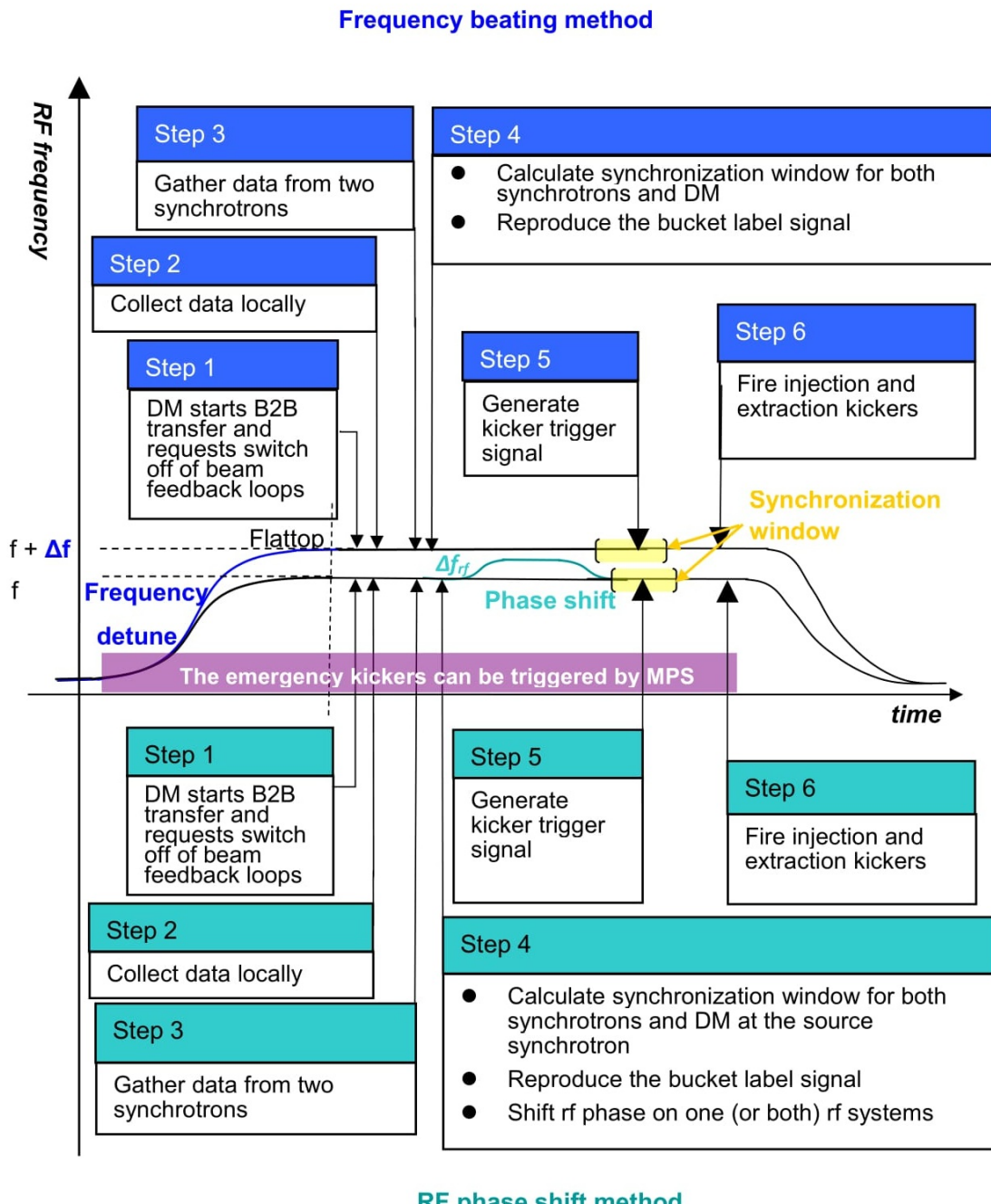


Figure 4.4: The procedure for the B2B transfer within one acceleration cycle.

As illustrated here the procedure with the frequency beating method (blue, top) and that with the phase shift method (green, bottom).

two synchrotrons around such a big FAIR campus for a direct phase measurement. Hence, a shared reference sinusoidal signal (which is called “synchronization reference signal” and denoted as f_{syn}^{REF}) derived from BuTiS is used for the indirect phase difference measurement. The synchronization reference signal has the same frequency and is in phase in different supply rooms. The phase measurement of each rf system is based on the frequency beating between the synchronization frequency and the synchronization reference signal, achieved by measuring the phase devia-

4.3. Realization

tion between these two frequencies. The phase advance is extrapolated based on the measured phase deviations. The phase difference is calculated by the subtraction of the extrapolated phase advance of the target synchrotron from the extrapolated phase advance of the source synchrotron.

For the reproduction of the bucket indication signal at the source synchrotron, the phase deviation between the bucket indication signal and the synchronization reference signal is measured and then the phase advance is extrapolated at the target synchrotron. For the target synchrotron, the extrapolated phase advance between the bucket indication signal and the synchronization reference signal and the extrapolated phase advance between the synchronization frequency and the synchronization reference signal are related to each other, so one phase deviation measurement and the corresponding phase advance extrapolation are sufficient for both the phase alignment and the reproduction of the bucket indication signal, reducing the data transfer of the system and the transfer delay on the WR network. Besides, every phase deviation measurement and the phase advance extrapolation process needs 500 us, so one phase deviation measurement and the corresponding phase advance extrapolation is preferred due to the time constraints (see Chap. 5).

Because the phase of the high harmonic frequency can be deduced from the phase of the low harmonic frequency, the frequency for the phase deviation measurement of the target synchrotron equals to the smaller one of the synchronization frequency and the frequency of the bucket indication signal. The frequency for the phase deviation measurement is called “phase measurement signal” and denoted as f_{B2B}^X . From the equation of the frequency of the bucket indication signal, see eq. 4.3, we know that f_{bucket} represents always the smaller one. Hence, the frequency of the phase measurement signal of the target synchrotron is

$$f_{B2B}^{trg} = \begin{cases} f_{syn}^{trg} & f_{bucket} = f_{syn}^{trg} \\ f_{rev}^{trg} & f_{bucket} = f_{rev}^{trg} \end{cases} \quad (4.5)$$

The measurement of the phase deviation is based on the frequency beating between the synchronization frequency and the synchronization reference signal, so the frequencies of these two signals must be slightly different for the phase measurement and prediction. Hence, there must be a proper frequency of the phase measurement signal of the source synchrotron corresponding to f_{B2B}^{trg} .

$$f_{B2B}^{src} = \begin{cases} f_{syn}^{src} & f_{bucket} = f_{syn}^{trg} \\ \frac{f_{rev}^{trg}}{f_{syn}^{trg}} f_{syn}^{src} & f_{bucket} = f_{rev}^{trg} \end{cases} \quad (4.6)$$

The synchronization reference signal has a fixed frequency and is always in phase in different supply rooms. It is a sinusoidal wave, whose frequency is a multiple of BuTiS T0 100 kHz and whose positive zero-crossings are always aligned with the first positive zero-crossings of C2 clocks after T0 edges (which is called the “T0 incidents”) [41, 42]. Thus, the synchronization reference signal is synchronous in different supply rooms by definition. The frequency of the synchronization reference signal f_{syn}^{REF} is determined by f_{B2B}^X and calculated as

$$f_{syn}^{REF} = \text{round}(f_{B2B}^X / 100 \text{ kHz}) \cdot 100 \text{ kHz} \quad (4.7)$$

The function *round* rounds $f_{B2B}^X / 100 \text{ kHz}$ up or down to an integer value, which is closest to $f_{B2B}^X / 100 \text{ kHz}$. e.g. $f_{B2B}^{SIS100} = f_{rev}^{SIS100} = 157.254 \text{ kHz}$, $f_{B2B}^{SIS100} / 100 \text{ kHz} =$

4.3. Realization

1.57, so $\text{round}(f_{B2B}^{\text{SIS100}}/100 \text{ kHz}) = 2$ and $f_{\text{syn}}^{\text{REF}} = 200 \text{ kHz}$. This is the FAIR use case of the U^{28+} B2B transfer from the SIS18 to the SIS100, more details, please see Chap. 6. When $|f_{B2B}^X/100 \text{ kHz}| < 1$, $f_{\text{syn}}^{\text{REF}} = 100 \text{ kHz}$. For the detailed realization of the synchronization reference signal, please see “Development of the LLRF system for a deterministic Bunch-to-Bucket transfer for FAIR“ [43].

4.3.1 Phase Measurement and corresponding Timestamp of each Rf System

The rf frequencies in the source and target synchrotron need to be stable and constant during the B2B transfer process. The phase measurement of each rf system follows the principles as shown below.

1. The measurement of the actual phase values.
2. The extrapolated phase values in the future based on the measured phase values.
3. The timestamp for the extrapolated phase values.

4.3.1.1 Measurement of Actual Phase Values of each Rf System

The phase measurement of each rf system is achieved by measuring the phase deviation between the phase measurement signal and the synchronization reference signal of a synchrotron. The phase deviation (denoted by $\Delta\varphi^X$) has a linear relationship with time, whose range is from -180° to $+180^\circ$.

$$\Delta\varphi^X(t) = [(k^X t + \Delta\varphi_0^X) \bmod 2\pi] - \pi \quad (4.8)$$

where k^X is the slope of the phase deviation and $\Delta\varphi_0^X$ the initial value of the phase deviation.

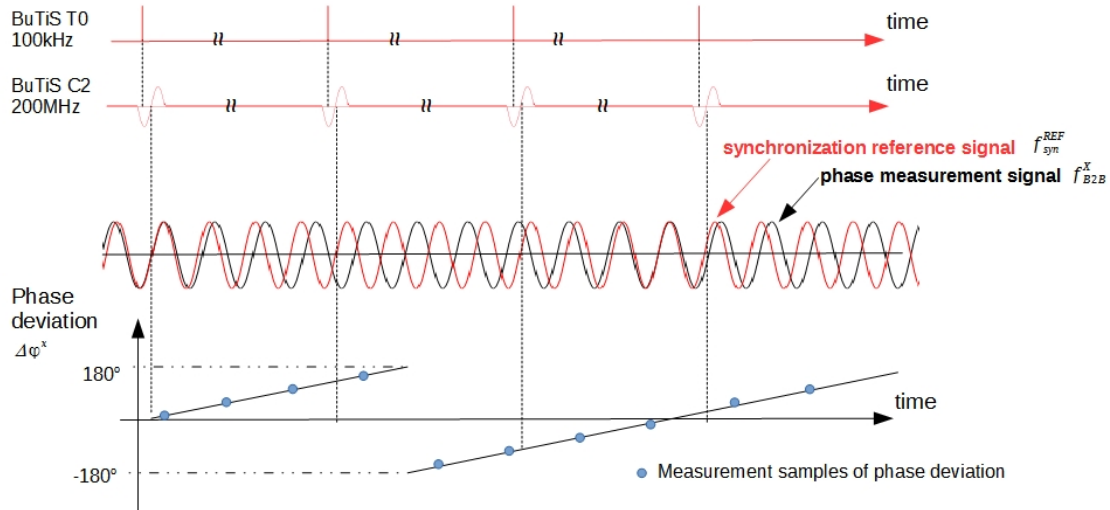


Figure 4.5: The realization of the phase deviation measurement at one synchrotron

4.3. Realization

Fig. 4.5 shows the phase measurement of the rf system at a dedicated synchrotron. The red sinusoidal wave represents the synchronization reference signal (e.g. 200 kHz) in a supply room and the black wave the phase measurement signal (e.g. 157.254 kHz) from the Group DDS. The phase deviation between the phase measurement signal and the synchronization reference signal is measured by the Phase Advance Measurement (PAM) module at the source synchrotrons and at the target synchrotron. The phase deviation measurement is performed synchronously to an internal clock and asynchronously to the BuTiS reference clock, which is represented by the blue dots. The measured phase deviation can be expressed as

$$\Delta\varphi^X(nT_{sample_PAM}) = [(k^X \cdot nT_{sample_PAM} + \Delta\varphi_0^X) \bmod 2\pi] - \pi \quad (4.9)$$

where T_{sample_PAM} is the measurement sampling period of the phase deviation by the PAM module.

For more details about the implementation and realization of the PAM module, please see “Development of the LLRF system for a deterministic Bunch-to-Bucket transfer for FAIR“ [43].

4.3.1.2 Phase Extrapolation of each Rf System

The phase deviation can be extrapolated due to the linear relationship between time and the phase deviation.

Based on a series of the measured samples of the phase deviation, the phase deviation at the T0 incidents (denoted by ψ^X and called the “extrapolated phase advance“) are extrapolated at the source and target synchrotrons by the Phase Advance Prediction (PAP) Module.

$$\psi^X(n) = \Delta\varphi^X(nT_{sample_PAP}) \quad (4.10)$$

where T_{sample_PAP} is the extrapolation sampling period of the phase extrapolation by the PAP module, $T_{sample_PAP} = 1/100$ kHz.

The extrapolated phase advance, ψ^{src} and ψ^{trg} at the source and target synchrotron, is represented by red diamonds in Fig. 4.6. Because the phase advance is extrapolated at the T0 incidents and the synchronization reference signal is zero phase aligned with the T0 incidents, ψ^{src} and ψ^{trg} are the phase of the phase measurement signals at the virtual rf cavities of two synchrotrons at the T0 incidents (represented as black dots in Fig. 4.6). For more details about the implementation and realization of the PAP module, please see “Development of the LLRF system for a deterministic Bunch-to-Bucket transfer for FAIR“ [43].

4.3.1.3 Timestamp of Extrapolated Phase

The extrapolated phase advance is synchronized with T0 incidents by the PAP module, but it does not synchronize with the absolute time. This is one of the task of the multipurpose B2B source and target SCUs [32, 44], which are located in the source and target synchrotrons. The PAP module is a SCU slave¹, respectively located in the B2B source SCU and B2B target SCU, see Fig. 4.7. Both the B2B source and target SCUs could get the timestamp of the T0 incidents.

¹[https://en.wikipedia.org/wiki/Master/slave_\(technology\)](https://en.wikipedia.org/wiki/Master/slave_(technology))

4.3. Realization

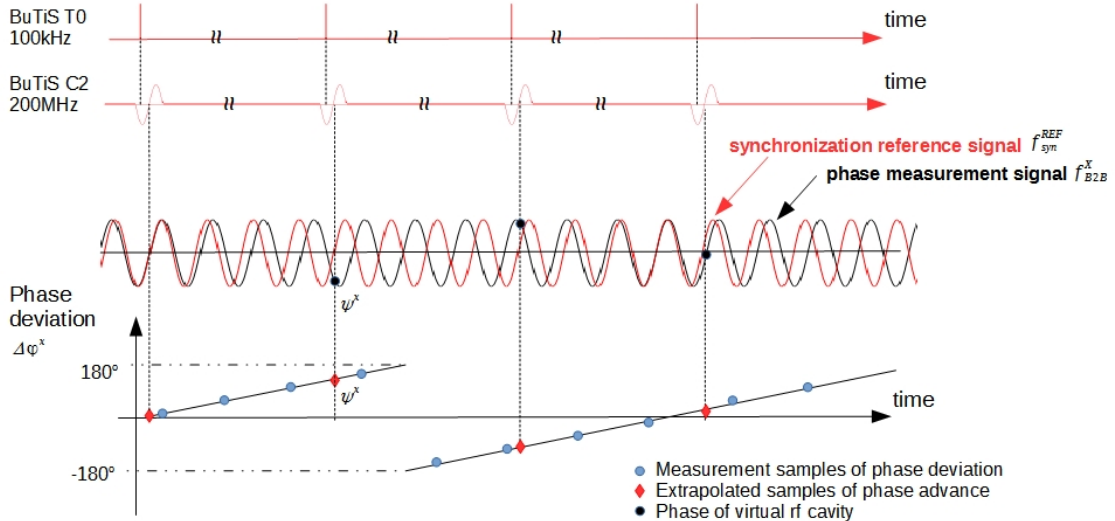


Figure 4.6: The realization of the phase advance extrapolation at one synchrotron

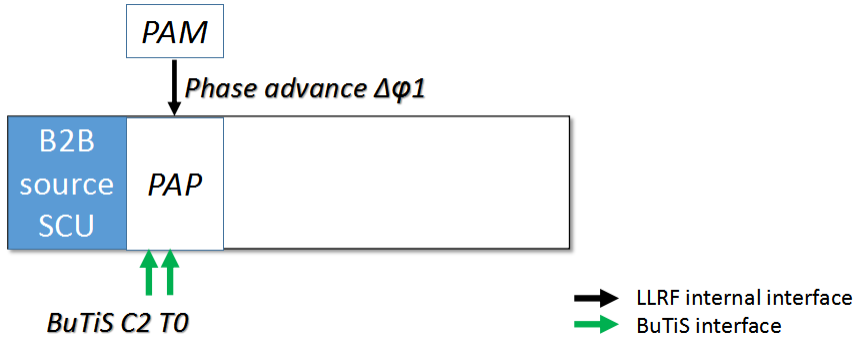


Figure 4.7: Implementation of the Phase Advance Prediction Module in the B2B source SCU

Fig. 4.8 illustrates the synchronization of the extrapolated phase to the timestamp. The DM broadcasts the timing frame of `CMD_B2B_START` to the WR network. This timing frame will be received by the B2B source SCU and the B2B target SCU. The B2B source and target SCUs start the B2B process at the designated time, the middle of a specified T0 incident (represented as the pink dot in Fig. 4.8). They need maximum 1 μ s to inform the PAP modules to start the phase advance extrapolation respectively. The PAP modules needs approximate 500 μ s for the phase extrapolation and updates the extrapolated phase value every T0 incident. After 500 μ s, the B2B source and target SCUs need another maximum 1 μ s to receive the extrapolated phase ψ_0^X (represented as the red diamond in Fig. 4.8) from the PAP modules, as well as the slope of the phase deviation k^X . It also timestamp the T0 incidents t_ψ^X which corresponds to the extrapolated phase. The B2B source SCU obtains ψ_0^{src} , t_ψ^{src} and k^{src} at the source synchrotron and the B2B target SCU obtains ψ_0^{trg} , t_ψ^{trg} and k^{trg} at the target synchrotron. In fact, $t_\psi^{src} = t_\psi^{trg}$.

Because the phase deviation of the phase measurement signal complies with the linear relation with time, the evolution of the phase deviation between the phase measurement signal and the synchronization reference signal can be calculated for any T0 incidents, see eq. 4.11, which will be used for the phase correction of the

4.3. Realization

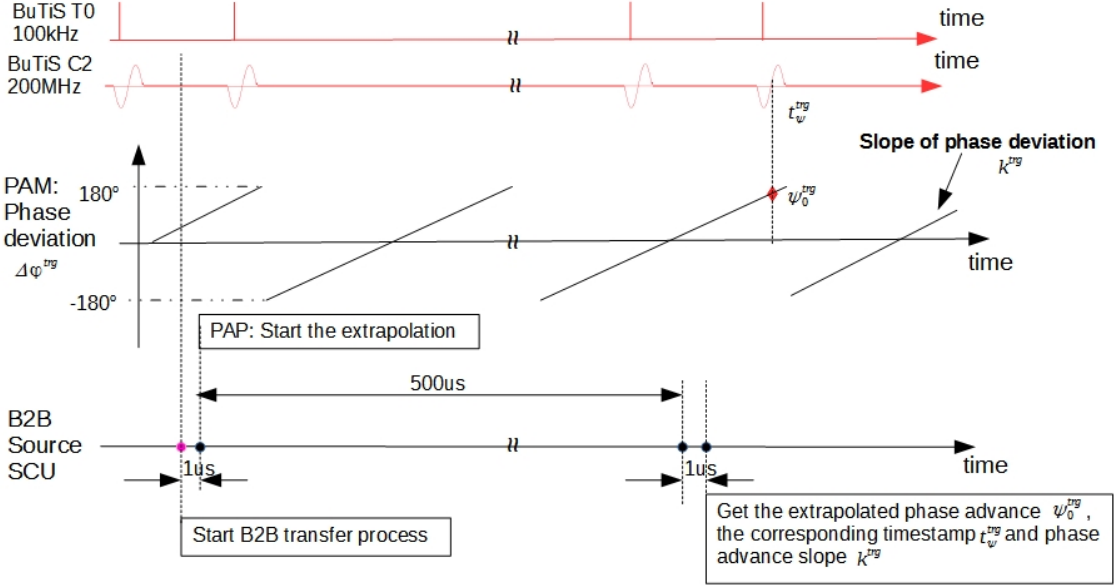


Figure 4.8: The synchronization of the extrapolated phase to the timestamp in one synchrotron

bucket indication signal in sec. 4.3.5.

$$\Delta\varphi^X(t_\psi^X + nT_{sample_PAP}) = [(\psi_0^X + k^X \cdot nT_{sample_PAP}) \bmod 2\pi] - \pi \quad (4.11)$$

4.3.2 Exchange of Measured Data

For the B2B transfer, there is a “B2B transfer master“, which is responsible for the data collection of two synchrotrons, the data calculation, the data redistribution and the B2B transfer status check. The data of the source and target synchrotron must be transferred to the “B2B transfer master“ via the deterministic WR network in the format of the timing frame.

For the simplicity, the B2B source SCU works as the “B2B transfer master“, so the extrapolated phase ψ_0^{trg} , the corresponding timestamp t_ψ^{trg} and the phase deviation slope k^{trg} are transferred by the B2B target SCU to the B2B source SCU via the WR network. The transfer of the data is achieved by the timing frame TGM_PHASE_TIME. The B2B transfer involves a certain amount of timing frames. More details about the B2B timing frames, please see Appendix A. The timing frames are not sent via the DM in order to reduce the traffic of the WR network and reduce the timing frame transfer delay on the WR network [45], so a specified VLAN, B2B VLAN, is defined for the B2B timing frames. All SCUs for the B2B transfer are assigned to the B2B VLAN. Fig. 4.9 illustrates an example of the transfer path of the B2B timing frames in the WR network. The frames are transferred along the path with orange color instead of the path with blue color. The test for the transfer delay of the B2B timing frames on the WR network is explained in Chap. 5.

4.3.3 Rf Synchronization

The FAIR B2B transfer system is available for both the phase shift and frequency beating methods, see Sec. 2.3. The rf synchronization of two synchrotrons is based

4.3. Realization

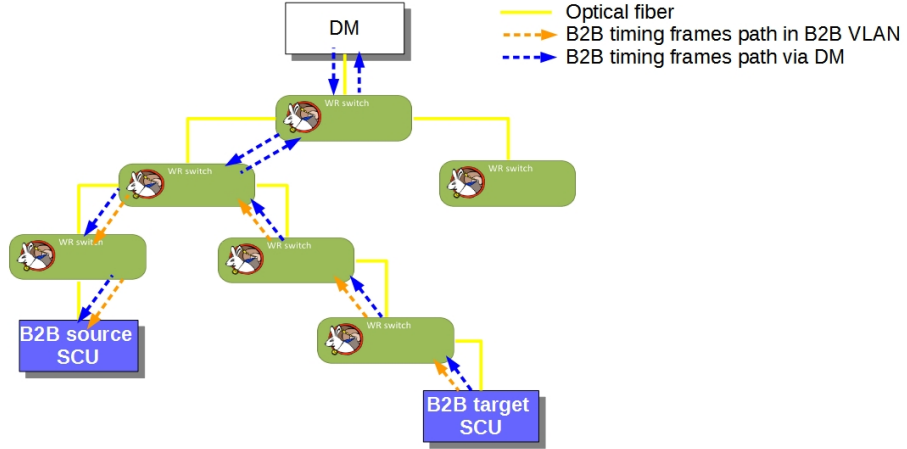


Figure 4.9: One example of the transfer path of the B2B timing frames in the WR network

on the phase difference between two synchronization frequencies of two rf systems $\Delta\phi_{syn}$. $\Delta\phi_{syn}$ is directly or indirectly calculated from the measurement of the phase difference between the phase measurement signals of two rf systems.

$$\Delta\phi_{syn} = \begin{cases} \psi_0^{trg} - \psi_0^{src} & f_{bucket} = f_{syn} \\ \frac{f_{syn}}{f_{rev}}(\psi_0^{trg} - \psi_0^{src}) \mod 2\pi & f_{bucket} = f_{rev} \end{cases} \quad (4.12)$$

$\Delta\phi_{syn}$ is within the range between -2π and 2π . The SM provides the target time difference between the synchronization frequencies of two rf systems t_{diff_sync} , which considers the delay compensation for TOF, all propagation and the extra phase shift. The B2B source SCU calculates the required phase shift (denoted as $\Delta\phi_{shift}$) based on t_{diff_sync} and $\Delta\phi_{syn}$.

With the phase shift method, a frequency modulation with a fixed duration is applied to the Group DDS with the synchronization frequency of one (or both) rf system. The rf frequency modulation achieves the phase shift of $\Delta\phi_{shift}$. With the frequency beating method, the phase difference varies at the rate of the synchronization frequency difference between two rf systems. Two rf systems are synchronized when the phase difference between two synchronization frequencies equals to $\Delta\phi_{shift}$.

- Rf synchronization with the phase shift method

For the rf synchronization, the maximum required phase shift of the synchronization frequency is 360° . In order to accomplish the phase alignment as fast as possible, the phase shift will be conducted backward or forward. Therefore a phase shift of up to $\pm 180^\circ$ will be implemented for the Group DDS with regard to the synchronization frequency f_{syn}^X . The required phase shift is calculated as

$$\Delta\phi_{shift} = \begin{cases} 4\pi + \Delta\phi_{shift_raw} & -4\pi < \Delta\phi_{shift_raw} \leq -3\pi \\ 2\pi + \Delta\phi_{shift_raw} & -3\pi < \Delta\phi_{shift_raw} \leq -\pi \\ \Delta\phi_{shift_raw} & -\pi < \Delta\phi_{shift_raw} \leq \pi \\ \Delta\phi_{shift_raw} - 2\pi & \pi < \Delta\phi_{shift_raw} \leq 2\pi \end{cases} \quad (4.13)$$

4.3. Realization

where $\Delta\phi_{shift_raw}$ is the raw value of the required phase shift within the range between -4π and 2π .

$$\Delta\phi_{shift_raw} = \Delta\phi_{syn} - t_{diff_sync} \cdot f_{syn}^{trg} \cdot 2\pi \quad (4.14)$$

A normalized frequency modulation profile $f_{normalized}$ for 180° can be precalculated, which guarantees the adiabaticity. The actual frequency modulation profile f_{actual} is decided by $f_{normalized}$ and $\Delta\phi_{shift}$, see eq. 4.15.

$$\frac{\Delta\phi_{shift}}{180^\circ} = \frac{f_{actual}}{f_{normalized}} \quad (4.15)$$

Fig. 4.10 shows an example of a normalized and several actual frequency modulation profiles and the corresponding phase shift profiles. The magenta profile is the normalized profile $f_{normalized}$ with the phase shift of 180° . The blue one is $1/2f_{normalized}$ with the phase shift of 90° and the green one is $1/3f_{normalized}$ with 60° .

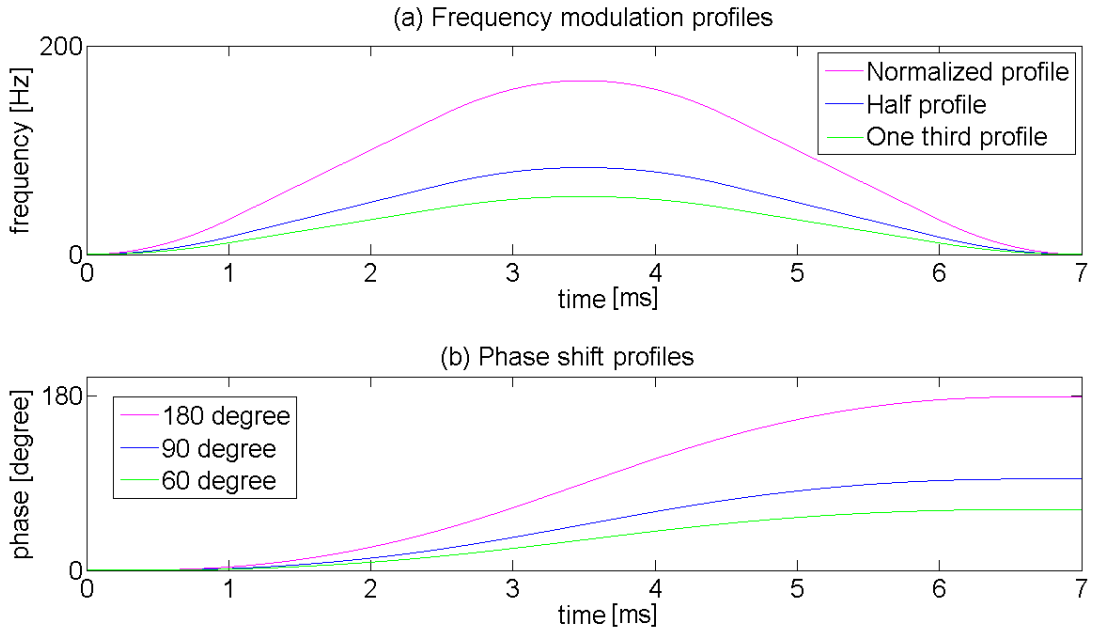


Figure 4.10: The normalized frequency and phase modulation profile and the actual profiles

Fig. 4.11 shows the implementation of the Phase Shift Module (PSM) in the B2B source SCU. The B2B source SCU sends the required phase shift to the PSM, which controls the phase shift of the phase measurement signal of Group DDS by means of either the frequency modulation (Fig. 4.10 (a)) or the phase modulation (Fig. 4.10 (b)). The required phase shift is distributed star-shaped to all the Group DDS of the synchrotron. The phase measurement signal is routed to the different cavity systems by a Switch Matrix to realize the phase shift of all cavities on the synchrotron. For more details about the implementation and realization of the PSM module, please see “Development of the LLRF system for a deterministic Bunch-to-Bucket transfer for FAIR” [43].

4.3. Realization

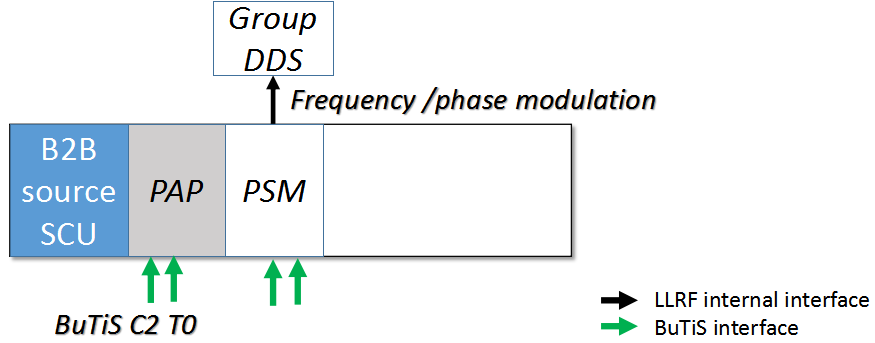


Figure 4.11: Implementation of the Phase Shift Module in the B2B source SCU

A particular case of the B2B synchronization occurs, when the target synchrotron is empty, i.e. it does not capture any bunch yet, the phase shift can be done for the target synchrotron without adiabatical consideration (e.g. the phase jump is possible). In this case, the B2B source SCU sends the timing frame TGM_PHASE_JUMP to the B2B target SCU, which contains the required phase shift. After the B2B target SCU receives the timing frame, it sends the value to the PSM for the phase jump of the Group DDS with the synchronization frequency of the target synchrotron.

- Rf synchronization with the frequency beating method

The frequency beating method can achieve only positive phase adjustment, so $\Delta\phi_{shift}$ is from 0° to 360° and calculated as

$$\Delta\phi_{shift} = \begin{cases} 4\pi + \Delta\phi_{shift_raw} & -4\pi < \Delta\phi_{shift_raw} \leq -2\pi \\ 2\pi + \Delta\phi_{shift_raw} & -2\pi < \Delta\phi_{shift_raw} \leq 0 \\ \Delta\phi_{shift_raw} & 0 < \Delta\phi_{shift_raw} \leq 2\pi \end{cases} \quad (4.16)$$

The circumference ratio between many pair of machines in FAIR is not an integer, the synchronization frequencies of two synchrotrons begin beating automatically. For the pairs with an integral circumference ratio, the synchronization frequency of the source synchrotron has to be detuned. The Group DDS produces the detuned phase measurement signal provided by the SM.

4.3.4 Coarse Synchronization

The coarse synchronization is achieved by the synchronization window with a certain length. Within this window, bunches are transferred into buckets with the center mismatch smaller than the upper bound². The length of the synchronization window T_w is one period of the bucket indication signal. For the phase shift method, the bunch-to-bucket injection center mismatch within the synchronization window is almost 0° . For the frequency beating method, the maximum bunch-to-bucket injection center mismatch $\Delta\phi_{rf}$ within the synchronization window is calculated by

²B2B transfer from the SIS18 to the SIS100: upper bound of the bunch-to-bucket center mismatch is $\pm 1^\circ$

4.3. Realization

eq. 4.17. More details, please see Sec. 2.3.2.

$$\Delta\phi_{rf} = \pm \frac{1}{2} \cdot 2\pi |f_{syn}^{src} - f_{syn}^{trg}| \cdot T_w \cdot \frac{f_{rf}^{trg}}{f_{syn}^{trg}} \quad (4.17)$$

The B2B source SCU obtains the delay compensation for the TOF, all propagation delays, the kicker preparation time and the bucket delay (denoted as t_{delay}) from the SM. It calculates the start of the synchronization window (denoted as t_w), taking the delay compensation into consideration and transfers t_w to the DM and the source and target Trigger SCUs via the WR network by the timing frame TGM_SYNCH_WIN. The Trigger SCUs are used to produce the kicker trigger signals. The DM must transfer TGM_SYNCH_WIN further to the BI for the indication of the beam. For the phase shift method, the rf frequency detuning has a fixed duration T . The start of the synchronization window for the phase shift method is calculated as

$$t_w = t_\psi^X + 600 \mu s + T - \frac{T_w}{2} - t_{delay} \quad (4.18)$$

where $600 \mu s$ consists of the upper bound transfer delay on the WR network ($500 \mu s$) and the B2B source SCU calculation time ($100 \mu s$), more details, please see Chap. 5. T is long enough to guarantee that the BI receives TGM_SYNCH_WIN and is activated before the start of the synchronization window.

The start of the synchronization window for the frequency beating method is calculated as

$$t_w = t_\psi^X + \frac{\Delta\phi_{shift}}{2\pi} \cdot \frac{1}{|f_{syn}^{src} - f_{syn}^{trg}|} + n \cdot \frac{1}{|f_{syn}^{src} - f_{syn}^{trg}|} - \frac{T_w}{2} - t_{delay} \quad (4.19)$$

where the term of $n \cdot \frac{1}{|f_{syn}^{src} - f_{syn}^{trg}|}$ is used to guarantee the activation of the BI timely.

4.3.5 Bucket Label

The bucket label is realized based on the bucket indication signal for the first bucket plus a fixed delay for the indication of the correct buckets to be filled.

The evolution of the phase deviation between the phase measurement signal and the synchronization reference signal of the target synchrotron is calculated for any T0 incidents (same as eq. 4.11).

$$\Delta\varphi^{trg}(t_\psi^{trg} + nT_{sample_PAP}) = [(\psi_0^{trg} + k^{trg} \cdot nT_{sample_PAP}) \bmod 2\pi] - \pi \quad (4.20)$$

where ψ_0^{trg} is the phase advance extrapolated by the PAP module at t_ψ^{trg} of the target synchrotron.

Therefore, the bucket indication signal can be corrected exactly in phase with the phase measurement signal of the target synchrotron by $\Delta\varphi^{trg}(t_\psi^{trg} + nT_{sample_PAP})$ at the T0 incidents. The bucket indication signal is exactly a copy of the revolution frequency or the synchronization frequency of the target synchrotron, so it is also called the "reproduced signal". The bucket indication signal can be reproduced campus-wide. A specific bucket is just a certain number of the cavity rf periods of the target synchrotron delay based on the bucket indication signal.

The FAIR B2B transfer system needs the bucket indication not only at the rf flattop, but also during the whole acceleration cycle. The bucket indication at the

4.3. Realization

rf flattop is used for the normal extraction and injection and the bucket indication during the whole acceleration cycle is used for the emergency dump. For the SIS100 emergency kick, the reproduced signal has always the same frequency and is always in phase with the SIS100 revolution signal, so it is called the "real-time reproduced signal". The delay based on the real-time reproduced signal always indicates the bunch gaps.

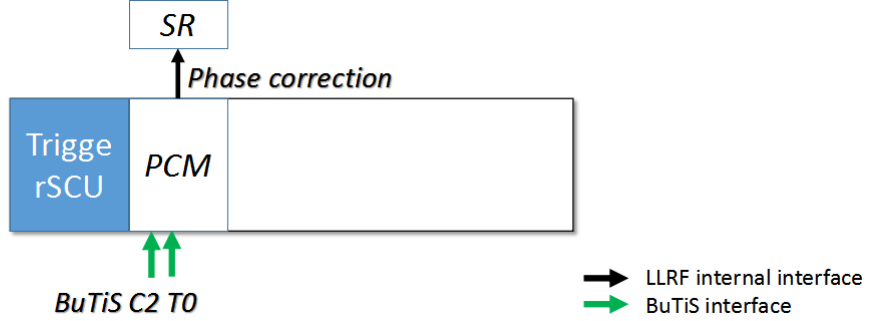


Figure 4.12: Implementation of the Phase Correction Module in the Trigger SCU

The bucket label is realized by the Trigger SCU, the Signal Reproduction (SR) module and the Phase Correction Module (PCM), see Fig. 4.12. The reproduced signal is produced by SR module. The Trigger SCU is responsible for the receipt of the phase correction value from the B2B source SCU and the transfer of this value to the PCM. The PCM module is used to correct the phase of the reproduced signal. The PCM module is a SCU slave in the Trigger SCU. The SR module produces the bucket indication signal marker in the format of the TTL signal, whose rising edges are aligned with the positive zero-crossings of the rf signal of the revolution frequency or the synchronization frequency. For more details about the implementation and realization of the PCM and the SR module, please see "Development of the LLRF system for a deterministic Bunch-to-Bucket transfer for FAIR" [43].

- Bucket label for the normal extraction and injection

For the bucket label for the normal extraction and injection, three steps are necessary. Fig. 4.13 shows these three steps for the reproduction of the bucket label. Here the B2B transfer from the SIS18 to the SIS100 is taken as an example.

- Step 1. Frequency correction

The SR module produces the "reproduced signal" with the frequency f_{bucket} . The positive zero-crossing of the reproduced signal always indicates the start of the 1st bucket.

- Step 2. Phase correction

The reproduced signal must do the phase correction at a specified T0 incident. The phase correction value is calculated by the B2B source SCU and transferred by the timing frame `TGM_PHASE_CORRECTION` to the Trigger SCU. Then the Trigger SCU gives the phase correction value to the SR module via the PCM.

- Step 3. Bucket indication

4.3. Realization

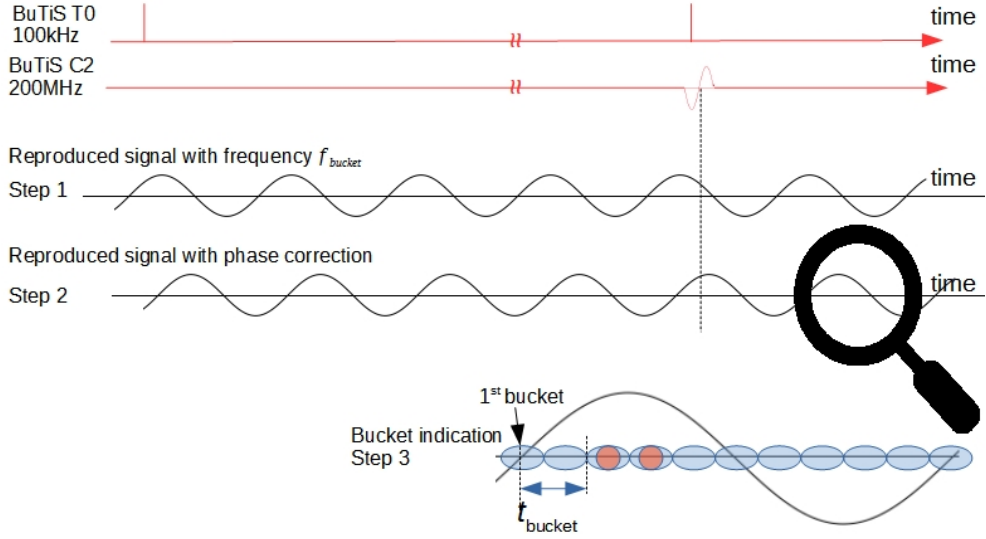


Figure 4.13: The realization of the bucket label for the normal extraction and injection.

The SM considers the bucket delay t_{bucket} within the kicker delay compensation, see Sec. 4.1.2. In Fig. 4.13, the reproduced signal is with the SIS100 revolution frequency and the 3rd and 4th buckets of ten buckets will be filled with $t_{bucket} = 1 \cdot T_{rev}^{SIS18}$.

- Bunch gap label for the emergency extraction

Only for the SIS100 emergency procedure, the bunch gap label is important during the whole acceleration cycle. There are two steps for the realization of the bunch gap label, see Fig. 4.14.

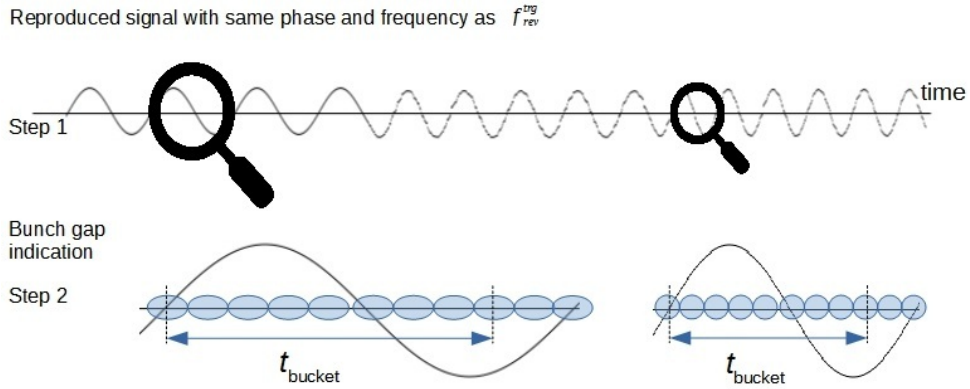


Figure 4.14: The realization of the bunch gap for the emergency extraction.

- Step 1. Reproduced signal synchronized with the phase measurement signal of the revolution frequency

4.3. Realization

The real-time reproduced signal is directly distributed from the switch matrix, which synchronizes with the phase measurement signal of the revolution frequency in frequency and phase.

- Step 2. Bunch gap indication

The SM considers the bunch gap t_{bucket} within the kicker delay compensation. In Fig. 4.14, the real-time reproduced signal is with the SIS100 revolution frequency and the 9th and 10th buckets of ten buckets are taken as an example as the bunch gap. The $t_{bucket} = 4 \cdot T_{rev}^{SIS18}$.

4.3.6 Fine Synchronization of Extraction and Injection Kickers

After the synchronization of the rf systems between two synchrotrons, the TOF, all propagation and kicker preparation delays are compensated. Now, the extraction and injection kickers must be fired at the calculated trigger time within the bunch gap before the specific bunch or bucket passes the kickers.

This is the task of the Trigger Decision (TD) module in the Trigger SCU. The TD receives the synchronization window in the form of an enable signal. The fine synchronization will be accomplished by the marker of the reproduced signal plus the extraction or injection kicker delay compensation from the SM. This achieves the fine synchronization of the B2B transfer. The TD transmits the kicker pulse directly to the kicker electronic.

In case of fatal errors or considerable damage, the emergency kicker must kick the beam immediately but within the bunch gap into the emergency dump.

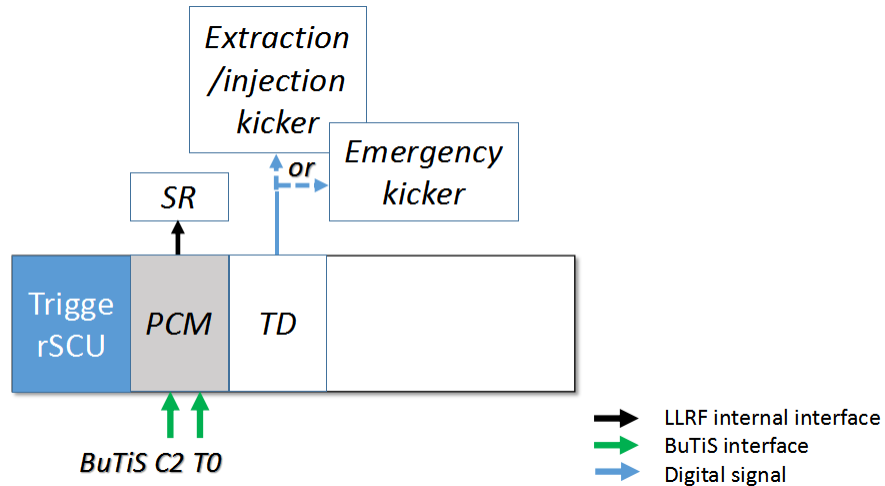


Figure 4.15: Implementation of the Trigger Decision module in the Trigger SCU

Fig. 4.15 shows the implementation of the Trigger Decision (TD) module in the Trigger SCU. The TD module is responsible for the production of triggers for the kickers.

The kicker trigger is realized based on the first rising edge of the bucket indication signal marker within the synchronization window plus the kicker delay compensation. For the normal B2B extraction/injection, the synchronization window is received by the source and target Trigger SCUs from the WR network by TGM_SYNCH_WIN. The extraction kick delay compensation is $T_{rev}^{SIS100} + T_{rev}^{SIS18} - (t_{TOF}$

4.3. Realization

$+t_{v_inj} + t_{ext}$) and the injection kicker delay compensation is $T_{rev}^{SIS100} + T_{rev}^{SIS18} - (t_{v_inj} + t_{inj})$ in the example in Fig. 4.1, when the bucket indication signal has the frequency of f_{syn}^{trg} .

For FAIR use cases, there is always only one bucket in the target synchrotron when $f_{bucket} = f_{syn}^{trg}$. In this case, the bucket delay is not taken into consideration. The extraction kick delay compensation is $T_{syn}^{trg} - (t_{TOF} + t_{v_inj} + t_{ext})$ and the injection kicker delay compensation is $T_{syn}^{trg} - (t_{v_inj} + t_{inj})$, see Fig. 4.16.

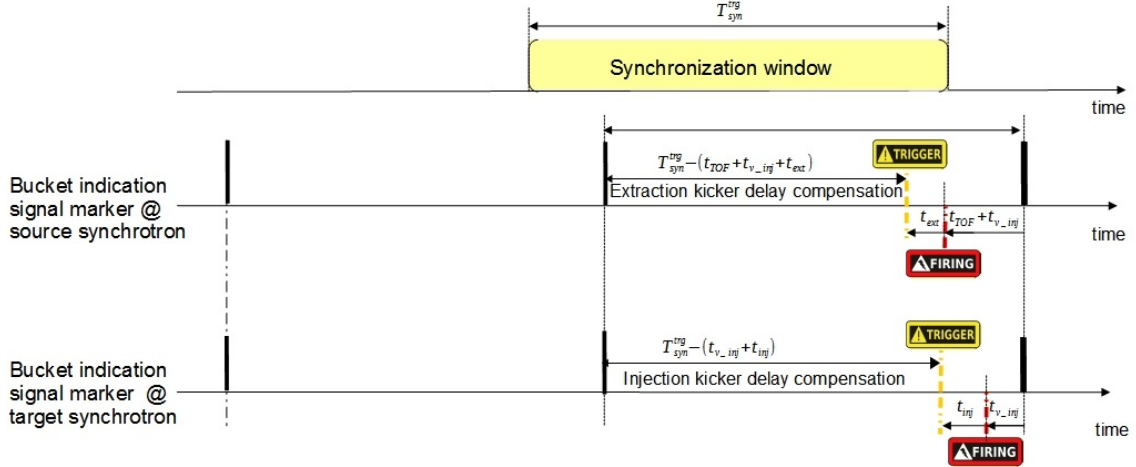


Figure 4.16: The illustration of the kicker delay compensation when the bucket indication signal has the frequency of f_{syn}^{trg} .

Both extraction and injection kick delay compensation values are preloaded from the SM to the Trigger SCU and the Trigger SCU gives these values to the TD module. When the beam injection inhibit signal from the MPS is on, the TD module will block the extraction/injection trigger.

For the SIS100 emergency kick, the extraction delay compensation is calculated by $T_{rev}^{SIS100} + t_{bucket} - (t_{v_emg} + t_{emg})$, where t_{v_emg} is the time delay between the virtual rf cavity and the emergency extraction position, t_{emg} the emergency kicker delay and t_{bucket} always indicates the bunch gap. The emergency extraction delay compensation values are preloaded from the SM to the Trigger SCU and the Trigger SCU gives these values to the TD module. The kicker delay compensation is applied to the real-time reproduced signal by TD module. Only when the emergency dump signal from MPS is valid, the emergency kicker will be triggered by the TD module.

4.3.7 B2B Transfer Status Check

The B2B transfer status must be known by the DM. The B2B source SCU, the B2B transfer master, is responsible for the status check. The B2B source SCU receives the trigger time of the extraction kicker and actual beam extraction time, `TGM_KICKER_TRIGGER_TIME_S`, from the source Trigger SCU via the WR network and also the trigger time of the injection kicker and actual beam injection time, `TGM_KICKER_TRIGGER_TIME_T`, from the target Trigger SCU via the WR network. The Trigger SCU collects the kicker trigger time and the beam extraction/injection time. The B2B source SCU examines the status of the B2B transfer system and transfers the status and the actual beam injection time, `TGM_B2B_STATUS`, to the

4.4. Data Flow

DM. If all components of the B2B transfer system work correctly and the B2B transfer process is successful. Otherwise it is failed.

4.4 Data Flow

In this section, the procedure for the B2B transfer is explained from the perspective of the data flow, which follows the basic six steps in Fig. 4.4. Fig. 4.17 shows the data flow in the source and target synchrotrons and between two synchrotrons. The rectangle with the different color represents the basic six steps. The left part in each rectangle presents the data flow in the source synchrotron and the right part the data flow in the target synchrotron.

1. The DM sends the timing frame `CMD_START_B2B` to the B2B source and target SCUs for the start of the B2B transfer via the WR network. Besides, it requests the switch-off of the feedback loop.
2. After receiving `CMD_START_B2B`, the B2B source and target SCUs start the PAM module to measure the phase deviation $\Delta\varphi^X$ with the help of the PAP module locally and the PAP module extrapolates the phase advance in the future. After a period of time, the B2B source and target SCU reads the extrapolated phase advance ψ_0^X and the slope of the phase deviation k^X from the PAP module locally, timestamping the ψ_0^X .
3. The B2B target SCU sends the extrapolated phase ψ_0^{trg} , the corresponding timestamp t_ψ^{trg} and the slope k^{trg} in the format of the timing frame `TGM_PHASE_TIME` to the B2B source SCU via the WR network.
4. When the B2B source SCU receives the timing frame `TGM_PHASE_TIME`, it calculates the synchronization window and transfers the timestamp of the start of the window to the DM in the format of the timing frame `TGM_SYNCH_WIN`, as well as to the Trigger SCUs at the source and target synchrotrons. The B2B source SCU calculates the phase correction value and transfers it to all Trigger SCUs via the WR network in the format of the timing frame `TGM_PHASE_CORRECTION`. Then the Trigger SCUs transfer the phase correction value to its PCM. The PCM starts the phase correction of the SR module.

Only for the phase shift method, the B2B source SCU calculates the required phase shift $\Delta\phi_{shift}$ and transfers it to the PSM. Then the PSM transfers the phase or frequency modulation profile to the Group DDS.

5. When the source and target Trigger SCUs receive the timing frame `TGM_SYNCH_WIN`, they produce the synchronization window pulse for the TD module. With the help of the reproduced signal from the SR module, the kicker delay compensation from the Trigger SCU and the indication signals (the emergency dump signal and the beam injection inhibit signal) from the MPS, the TD module produces the normal extraction/injection trigger signals or the emergency kick trigger for the kicker.
6. The extraction and injection kickers or emergency kicker are fired. After that, the source Trigger SCU gets the actual beam extraction time and the timestamp of the extraction trigger signal from the TD module and transfers them to

4.5. Comparison between FAIR B2B Transfer System and current B2B Transfer

the B2B source SCU in the format of the timing frame TGM_KICKER_TRIGGER_TIME_S. The target Trigger SCU gets the timestamp of actual beam injection time and the timestamp of the injection trigger signal from the TD module and transfers them to the B2B source SCU in the format of the timing frame TGM_KICKER_TRIGGER_TIME_T. Then the B2B source SCU checks the B2B transfer status and transfers the status together with the beam injection time to the DM in the format of the timing frame TGM_B2B_STAUS (represented as the red line in the rectangle of step 6 in Fig. 4.17).

4.5 Comparison between FAIR B2B Transfer System and current B2B Transfer

The existing GSI control system realizes the B2B transfer from the SIS18 to the ESR. It is an event based system, that event execution will start immediately at the event receipt. Events are directly sent from a “timing master”, who makes the schedule. Each accelerator has its own timing master, e.g. the ESR is equipped with the ESR-timing master and the SIS18 with the SIS-timing master. All devices are connected to distributed Equipment Controllers (EC) via field bus. EC is responsible for the receipt of the event and produces the pulse for the devices [46, 47].

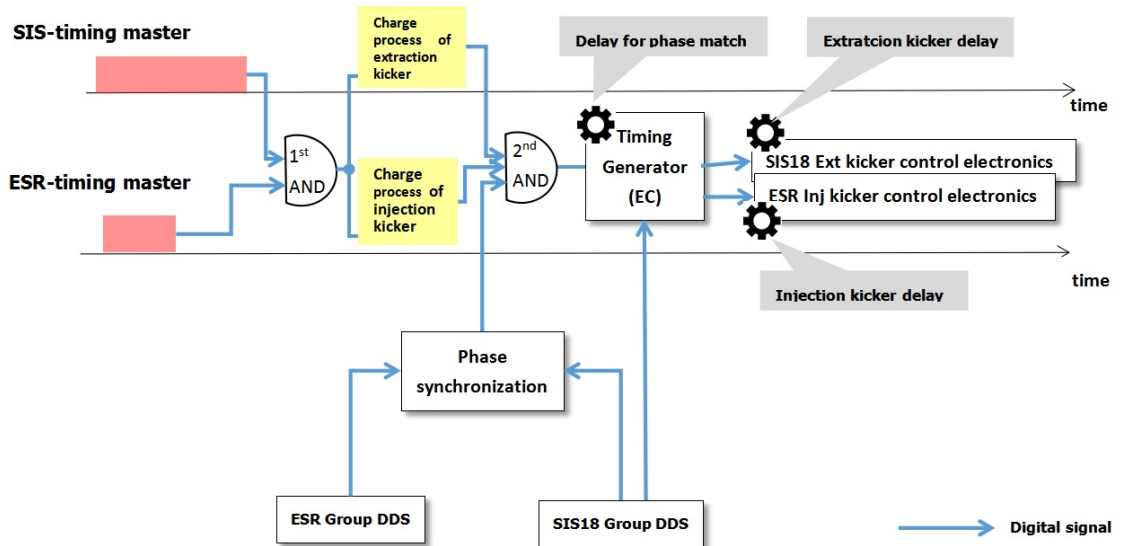


Figure 4.18: The current realization of the bunch-to-bucket transfer between the SIS18 and the ESR with the GSI control system.

Gear sign represents the configuration from operators.

Fig. 4.18 illustrates the current realization of the B2B transfer from the SIS18 to the ESR with the GSI control system. The SIS18 needs longer time for the preparation, e.g. the beam injection and the beam acceleration, before the extraction than that of the ESR before the injection, so the ESR is earlier fully prepared for the transfer. The preparation process is represented as red rectangle in Fig. 4.18. When the SIS18 is fully prepared with bunches to be transferred, the ready signal from the ESR-timing master and the SIS-timing master are forwarded into a logic *AND* gate.

4.5. Comparison between FAIR B2B Transfer System and current B2B Transfer

When both the SIS18 and the ESR are prepared, namely the output of the logic *AND* gate is high, the extraction kicker charge event is sent from the SIS-timing master and the injection kicker charge event from the ESR-timing master. The charge process of kicker is represented as yellow rectangle in Fig. 4.18. When two kickers are fully charged, the ready signal of the extraction and injection kickers from the ESR-timing master and the SIS-timing master are forwarded into the second logic *AND* gate, as well as the “phase synchronization signal” from the rf system. The phase synchronization signal indicates the alignment of the zero-crossing of the phase measurement signals from Group DDS of the SIS18 and the ESR. The output of the second *AND* gate is an indication signal, starting the delay compensation of the time-of-flight and all propagation delays on the SIS18 cavity rf signal for the correct phase match between the SIS18 and ESR rf systems, denoted as “delay for phase match” in Fig. 4.18. The ESR uses the injection orbit instead of the design orbit, so the circumference ratio between the SIS18 and the ESR is close to an integer, $C^{SIS18}/C^{ESR} = 2 - 0.003$, the SIS18 has four bunches, $h^{SIS18} = 4$ and ESR has two buckets, $h^{ESR} = 2$, so $f_{rf}^{SIS18}/f_{rf}^{ESR} = 4/(4 - 0.006)$. The phase difference between rf systems of the SIS18 and the ESR varies at the speed of the beating frequency $\Delta f = |f_{rf}^{SIS18} - f_{rf}^{ESR}| = 1898$ Hz, see Appendix. C.2. The required phase difference (denoted as $\Delta\phi_{shift}$) happens Δt after the indication signal, see eq. 4.21.

$$\Delta t = \frac{\Delta\phi_{shift}}{2\pi} \cdot \frac{1}{\Delta f} \quad (4.21)$$

When the delay for the required phase difference is expired, trigger pulses are produced by the timing generator for both the SIS18 extraction and ESR injection kicker control electronics. Every kicker control electronics adds a separate delay to trigger pulses, denoted as “extraction kicker delay” and “injection kicker delay” in Fig. 4.18. The delay for the required phase match, extraction kicker delay and injection kicker delay are configurable by operators. The precision of the ignition signal from the kicker control electronics is 1 ns.

The existing B2B transfer with the GSI control system only supports the B2B transfer with the frequency beating method. It dose not support B2B transfer with the phase shift method. It gets the phase difference between two rf systems of the SIS18 and the ESR via the direct phase comparison by the phase synchronization module. Parameters (e.g. the delay for the required phase match, the extraction kicker delay and the injection kicker delay) must be properly configured and adjusted by operators. The phase synchronization signal is delay compensated, but the transfer of the signal to the second *AND* gate is not delay compensated and with the jitter of 1 μ s, resulting a spread of the bunch-to-bucket injection center mismatch with the order of the magnitude $\pm 1^\circ$. Besides, it does not support buckets filling by multiple batches, e.g. eight out of ten SIS100 buckets are filled by four SIS18 batches, each of them has two bunches.

Compared with the current B2B transfer with the GSI control system, the FAIR B2B transfer system has many advantages. It supports both the phase shift and frequency beating methods. For the B2B transfer from the SIS18 to the ESR, it is with a smaller bunch-to-bucket injection center mismatch (see Chap. 6). The FAIR B2B transfer system is based on the GMT system, which is a time based system. All FECs of the GMT system are time synchronized with nano second accuracy, which achieves the smaller bunch-to-bucket injection center mismatch. Besides, the FAIR

4.5. Comparison between FAIR B2B Transfer System and current B2B Transfer

B2B transfer system is more flexible. It supports several B2B transfers running at the same time, e.g. the B2B transfer from the SIS18 to the SIS100 and B2B transfer from the ESR to the CRYRING. It is capable to transfer different species beam from one machine cycle to another without the operator's configuration. It is capable to transfer the beam between two synchrotrons via a FRS, Pbar or Super FRS. It can achieve various complex bucket pattern. What is more, the FAIR B2B transfer system coordinates with the MPS system, which protects SIS100/SIS300 from unacceptable failure or situation.

4.5. Comparison between FAIR B2B Transfer System and current B2B Transfer

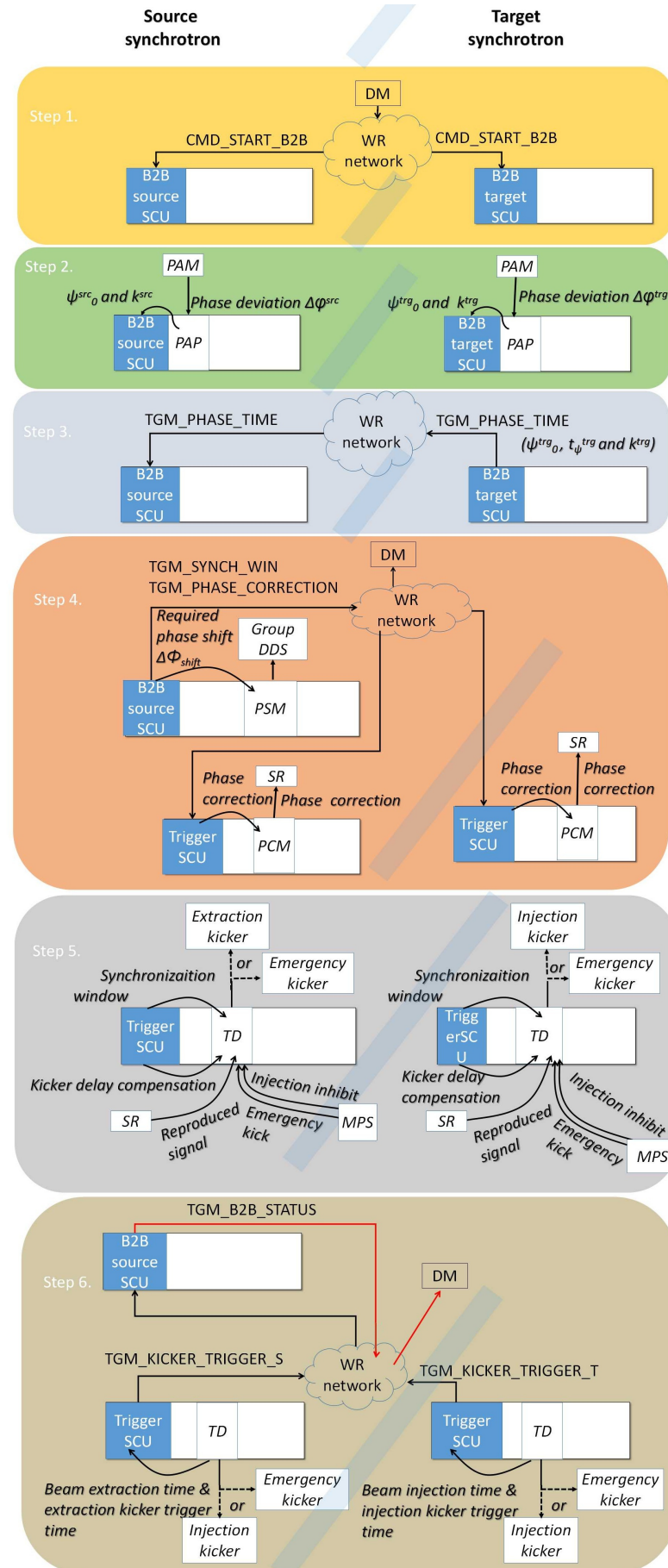


Figure 4.17: The data flow of the B2B transfer system

Chapter 5

Realization and systematic Investigation of FAIR B2B Transfer System

This chapter concentrates on the realization and systematic investigation of the B2B transfer system. In Sec. 6.1, both the phase shift and frequency beating synchronization methods are analyzed from the beam dynamic perspective. The WR network is investigated for the B2B transfer and the calculation of the synchronization window are presented in Sec. 6.2. The B2B transfer system for FAIR focuses first of all on the transfer from the SIS18 to the SIS100, so the trigger possibility of the SIS18 extraction and SIS100 injection kicker are systematically investigated in Sec. 6.3. Besides, the test setup from the timing aspect is introduced and the test result is analyzed in Sec. 6.4.

5.1 Beam Dynamic Analysis of two Synchronization Methods for B2B Transfer from SIS18 to SIS100

This section analyzes the phase shift and frequency beating methods from the beam-dynamics perspective for the synchronization of the SIS18 with the SIS100. Because the most stringent requirement are from the boundary ion species, the beam dynamics of the H^+ and U^{28+} beams are analyzed. The acceptable range of the parameters for the frequency adjustment accompanying these two methods for the SIS18 are summarized in Tab. 5.1.

5.1.1 Beam Dynamics of Phase Shift Method for U^{28+}

The obtained phase shift $\Delta\phi$ is determined by the rf frequency modulation Δf_{rf} and the duration of the frequency modulation T (same as eq. 2.22).

$$\Delta\phi = 2\pi \int_{t_0}^{t_0+T} \Delta f_{rf}(t) dt \quad (5.1)$$

In order to make the rf frequency modulation effective, the beam feedback loops on the rf system are switched off before the B2B starts. Sec. 2.3.1 shows that there

5.1. Beam Dynamic Analysis of two Synchronization Methods for B2B Transfer from SIS18 to SIS100

Table 5.1: Acceptable range of the parameters accompanying with the frequency adjustment of SIS18

Average radial excursion	Relative moment shift	Synchronous phase	Bucket size	Adiabaticity	Chromaticity tune shift/tune
$H^+ \pm 0.8 \times 10^{-4}$	± 0.008	$\pm 10^\circ$	$> 80\%$	$< 2 \times 10^{-4}$	$< \pm 10^{-3}$
$U^{28+} \pm 2.4 \times 10^{-4}$					

are several criterion for the rf frequency modulation for the longitudinal emittance to be preserved.

- There exists a maximum rf frequency offset Δf_{rf_max} .
- $\frac{d\Delta f_{rf}}{dt}$ must be continuous and small enough.
- $\frac{d^2\Delta f_{rf}}{dt^2}$ must be small enough.

According to these criterion, some rf frequency modulations are obviously ruled out of consideration. e.g. a trapezoid modulation and a triangular modulation, whose first derivative are not continuous. The following three examples of rf frequency modulation are analysed, which comply with the above mentioned criterion. The case (1) is a sinusoidal modulation, the case (2) is a parabolic modulation, which consists of three parabolas and two lines between every two parabolas, and the case (3) is also a parabolic modulation, including of three parabolas. The phase shift is assumed to be achieved within 7 ms, namely $T = 7$ ms. Three rf frequency modulation cases are shown in Fig. 5.1. All three cases give the same phase shift, $\Delta\phi = \pi$, which is proved by substituting each form of $\Delta f_{rf}(t)$ into eq. 5.1 and performing integration.

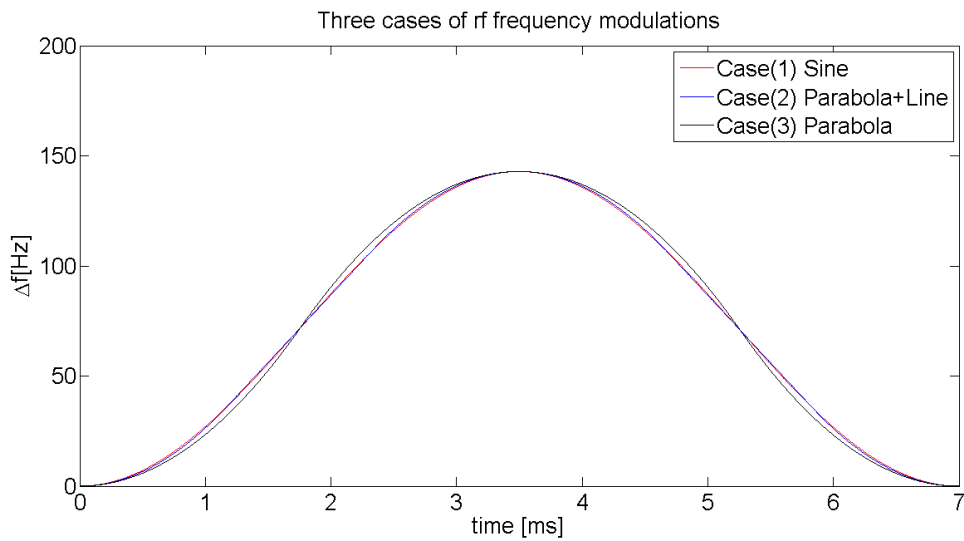


Figure 5.1: Examples of rf frequency modulation.

5.1. Beam Dynamic Analysis of two Synchronization Methods for B2B Transfer from SIS18 to SIS100

Case (1)

$$\Delta f_{rf}(t) = \frac{1}{2T} [1 - \cos(\frac{2\pi}{T}(t - t_0))] \quad t_0 + 0 < t \leq t_0 + T \quad (5.2)$$

Case (2)

$$\Delta f_{rf}(t) = \begin{cases} \frac{9}{T^3}(t - t_0)^2 & t_0 + 0 < t \leq t_0 + \frac{T}{6} \\ \frac{1}{4T} + \frac{3}{T^2}(t - t_0 - \frac{T}{6}) & t_0 + \frac{T}{6} < t \leq t_0 + \frac{2T}{6} \\ \frac{1}{T} - \frac{9}{T^3}(t - t_0 - \frac{T}{2})^2 & t_0 + \frac{2T}{6} < t \leq t_0 + \frac{4T}{6} \\ \frac{3}{4T} - \frac{3}{T^2}(t - t_0 - \frac{4T}{6}) & t_0 + \frac{4T}{6} < t \leq t_0 + \frac{5T}{6} \\ \frac{9}{T^3}(t - t_0 - T)^2 & t_0 + \frac{5T}{6} < t \leq t_0 + T \end{cases} \quad (5.3)$$

Case (3)

$$\Delta f_{rf}(t) = \begin{cases} \frac{8}{T^3}(t - t_0)^2 & t_0 + 0 < t \leq t_0 + \frac{T}{4} \\ \frac{1}{T} - \frac{8}{T^3}[(t - t_0) - \frac{T}{2}]^2 & t_0 + \frac{T}{4} < t \leq t_0 + \frac{3T}{4} \\ \frac{8}{T^3}[T - (t - t_0)]^2 & t_0 + \frac{3T}{4} < t \leq t_0 + T \end{cases} \quad (5.4)$$

Fig. 5.2 and Fig. 5.3 show the first and second derivative of three rf frequency modulations.

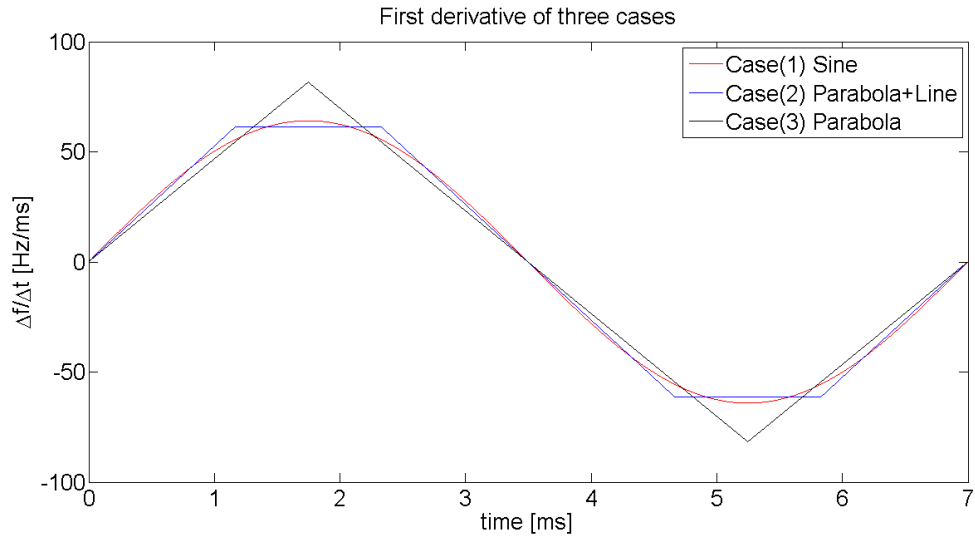


Figure 5.2: First derivation of three cases.

5.1. Beam Dynamic Analysis of two Synchronization Methods for B2B Transfer from SIS18 to SIS100

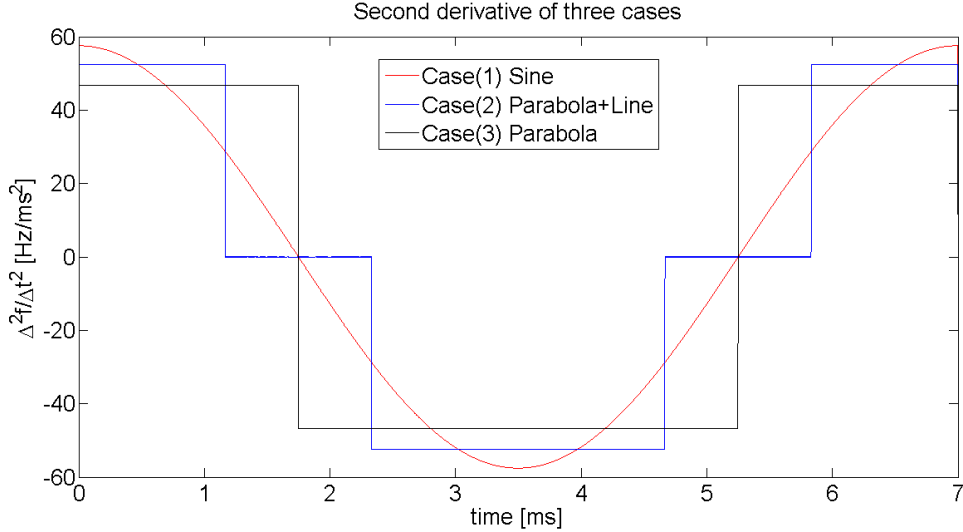


Figure 5.3: Second derivation of three cases.

Fig. 5.4 shows the corresponding phase shift modulation of three cases.

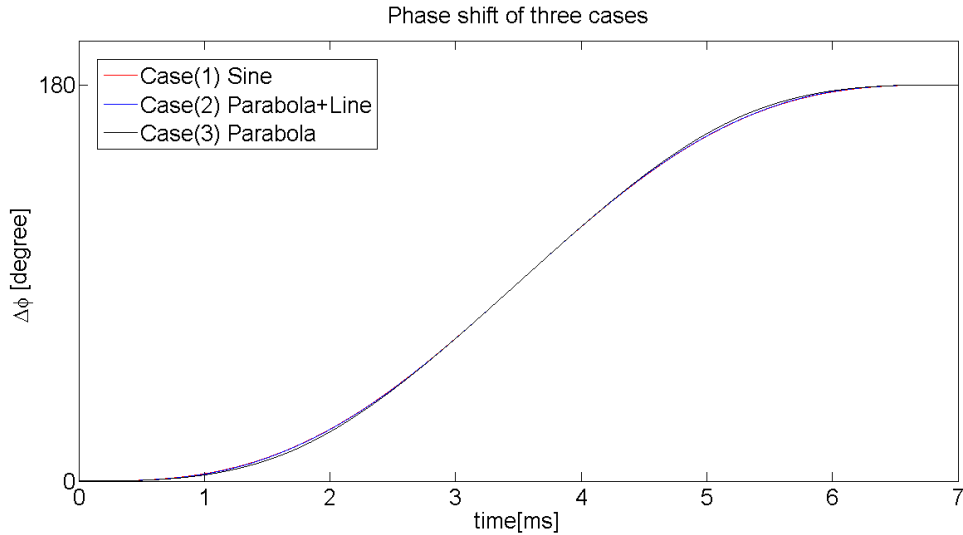


Figure 5.4: The phase shift modulation of three cases.

5.1.1.1 Longitudinal Dynamic Analysis for Frequency Modulation

In this section, the average radial excursion, the relative momentum shift, the synchronous phase, the bucket size and the adiabaticity of three rf frequency modulations are analyzed.

- Average radial excursion

The average radial excursion is calculated for the three cases by eq. (2.54). Fig. 5.5 shows the calculation result [48].

5.1. Beam Dynamic Analysis of two Synchronization Methods for B2B Transfer from SIS18 to SIS100

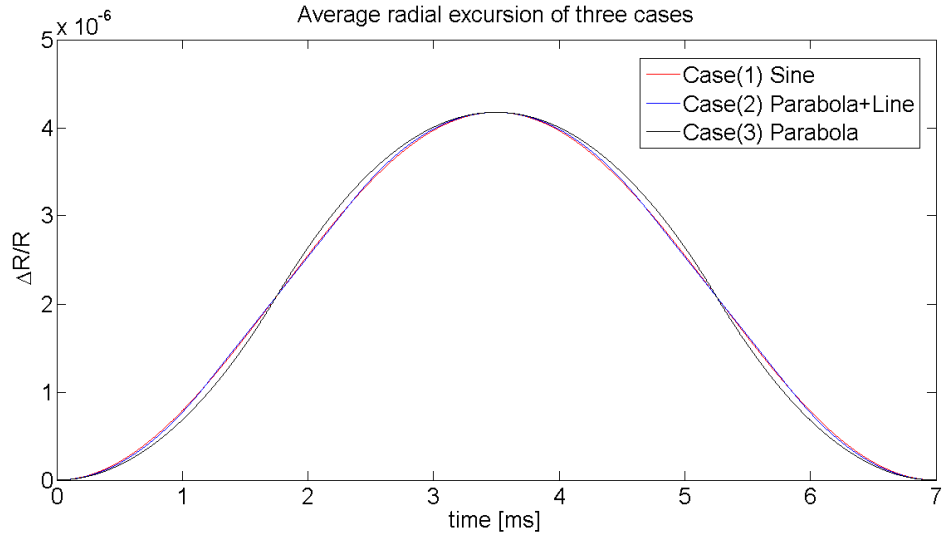


Figure 5.5: Average radial excursions of three cases.

Table 5.2: The maximum average radial excursion of three cases

	Case (1)	Case (2)	Case (3)
Max average radial excursion	4.18×10^{-6}	4.18×10^{-6}	4.18×10^{-6}
Time	3.5 ms	3.5 ms	3.5 ms

As shown in Tab. 5.2 the maximum average radial excursion is 4.18×10^{-6} for all three cases, which is within the acceptable range in Tab. 5.1. Hence, all cases are applicable.

- Relative momentum shift

The relative momentum shift is calculated for three cases by eq. 2.53. Fig. 5.6 shows the calculation result.

5.1. Beam Dynamic Analysis of two Synchronization Methods for B2B Transfer from SIS18 to SIS100

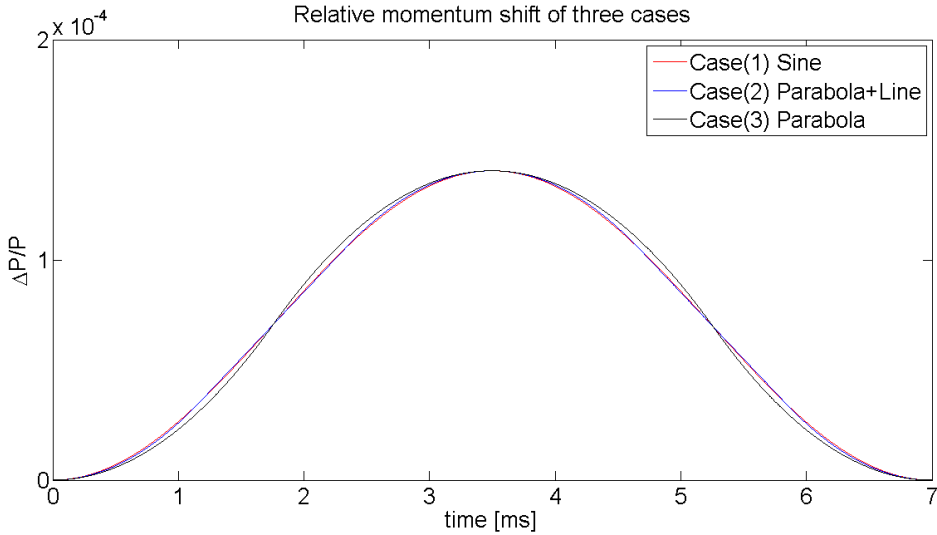


Figure 5.6: Relative momentum shift of three cases.

Table 5.3: The maximum relative momentum shift of three cases

	Case (1)	Case (2)	Case (3)
Max relative momentum shift	1.40×10^{-4}	1.40×10^{-4}	1.40×10^{-4}
Time	3.5 ms	3.5 ms	3.5 ms

As shown in Tab. 5.3 the maximum relative momentum shift is 1.40×10^{-4} for all three cases, which is within the acceptable range in Tab. 5.1. Hence, all cases are applicable.

- Synchronous phase

The rf frequency modulations make the synchronous phase deviate from the nominal value 0° . Fig. 5.7 shows the changes in the synchronous phase $\phi_s(t)$. It is calculated by substituting values into eq. 2.56. For three cases, the synchronous phase $\Delta\phi_s(t)$ during the modulations are continuous without any phase jumps and small than $\pm 10^\circ$. Hence, all cases are applicable.

5.1. Beam Dynamic Analysis of two Synchronization Methods for B2B Transfer from SIS18 to SIS100

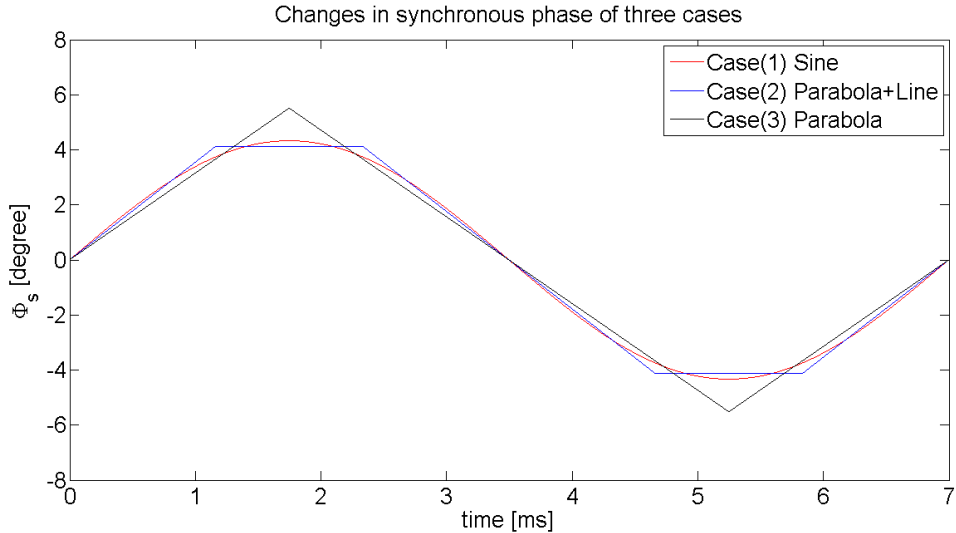


Figure 5.7: Changes in synchronous phase of three cases.

- Bucket size

The bucket area factor α_b varies during rf frequency modulations. Before the modulations, the synchronous phase $\phi_s=0^\circ$ and $\alpha_b(0^\circ) = 1$. By substituting the changes in synchronous phase into eq. 2.59, we get the ratio of bucket areas of a running bucket to the stationary bucket for three cases, see Fig. 5.8.

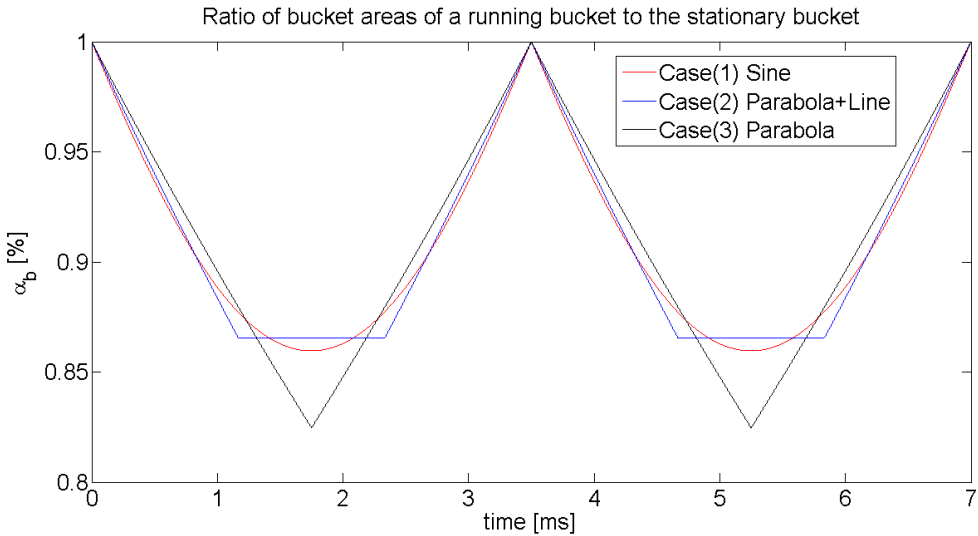


Figure 5.8: Ratio of bucket areas of a running bucket to the stationary bucket of three cases.

Tab. 5.4 shows the minimum bucket area factor for three cases. For case (1) and (2), the bucket area factor is larger than 86%, which is larger than that of the case (3). Hence, case (1) and (2) are preferred compared with the case (3).

5.1. Beam Dynamic Analysis of two Synchronization Methods for B2B Transfer from SIS18 to SIS100

Table 5.4: The minimum bucket area factor of three cases

	Case (1)	Case (2)	Case (3)
Min bucket area factor	86.0%	86.5%	82.5%
Time	1.750 ms and 5.250 ms	1.167 ms-2.333 ms, 4.667 ms-5.833 ms	1.750 ms and 5.250 ms

- Adiabaticity

By substituting the values of $\phi_s(t)$, $\dot{\phi}_s(t)$ and ω_s into eq. 2.63, we get the adiabaticity parameter ε for three cases, see Fig. 5.9.

Tab. 5.5 shows the maximum adiabaticity parameter for three cases. For case (1), the maximum of ε is 0.000030. For case (2), the maximum of ε occurs at $1/6T$, $2/6T$, $4/6T$ and $5/6T$, when the change rate of the synchronous phase $\dot{\phi}_s(t)$ has a maximum, shown in Fig. 5.7. For case (3), the maximum of ε occurs at $1/4T$ and $3/4T$, when the change rate of the synchronous phase $\dot{\phi}_s(t)$ has a maximum. For all three cases, the adiabaticity parameter meets the requirement of the adiabaticity in Tab. 5.1, so all three cases are applicable.

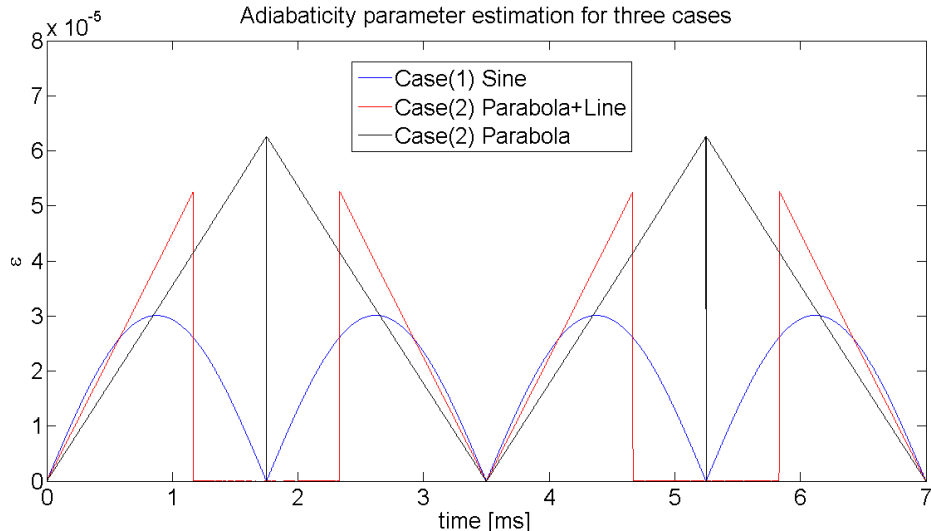


Figure 5.9: Adiabaticity parameter of three cases.

Table 5.5: The maximum adiabaticity of three cases

	Case (1)	Case (2)	Case (3)
Maximum adiabaticity	5.3×10^{-5}	5.9×10^{-5}	6.3×10^{-5}
Time	0.875 ms, 2.625 ms 4.250 ms and 6.125 ms	1.167 ms, 2.333 ms, 4.667 ms and 5.833 ms	1.750 ms and 5.250 ms

5.1. Beam Dynamic Analysis of two Synchronization Methods for B2B Transfer from SIS18 to SIS100

5.1.1.2 Transverse Dynamics Analysis

For the SIS18, the chromaticity Q'_x and Q'_y of U^{28+} is -6.5 and -4.1 . Substituting the chromaticity and the maximum momentum shift (see. Tab. 5.3) into eq. 2.64. The chromatic tune shift ΔQ_x and ΔQ_y during rf modulations for three cases can be calculated. Beacuse case (1), case (2) and case (3) have same maximum relative momentum shift, the chromatic tune shift is same for three rf frequency modulations.

$$\Delta Q_x = -6.5 \times 1.40 \times 10^{-4} = -9.1 \times 10^{-4} \quad (5.5)$$

$$\Delta Q_y = -4.1 \times 1.40 \times 10^{-4} = -5.74 \times 10^{-4} \quad (5.6)$$

The percentage of the chromatic tune shift to the tune is

$$\frac{\Delta Q_x}{Q_x} = \frac{-9.1 \times 10^{-4}}{4.17} = -2.18 \times 10^{-4} \quad (5.7)$$

$$\frac{\Delta Q_y}{Q_y} = \frac{-5.74 \times 10^{-4}}{3.4} = -1.69 \times 10^{-4} \quad (5.8)$$

The percentage of the chromatic tune shift to the tune for three cases are significantly small, which could be neglected.

Although all three cases meet the requirement of the parameters accompanying with the frequency adjustment, the case (1) of a sinusoidal modulation is the best one for the beam stability because of the smaller adiabaticity.

5.1.2 Beam Dynamics of Frequency Beating Method for U^{28+}

In the case of the frequency beating method, we guarantee the extraction and injection energy always match, which means that the momentum is not affected by the frequency detune, namely $\Delta p = 0$. Hence, the frequency detune has influence only on the longitudinal dynamics.

5.1.2.1 Longitudinal Dynamics Analysis

For the frequency beating method, the rf frequency detune is done during the SIS18 rf ramp or after the ramp. Due to the SIS18 U^{28+} lattice, the SIS18 U^{28+} accepted orbit excursion is [38]

$$\frac{\Delta R}{R} = \pm 2.4 \times 10^{-4} \quad (5.9)$$

From eq. 2.67, the tolerate rf frequency change for U^{28+} at the extraction energy 200 MeV/u is

$$\frac{\Delta f_{rf}}{f_{rf}} = \pm 2.4 \times 10^{-4} \quad (5.10)$$

where the maximum rf frequency detune approximates to 370 Hz for the cavity rf frequency of 1.572 536 MHz of U^{28+} . Fig. 5.10 shows the rf frequency detune during the rf ramp. In the simulation, the rf frequency is detuned at 0.2756 s with 6.08 Hz/us, see blue rectangle in Fig. 5.10. For the sake of simplicity, 200 Hz is used as the frequency detune. The SIS18 needs approximate 33 μ s to reach 200 Hz with 6.08 Hz/us.

5.1. Beam Dynamic Analysis of two Synchronization Methods for B2B Transfer from SIS18 to SIS100

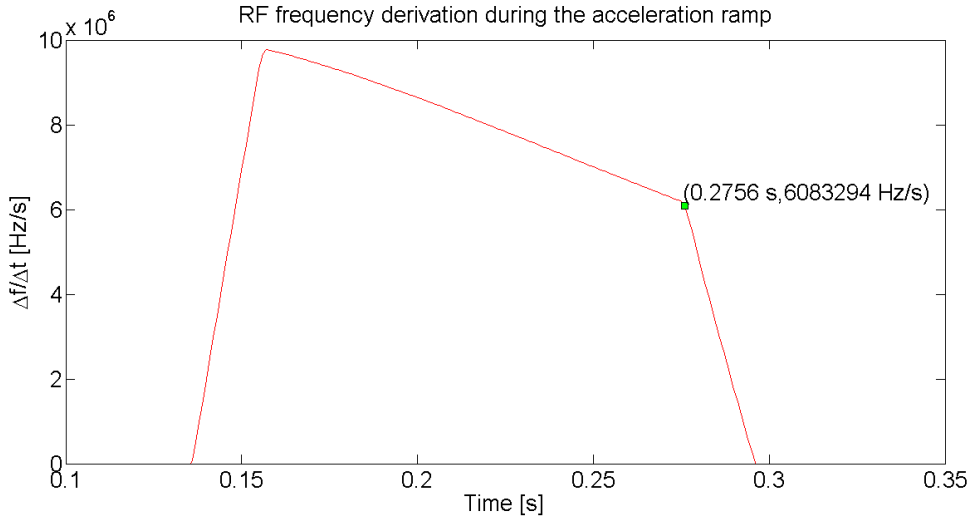


Figure 5.10: Frequency detune during the SIS18 U^{28+} rf ramp.

5.1.3 Beam Dynamics of Phase Shift Method for H^+

For the frequency adjustment of the SIS18 for the U^{28+} beam, we know that the sinusoidal modulation is best for the beam stability. Now we will check whether the sinusoidal modulation is also applicable for the H^+ beam of the SIS18.

5.1.3.1 Longitudinal Dynamics Analysis

When the case (1), a sinusoidal modulation (same as the eq. 5.2) with $T = 7\text{ ms}$, is used as the frequency modulation for the phase shift of π , we have the following parameters accompanying the modulation, see Tab. 5.6.

Case (1)

$$\Delta f_{rf}(t) = \frac{1}{2T} [1 - \cos(\frac{2\pi}{T}(t - t_0))] \quad t_0 + 0 < t \leq t_0 + T \quad (5.11)$$

Table 5.6: Parameters accompanying with a 7 ms sinusoidal modulation for the SIS18 H^+ beam

Average radial excursion	Relative moment shift	Synchronous phase	Bucket size	Adiabaticity
$< 4.09 \times 10^{-5}$	< 0.0041	$\pm 34.7^\circ$	$> 27\%$	< 0.04

Compared with the acceptable range of the parameters in Tab. 5.1, the synchronize phase, the bucket size and the adiabaticity accompanying with the 7 ms sinusoidal modulation are far beyond the acceptable range. Hence, a sinusoidal modulation with longer period must be used to guarantee these requirement. A sinusoidal modulation with $T = 20\text{ ms}$ is used as the frequency modulation for the

5.1. Beam Dynamic Analysis of two Synchronization Methods for B2B Transfer from SIS18 to SIS100

Table 5.7: Parameters accompanying with a 20 ms sinusoidal modulation for the SIS18 H^+ beam

Average radial excursion	Relative moment shift	Synchronous phase	Bucket size	Adiabaticity
$< 3.9 \times 10^{-6}$	$< 3.9 \times 10^{-4}$	$\pm 4.2^\circ$	> 86%	$< 1.9 \times 10^{-4}$

phase shift of π , we have the following parameters accompanying the modulation, see Tab. 5.7. In this case, all parameters meet the requirement.

For the frequency modulation of the SIS18 H^+ beam, a longer period sinusoidal modulation (e.g. 20 ms) must be used for the beam stability consideration.

5.1.3.2 Transverse Dynamics Analysis

For the SIS18, the chromaticity Q'_x and Q'_y of H^+ is -7.5 and -4.4 . Substituting the chromaticity and the maximum momentum shift (see. Tab. 5.7) into eq. 2.64. The maximum chromatic tune shift ΔQ_x and ΔQ_y during the 20 ms sinusoidal modulation can be calculated.

$$\Delta Q_x = -7.5 \times 3.9 \times 10^{-4} = -2.925 \times 10^{-3} \quad (5.12)$$

$$\Delta Q_y = -4.4 \times 3.9 \times 10^{-4} = -1.716 \times 10^{-3} \quad (5.13)$$

The percentage of the chromatic tune shift to the tune is

$$\frac{\Delta Q_x}{Q_x} = \frac{-2.925 \times 10^{-3}}{4.17} = -7.01 \times 10^{-4} \quad (5.14)$$

$$\frac{\Delta Q_y}{Q_y} = \frac{-1.716 \times 10^{-3}}{3.4} = -5.05 \times 10^{-4} \quad (5.15)$$

The percentage of the chromatic tune shift to the tune for three cases are significantly small, which could be neglected.

5.1.4 Beam Dynamics of Frequency Beating Method for H^+

The frequency detune has influence only on the longitudinal dynamics because of $\Delta p = 0$ during the frequency detune process.

5.1.4.1 Longitudinal Dynamics Analysis

Due to the SIS18 H^+ lattice, the SIS18 H^+ accepted orbit excursion is [38]

$$\frac{\Delta R}{R} = \pm 0.8 \times 10^{-4} \quad (5.16)$$

From eq. 2.67, the tolerate rf frequency change for H^+ at the extraction energy 4 GeV/u is

$$\frac{\Delta f_{rf}}{f_{rf}} = \pm 0.8 \times 10^{-4} \quad (5.17)$$

5.2. GMT systematic Investigation

where the maximum rf frequency detune approximates to 108 Hz for the cavity rf frequency of 1.359 358 MHz of H^+ .

5.2 GMT systematic Investigation

The B2B transfer system makes use of certain aspects of the GMT system to implement the data collection, merging and redistribution. The main task of the data merging is to calculate the start of the synchronization window, which is used for the selection of the bucket indication signal for the kicker trigger. The data collection and redistribution make use of the WR network, so the test and measurement of the WR network for the B2B transfer is important.

5.2.1 Calculation of the Start of the Synchronization Window

All calculations for the B2B transfer are based on the phase deviation measurement by the PAM module. With the help of the phase extrapolation by the PAP module and the timestamp for the extrapolated phase by the B2B source and target SCUs, the fine time point of the correct phase alignment between two synchronization frequencies is calculated, see Chap. 4. This fine time point is called the “best estimate of alignment” and denoted by t_{align} . There exists *uncertainty* for any measurement, which is defined as a non-negative parameter characterizing the dispersion of the values attributed to a measured quantity. The measurement uncertainty [49] of the phase deviation is reflected in the uncertainty of the extrapolated phase for the calculation of the phase alignment. Because of the propagation of the uncertainty of the extrapolated phase and that of the timestamp, the phase alignment lies between $t_{align} - \delta t_{align}$ and $t_{align} + \delta t_{align}$, where δt_{align} is the uncertainty of the phase alignment. $[t_{align} - \delta t_{align}, t_{align} + \delta t_{align}]$ is called the “probable range of alignment”. In order to achieve the highly precise bunch-to-bucket injection, the length of the probable range of alignment must be much shorter than the length of the synchronization window. In Sec. 6.2.1.1, the calculation and inspection of δt_{align} for the phase shift and frequency beating methods are explained. For the correct selection of the same rising edge of the bucket indication signal at different SCUs, the start of the synchronization window must be properly calculated. In Sec. 6.2.1.2, the calculation of the start of the synchronization window is explained. In Sec. 6.2.1.3, the requirement of the accuracy of the start of the synchronization window is calculated.

5.2.1.1 Uncertainty of Phase Alignment

In Chap. 4, we get the phase difference $\Delta\phi_{syn}$ between two synchronization frequencies at t_ψ^X .

$$\Delta\phi_{syn} = \begin{cases} \psi_0^{trg} - \psi_0^{src}, & f_{bucket} = f_{syn}^{trg} \\ \frac{f_{syn}^{trg}}{f_{rev}^{trg}}(\psi_0^{trg} - \psi_0^{src}) \bmod 2\pi, & f_{bucket} = f_{rev}^{trg} \end{cases} \quad (5.18)$$

The longer the time is used for the phase extrapolation, the smaller the uncertainty of the extrapolated phase will be. If the PAP module use 500 μ s to extrapolate the phase, the uncertainty of the extrapolated phase is 100 ps in the time domain

5.2. GMT systematic Investigation

[43]. The uncertainty of the extrapolated phase from the time domain to the phase domain (denoted as $\delta\psi^X$) is calculated by eq. 5.19.

$$\delta\psi^X = 100ps \times f_{B2B}^{trg} \times 2\pi \quad (5.19)$$

Both the B2B source SCU and the B2B target SCU measures the timestamp t_ψ^X for the extrapolated phase and the uncertainty of the measured timestamp (denoted as δt_ψ^X) is 1 ns.

$$\delta t_\psi^X = 1 \text{ ns} \quad (5.20)$$

- Phase shift method

For the phase shift method, the duration of the rf frequency modulation is T , so the best estimate of alignment is expressed by

$$t_{align} = t_\psi^X + T \quad (5.21)$$

The uncertainty of the phase alignment is only caused by the uncertainty of the timestamp, calculated by eq. 5.22.

$$\delta t_{align} = \sqrt{\left(\frac{\partial t_{align}}{\partial t_\psi^X} \delta t_\psi^X\right)^2} = \delta t_\psi^X = 1 \text{ ns} \quad (5.22)$$

For all FAIR B2B transfer use cases with the phase shift method, the uncertainty of the phase alignment is 1 ns, which is much smaller than T_w and is acceptable.

- Frequency beating method

The best estimate of alignment is determined by the required phase difference $\Delta\phi_{shift}$, see eq. 5.23.

$$t_{align} = t_\psi^X + \frac{\Delta\phi_{shift}}{2\pi} \cdot \frac{1}{|f_{syn}^{src} - f_{syn}^{trg}|} \quad (5.23)$$

The relation between $\Delta\phi_{shift}$ and $\Delta\phi_{syn}$ is explained in Chap. 4.

The uncertainty of the phase alignment is caused by the uncertainty of the phase extrapolation and the uncertainty of the timestamp, calculated by eq. 5.24

$$\begin{aligned} \delta t_{align} &= \sqrt{\left(\frac{\partial t_{align}}{\partial t_\psi^X} \delta t_\psi^X\right)^2 + \left(\frac{\partial t_{align}}{\partial \psi_0^{src}} \delta \psi_0^{src}\right)^2 + \left(\frac{\partial t_{align}}{\partial \psi_0^{trg}} \delta \psi_0^{trg}\right)^2} \\ &= \sqrt{(\delta t_\psi^X)^2 + \left(\frac{1}{2\pi} \frac{1}{|f_{syn}^{src} - f_{syn}^{trg}|} \frac{\partial \Delta\phi_{shift}}{\partial \psi_0^{src}} \delta \psi_0^{src}\right)^2 + \left(\frac{1}{2\pi} \frac{1}{|f_{syn}^{src} - f_{syn}^{trg}|} \frac{\partial \Delta\phi_{shift}}{\partial \psi_0^{trg}} \delta \psi_0^{trg}\right)^2} \end{aligned} \quad (5.24)$$

Because $\Delta\phi_{shift}$ and $\Delta\phi_{syn}$ have a linear relationship and the linear slope is 1, $\frac{\partial \Delta\phi_{shift}}{\partial \psi_0^{trg}} = \frac{\partial \Delta\phi_{syn}}{\partial \psi_0^{trg}}$ and $\frac{\partial \Delta\phi_{shift}}{\partial \psi_0^{src}} = \frac{\partial \Delta\phi_{syn}}{\partial \psi_0^{src}}$. Based on eq. 5.18, we get the partial derivative of $\Delta\phi_{shift}$ with respect to ψ_0^{src} and ψ_0^{trg} .

$$\left| \frac{\partial \Delta\phi_{shift}}{\partial \psi_0^{trg}} \right| = \left| \frac{\partial \Delta\phi_{shift}}{\partial \psi_0^{src}} \right| = \begin{cases} 1, & f_{bucket} = f_{syn}^{trg} \\ \frac{f_{syn}^{trg}}{f_{rev}^{trg}}, & f_{bucket} = f_{rev}^{trg} \end{cases} \quad (5.25)$$

5.2. GMT systematic Investigation

$\delta\psi_0^{src} = \delta\psi_0^{trg}$ and Substituting eq. 5.25 into eq. 5.24, we get

$$\delta t_{align} = \begin{cases} \sqrt{(\delta t_\psi^X)^2 + 2(\frac{1}{2\pi} \frac{1}{|f_{syn}^{src} - f_{syn}^{trg}|} \delta\psi_0^X)^2}, & f_{bucket} = f_{syn}^{trg} \\ \sqrt{(\delta t_\psi^X)^2 + 2(\frac{1}{2\pi} \frac{1}{|f_{syn}^{src} - f_{syn}^{trg}|} \frac{f_{syn}^{trg}}{f_{rev}^{trg}} \delta\psi_0^X)^2}, & f_{bucket} = f_{rev}^{trg} \end{cases} \quad (5.26)$$

Tab. 5.8 shows the uncertainty of the phase alignment for all FAIR use cases. More details about parameters, please see Chap. 6.

Table 5.8: Uncertainty of the phase alignment of all FAIR B2B use cases

Use cases of FAIR accelerators	$\delta\psi_0^X$	$ f_{syn}^{src} - f_{syn}^{trg} $	δt_{align}	T_w
U^{28+} B2B transfer from the SIS18 to the SIS100	0.006°	200 Hz	1.174 μ s	6.359 μ s
H^+ B2B transfer from the SIS18 to the SIS100	0.010°	200 Hz	0.983 μ s	3.678 μ s
$h=4$ B2B transfer from the SIS18 to the ESR	0.025°	1899 Hz	0.103 μ s	1.456 μ s
$h=1$ B2B transfer from the SIS18 to the ESR	0.036°	1368 Hz	0.104 μ s	1.017 μ s
B2B transfer from the ESR to the CRYRING	0.025°	949 Hz	0.102 μ s	1.456 μ s
H^+ B2B transfer from the SIS100 to the CR via a Pbar	0.002°	450 Hz	0.019 μ s	18.226 μ s
RIB B2B transfer from the SIS100 to the CR via a Super FRS	0.004°	108 Hz	0.154 μ s	9.779 μ s
Antiproton B2B transfer from the CR to the HESR	0.004°	136 Hz	0.123 μ s	9.860 μ s
B2B transfer from the SIS18 to the ESR via a FRS	0.008°	4249 Hz	7 ns	4.553 μ s

The uncertainty of the phase alignment for all FAIR use cases is much smaller than the length of the synchronization window. Hence, the influence of the propagation of the uncertainty on the bunch-to-bucket injection center mismatch within the synchronization window is negligible. The uncertainty of the phase extrapolation 100 ps and the uncertainty of the timestamp t_{psi}^X are acceptable for the FAIR B2B transfer system.

5.2.1.2 Uncertainty of the Start of the Synchronization Window

The start of the synchronization window is expressed as

$$t_w = t_\psi^X + \Delta t_w \quad (5.27)$$

5.2. GMT systematic Investigation

with

$$\Delta t_w = \begin{cases} T - \frac{T_w}{2} - t_{delay} & \text{Phase shift method} \\ \frac{\Delta\phi_{shift}}{2\pi} \cdot \frac{1}{|f_{syn}^{src} - f_{syn}^{trg}|} - \frac{T_w}{2} - t_{delay} & \text{Frequency beating method} \end{cases} \quad (5.28)$$

More details, please see Chap. 4.

The synchronization window is used to select the first rising edge of the bucket indication signal. In reality, the relative position between the start of the synchronization window and the first rising edge of the bucket indication signal is random. In order to guarantee the correct selection of the rising edge of the bucket indication signal at both the source and target synchrotrons, the start of the synchronization window will be rectified to half the period of the bucket indication signal before the selected rising edge. The rectified start is called the “best estimate of the start of the synchronization window”, denoted as t_{w_rect} . The value used for the rectification is denoted as Δt_{w_rect} , see Fig. 5.11. However, the actual start of the synchronization window is impossible to be exactly at t_{w_rect} because of the propagation of the uncertainty. The start of the synchronization window lies between $t_{w_rect} - \delta t_{w_rect}$ and $t_{align} + \delta t_{w_rect}$, where δt_{w_rect} is the uncertainty of the start of the synchronization window.

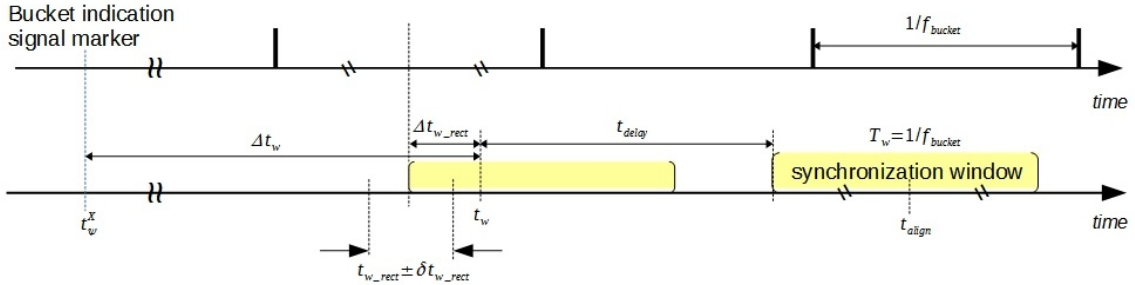


Figure 5.11: The rectification of the start of the synchronization window.

The rectification for the start of the synchronization window is calculated by

$$\Delta t_{w_rect} = \frac{1}{2f_{B2B}^{trg}} - [(\Delta t_w - \frac{2\pi - \psi_0^{trg}}{2\pi} \frac{1}{f_{B2B}^{trg}}) \bmod \frac{1}{f_{B2B}^{trg}}] \quad (5.29)$$

The best estimate of the start of the synchronization window is calculated by

$$t_{w_rect} = t_\psi^X + \Delta t_w + \Delta t_{w_rect} \quad (5.30)$$

The uncertainty of t_{w_rect} is caused by the uncertainty of the phase extrapolation and the uncertainty of the timestamp, calculated by

$$\begin{aligned} \delta t_{w_rect} &= \sqrt{\left(\frac{\partial t_{w_rect}}{\partial t_\psi^X} \delta t_\psi^X\right)^2 + \left(\frac{\partial t_{w_rect}}{\partial \psi_0^{src}} \delta \psi_0^{src}\right)^2 + \left(\frac{\partial t_{w_rect}}{\partial \psi_0^{trg}} \delta \psi_0^{trg}\right)^2} \\ &= \sqrt{(\delta t_\psi^X)^2 + \left(\frac{\partial \Delta t_w}{\partial \psi_0^{src}} + \frac{\partial \Delta t_{w_rect}}{\partial \psi_0^{src}}\right)^2 (\delta \psi_0^{src})^2 + \left(\frac{\partial \Delta t_w}{\partial \psi_0^{trg}} + \frac{\partial \Delta t_{w_rect}}{\partial \psi_0^{trg}}\right)^2 (\delta \psi_0^{trg})^2} \quad (5.31) \\ &= \sqrt{(\delta t_\psi^X)^2 + \left(\frac{1}{2\pi} \frac{1}{f_{B2B}^{trg}} \delta \psi_0^{trg}\right)^2} \end{aligned}$$

For FAIR use cases, f_{B2B}^{trg} is in the 100 kHz range and $\delta \psi_0^{trg}$ is less than 0.05° (see Tab. 5.8). Hence, $\delta t_{w_rect} < 2ns$, which can be negligible.

5.2. GMT systematic Investigation

5.2.1.3 Accuracy of the Start of the Synchronization Window

The actual start of the synchronization window is impossible to be exactly at the best estimate of the start of the synchronization window because of random uncertainty (e.g. the transition time from low to high voltage of digital IO ports) and systematic uncertainty (e.g. the FPGA process time). The accuracy of the start of the synchronization window is the deviation between the theoretically calculated start time and the actual observed start time on SCUs. The FAIR B2B transfer system will be used for all FAIR use cases. Therefore, we have to find the most stringent accuracy requirement. The shortest synchronization window is $1.017\text{ }\mu\text{s}$, which comes from $h=1$ B2B transfer from the SIS18 to the ESR. We keep 20 ns as a forbidden range, which means that the actual start is not allowed 20 ns before and after the bucket indication signal marker. The green region in Fig. 5.12 represents the safety margin for the start of the synchronization window and the red region the forbidden range. So the requirement of the accuracy of the start of the synchronization window is

$$\text{Accuracy} = \pm \frac{1.017\text{ }\mu\text{s} - 20\text{ ns} \cdot 2}{2} \approx \pm 488\text{ ns} \quad (5.32)$$

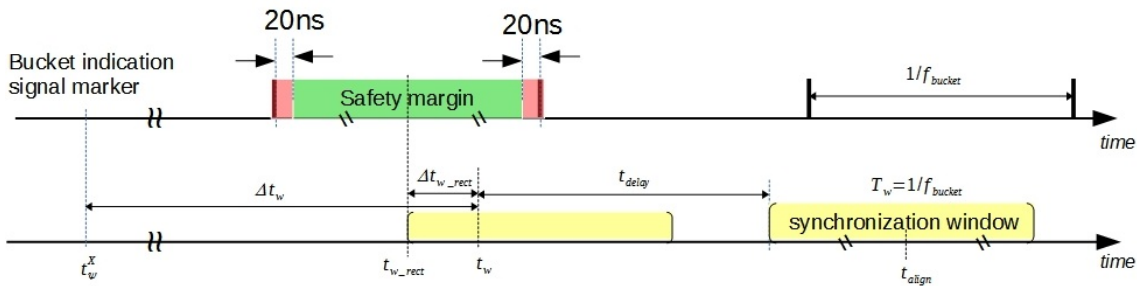


Figure 5.12: The accuracy of the start of the synchronization window.

5.2.2 Characterization of WR Network

Within this dissertation, a network analyzer, a Xena traffic generator¹, is used to characterize the properties of the WR network, which are relevant to the B2B transfer. The Xena traffic generator offers a new class of professional Layer 2-3 Gigabit Ethernet test platform. It is used to measure the frame loss rate², the frame transfer latency³ and the frame transfer jitter⁴ for a network. The Xena traffic generator sends traffic streams with a unique stream ID and receives the identical traffic streams for identifying the latency, jitter and packet loss. For the measurements reported here, the following types of traffic are considered.

¹<http://xenanetworks.com/layer-2-3-platform/>

²The ratio of the number of the lost frames to the number of the theoretic received frames of a tested port.

³The time interval between the time of Xena port receiving frame and the time of another Xena port sending frame.

⁴The absolute value of the difference between the latency of two consecutive received frames belonging to the same stream from one Xena port to another Xena port.

http://www.xenanetworks.com/wp-content/uploads/Measuring_Frame_latency_Variation.pdf

5.2. GMT systematic Investigation

- DM Broadcast

The DM forwards broadcast timing frames downwards to all FECs. The average bandwidth for the DM broadcast is 100 Mbit/s. The burst⁵ speed is 12 packets per 100 µs.

- DM Unicast

The DM sends 10 Mbit/s unicast timing frames to some specified FECs at the burst speed of 3 packets per 300 µs.

- B2B Unicast

The B2B source SCU sends two timing frames upwards to the DM within 10 ms for each cycle. Every supercycle contains four cycles. The maximum supercycle repetition frequency for FAIR is the repetition frequency of the U^{28+} supercycle, 2.82 Hz. The bandwidth is $2.82 \times 4 \times 2 \times 880 < 20$ kbit/s.

- B2B Broadcast

Maximum 10 B2B broadcast timing frames are sent within 10 ms for each cycle. So the bandwidth is $2.82 \times 4 \times 10 \times 880 < 100$ kbit/s.

- Management Traffic

The average bandwidth for the management traffic is 10 Mbit/s. It broadcasts packets with random Ethernet frame length from 64 bytes to 1518 bytes.

The requirements for the B2B Broadcast and Unicast traffic are summarized in Tab. 5.9.

Table 5.9: B2B transfer requirements on the WR network

	Frame Loss Rate	Upper bound latency of WR network	Upper bound latency per WR switch layer
B2B Broadcast	$< 10^{-12}$	500 µs	60 µs
B2B Unicast	$< 10^{-12}$	500 µs	60 µs

For the WR network for FAIR, three VLANs with different priorities are applied according to the importance of the traffic. The DM Broadcast, DM Unicast and B2B Unicast are assigned to the VLAN 7 with the highest priority. The B2B Broadcast is assigned to the VLAN 6 with the secondary high priority and the Management Traffic is assigned to the VLAN 5 with the lowest priority.

⁵A group of consecutive frames with shorter interframe gaps than frames arriving before or after the burst of frames.

5.2. GMT systematic Investigation

5.2.2.1 WR Network Test Setup

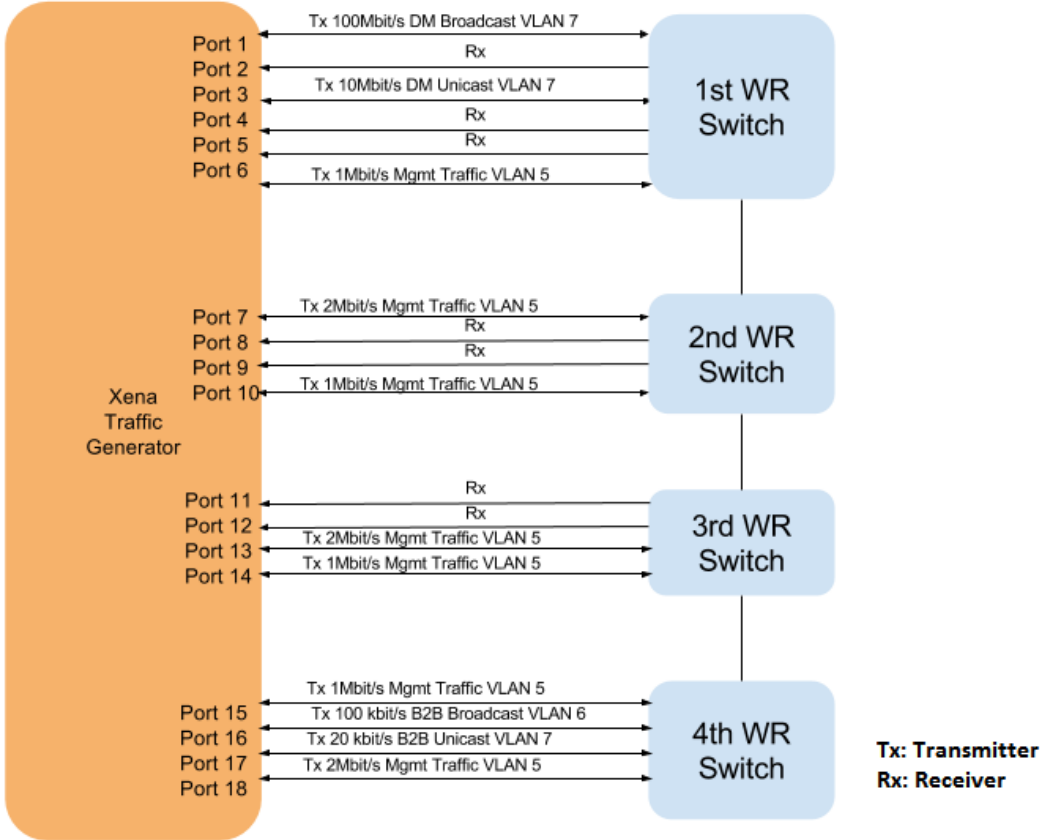


Figure 5.13: The WR network test setup.

Based on the mentioned traffic, the measurement setup is built, see Fig. 5.13. Four WR switches are connected to the port 1 to 18 of the Xena traffic generator. All ports of four WR switches are assigned to three VLANs, VLAN 5, VLAN 6 and VLAN 7. Tab. 5.10 shows the bandwidth, VLAN, VLAN priority and usage of the traffic of each Xena port in details. The test is running for 45 days. More test configuration and results, please see “Testing the WR Network of the FAIR General Machine Timing System” [50].

5.2.2.2 Test Result of Frame Loss Rate

The frame loss rate of the stream from the port 17 to the port 1 is measured for the B2B Unicast frames. The frame loss rate of the stream from the port 16 to other ports is measured for the B2B Broadcast traffic. The B2B Unicast frames have no frame loss. For the B2B Broadcast frames, the frame loss rate from the port 16 to the port 11, 12, 17 and 18 is 1.78×10^{-8} , see Fig. 5.14.

5.2. GMT systematic Investigation

Table 5.10: The connection between the traffic generator and WR switches

Switch	Xena Port	Traffic	VLAN	Priority	Usage
WR switch 1	Port 1	100 Mbit/s 110bytes	7	7	DM Broadcast
	Port 2	Rx traffic			
	Port 3	10 Mbit/s 110bytes	7	7	DM Unicast
	Port 4	Rx traffic			
	Port 5	Rx traffic			
	Port 6	1 Mbit/s 64 - 1518 bytes	5	5	Management Broadcast
WR switch 2	Port 7	2 Mbit/s 64 - 1518 bytes	5	5	Management Broadcast
	Port 8	Rx traffic			
	Port 9	Rx traffic			
	Port 10	1 Mbit/s 64 - 1518 bytes	5	5	Management Broadcast
WR switch 3	Port 11	Rx traffic			
	Port 12	Rx traffic			
	Port 13	2 Mbit/s 64 - 1518 bytes	5	5	Management Broadcast
	Port 14	1 Mbit/s 64 - 1518 bytes	5	5	Management Broadcast
WR switch 4	Port 15	1 Mbit/s 64 - 1518 bytes	5	5	Management Broadcast
	Port 16	100 kbit/s 110bytes	6	6	B2B Broadcast
	Port 17	20 kbit/s 110bytes	7	7	B2B Unicast
	Port 18	2 Mbit/s 64 - 1518 bytes	5	5	Management Broadcast

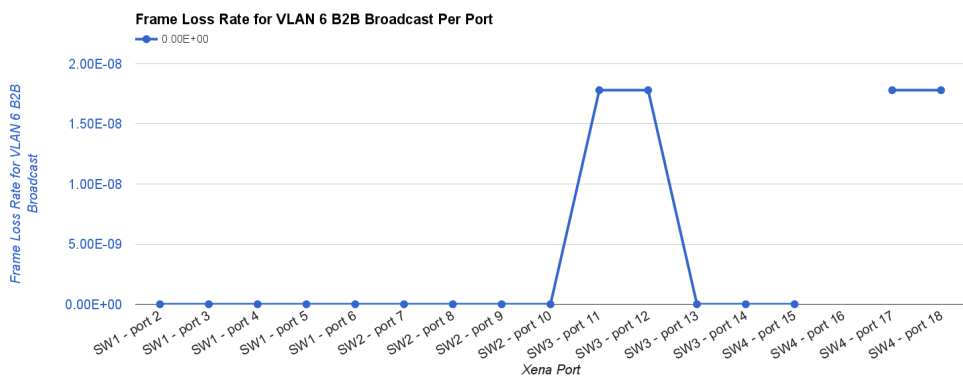


Figure 5.14: Frame loss rate of the B2B Broadcast frames.

5.2.2.3 Test Result of Latency and Jitter

- Latency and jitter for the B2B Broadcast frames

5.2. GMT systematic Investigation

For the B2B Broadcast frames, the latency and jitter of the stream from the port 16 to other ports is measured.

- Average latency and jitter

Fig. 5.15 shows the test result for the average latency and jitter for the B2B Broadcast frames. Tab. 5.11 shows the average latency and jitter of different WR switch layers. They meet the requirements of the B2B transfer, see Tab. 5.9.

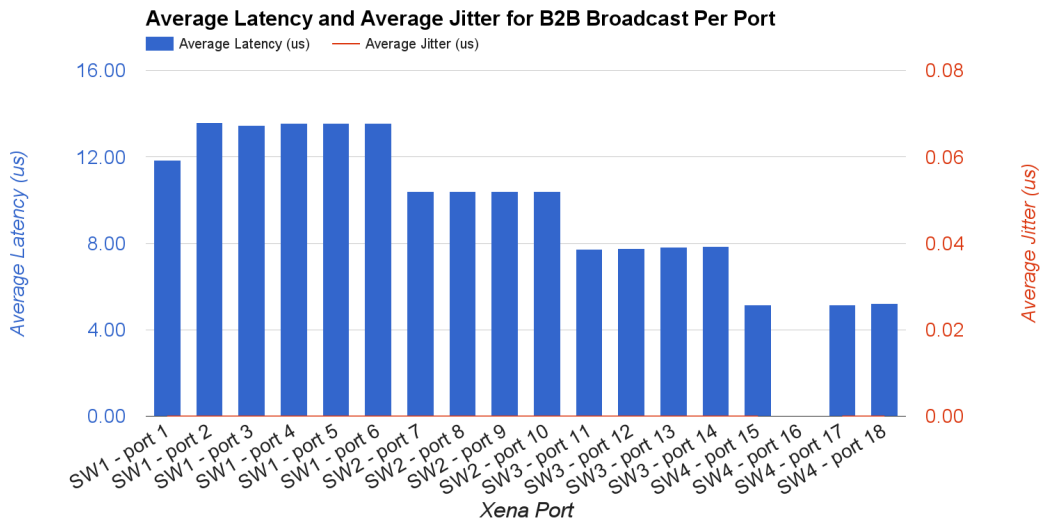


Figure 5.15: The average latency and jitter for B2B Broadcast frames.

Table 5.11: The average latency and jitter of the B2B Broadcast frames

	WR switch 4	WR switch 4, 3	WR switch 4, 3, 2	WR switch 4, 3, 2, 1
Avg latency	6 μ s	8 μ s	11 μ s	14 μ s
Avg jitter	0 ns	0 ns	0 ns	0 ns

- Maximum Latency and jitter

Fig. 5.16 shows the test result for the maximum latency and jitter for the B2B Broadcast frames. Tab. 5.12 shows the maximum latency and jitter of different WR switch layers. They meet the requirements of the B2B transfer, see Tab. 5.9.

5.2. GMT systematic Investigation

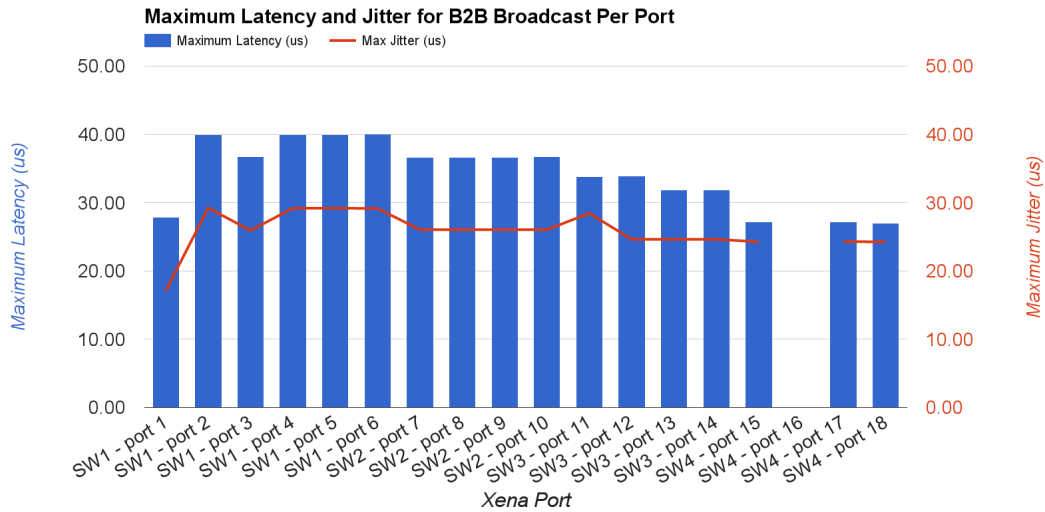


Figure 5.16: The maximum latency and jitter for B2B Broadcast frames.

Table 5.12: The maximum latency and jitter of the B2B Broadcast frames

	WR switch 4	WR switch 4, 3	WR switch 4, 3, 2	WR switch 4, 3, 2, 1
Max latency	28 μ s	34 μ s	37 μ s	41 μ s
Max jitter	25 μ s	25 μ s	27 μ s	30 μ s

- Latency and jitter for the B2B Unicast frames

For the B2B unicast frames, the latency and jitter of the stream from the port 17 to the port 1 are measured.

- Average latency and jitter

For the B2B Unicast frames, 4 WR switch network has approximate 11 μ s average latency and 0 μ s average jitter.

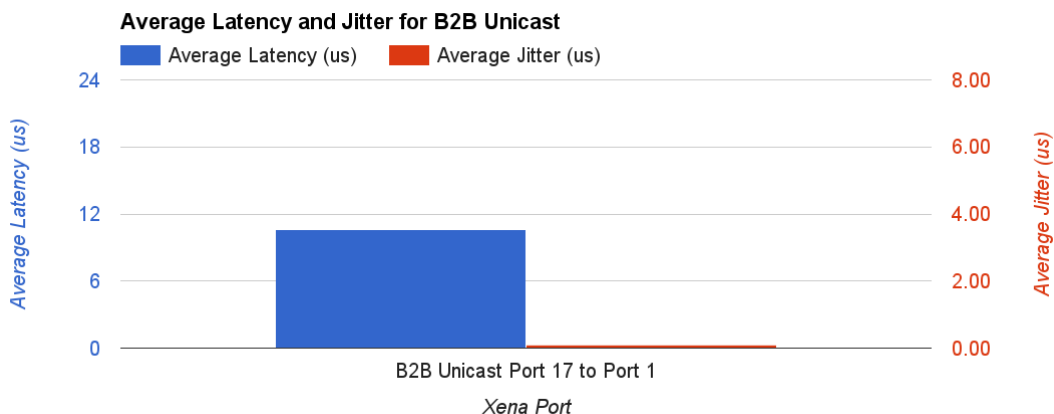


Figure 5.17: The average latency and jitter for B2B Unicast frames.

5.2. GMT systematic Investigation

- Maximum Latency and jitter

For the B2B unicast frames, 4 WR switch network has approximate 23 μ s maximum latency and 13 μ s maximum jitter.

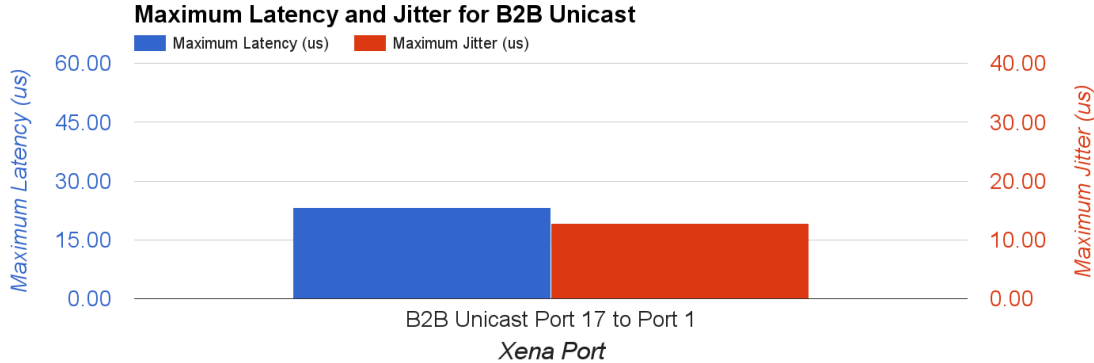


Figure 5.18: The maximum latency and jitter for B2B Unicast frames.

5.2.2.4 Conclusion

Tab. 5.13 shows the result of the test. The latency and jitter meet the requirements of the B2B Broadcast and B2B Unicast traffic. But the frame loss rate for the B2B Broadcast frames doesn't meet the requirement. The firmware of the WR switch is still under development by CERN.

Table 5.13: The result of the WR network test for the B2B transfer

	Frame Loss Rate	Average Latency	Maximum Latency	Average Jitter	Maximum Jitter
B2B Broadcast	7.12×10^{-8}	6 μ s/switch	28 μ s/switch	0 μ s/switch	25 μ s/switch
B2B Unicast	0 %	11 μ s/4switch 3 μ s/switch	23 μ s/4switch 6 μ s/switch	0 μ s/4switch 0 μ s/switch	13 μ s/4switch 4 μ s/switch

For the B2B transfer system, the upper bound latency of the frames on the WR network is 500 μ s and the upper bound latency for each WR layer is 60 μ s, see Tab.5.9. The latency of the WR network is decided by the layers of WR switches and the length of the optical fiber. The propagation of light through the core of an optical fiber is roughly about 200 m/ μ s [51] and the longest distance in the FAIR campus is around 2 km, so the latency of a 2 km optical fiber is about 10 μ s. The layers of WR switches play a more important role in the latency.

- B2B Broadcast

Here we calculate the tolerate layer of the WR switch between the B2B source SCU and the B2B target SCU, between the B2B source SCU and the source Trigger SCU and between the B2B source SCU and the target Trigger SCU.

$$\frac{500 \mu\text{s} - 10 \mu\text{s}}{60 \mu\text{s}/\text{switch}} > 8 \quad (5.33)$$

5.3. Kicker systematic Investigation

- B2B Unicast

Here we calculate the tolerate layer of the WR switch between the B2B source SCU and the DM.

$$\frac{500 \mu\text{s} - 10 \mu\text{s}}{60 \mu\text{s}/\text{switch}} > 8 \quad (5.34)$$

5.3 Kicker systematic Investigation

The SIS18 extraction kicker is consisted of nine kicker magnets. In the existing topology, five kicker magnets are equally located in the 1st crate and the other four kicker magnets are equally located in the 2nd crate. The investigation is based on the assumption that the kicker magnets in one crate are controlled by a common kicker control electronics, which received a trigger signal from a common TD module. The nine kicker magnets could also be controlled by their own kicker control electronics and TD module. It is still an open issue. The kicker magnets in the same crate are triggered instantaneous by the trigger signal with the local delay compensation of the electronics, the length of the energy transmission cable and etc. Fig. 5.19 shows the schematic diagram of the kicker magnets in the 2nd crate of the SIS18 extraction kicker. The width of each kicker magnet is 0.25 m and the distance between two kicker magnets is 0.09 m. The distance between two crates is 19.17 m [52].

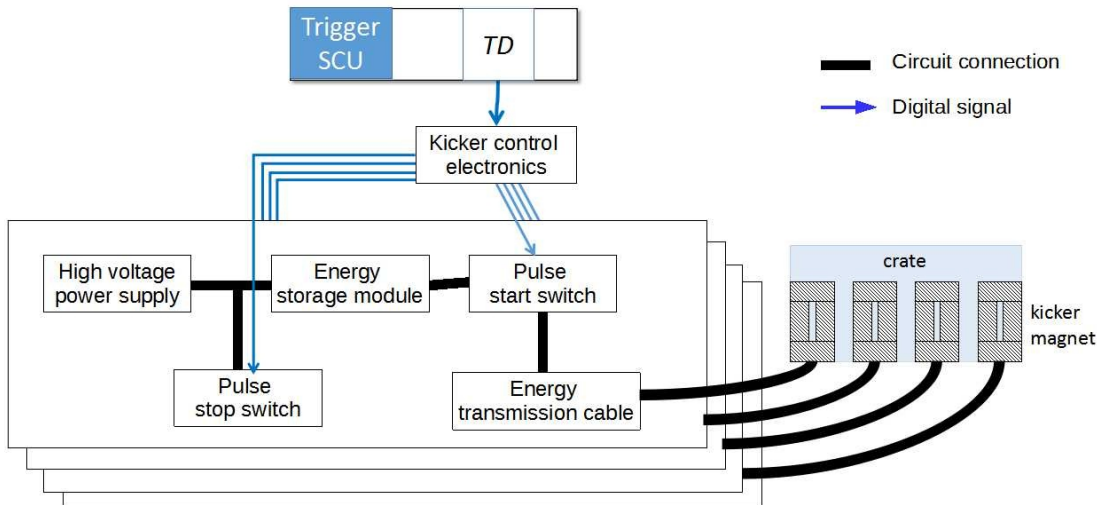


Figure 5.19: The schematic diagram of the kicker magnets in the 2nd crate of the SIS18 extraction kicker.

The SIS100 injection kicker is consisted of six kicker magnets, which are equally located in a common crate. The width of each kicker magnet is 0.22 m and the distance between two magnets is 0.23 m. For the B2B transfer, the rise time of SIS18 extraction kicker and SIS100 injection kicker magnet are 90 ns and 130 ns [53]. The kicker rise time must fit within the bunch gap, e.g. 25% of the cavity rf period [27, 39]. The bunch gap is denoted by t_{gap} . All the analysis in this section dose not take the jitter of the kicker trigger signal into consideration (approximate 1 ns). Here we are discussing about the following possibilities of the kicker trigger, which are still open issues.

5.3. Kicker systematic Investigation

- For the SIS18 extraction kicker, whether the kicker magnets in the 2nd crate could be fired a fixed delay after the firing of the kicker magnets in the 1st crate for ion beams over the whole range of stable isotopes.
- For the SIS100 injection kicker, whether the kicker magnets could be fired instantaneously.

5.3.1 SIS18 Extraction Kicker

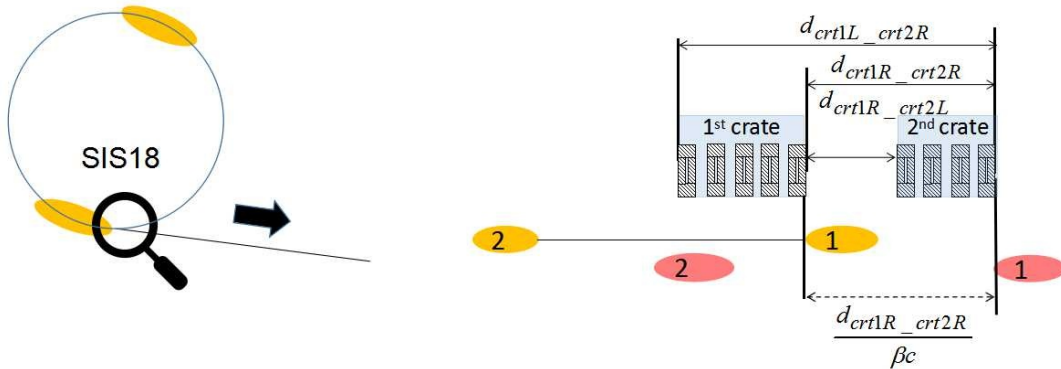


Figure 5.20: A possible firing delay between kicker magnets in two crates of SIS18 extraction kicker.

The bunch is firstly kicked by kicker magnets in the 1st crate and then kicked by the kicker magnets in the 2nd crate to the transfer line. The yellow and red ellipse represents the position of the bunches, when the kicker magnets in the 1st and 2nd crate are fired. The number in the ellipse is used to tell different bunches. The head of the bunch is at the right side. The bunch 2 is firstly kicked.

Fig. 5.20 shows a possible firing delay between kicker magnets in two crates. $d_{crt1R-crt2L}$ denotes the distance between two crates, which equals to 19.17 m. $d_{crt1L-crt2R}$ denotes the distance from the leftmost to the rightmost kicker magnet, which equals to 22.05 m = $d_{crt1R-crt2L} + 9 \times 0.25\text{ m} + 7 \times 0.09\text{ m}$. $d_{crt1R-crt2R}$ denotes the distance between the rightmost of the 1st crate to the rightmost of the 2nd crate, which equals to 20.44 m = $d_{crt1R-crt2L} + 4 \times 0.25\text{ m} + 3 \times 0.09\text{ m}$. The kicker magnets in the 1st crate are fired when the tail of the bunch 1 passes by the 1st crate completely. The kicker magnets in the 2nd crate are fired when the tail of the bunch 1 passes by the 2nd crate completely. The delay for the firing two crates in this scenario is $d_{crt1R-crt2R}/\beta c$.

5.3. Kicker systematic Investigation

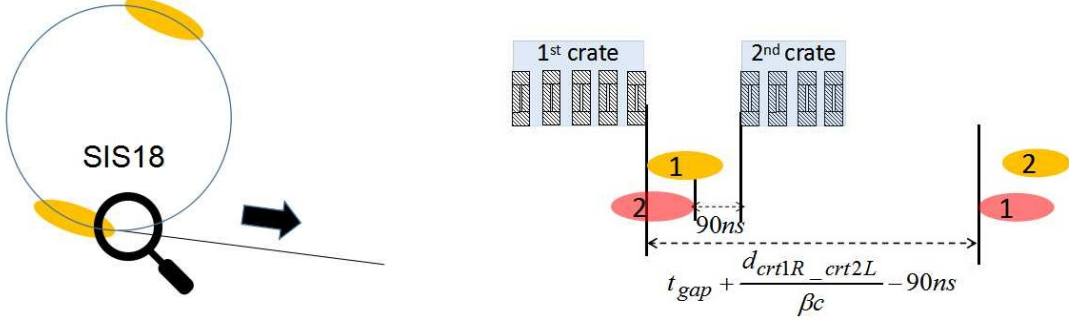


Figure 5.21: The maximum firing delay between kicker magnets in two crates of SIS18 extraction kicker.

Fig. 5.21 shows the scenario of the maximum firing delay between kicker magnets in two crates. The kicker magnets in the 1st crate are fired when the tail of the bunch 1 passes by the 1st crate completely. The kicker magnets in the 2nd crate are fired 90 ns before the head of the bunch 2 passes by it. The delay equals to $t_{gap} + d_{crt1R_crt2L}/\beta c - 90\text{ ns}$.

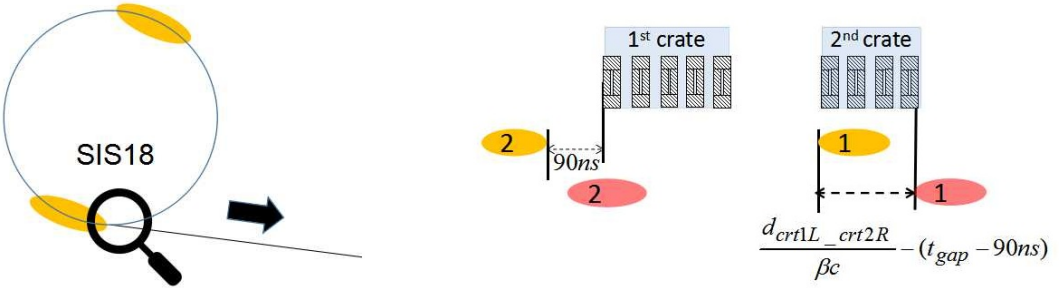


Figure 5.22: The minimum firing delay between kicker magnets in two crates of SIS18 extraction kicker.

Fig. 5.22 shows the scenario of the minimum firing delay. The kicker magnets in the 1st crate are fired 90 ns before the head of the bunch 2 passes by it. The kicker magnets in the 2nd crate are fired when the bunch 1 passes by the 2nd crate. The delay is $d_{crt1L_crt2R}/\beta c - (t_{gap} - 90\text{ ns})$.

Here we take three ion beams, H^+ , U^{28+} and U^{73+} , to check the maximum and minimum firing delay for kicker magnets in two crates, because the boundary ion species have the most stringent requirements. Tab. 5.14 shows the longest, a possible and the shortest firing delay for three ion beams.

5.3. Kicker systematic Investigation

Table 5.14: The firing delay for SIS18 kicker magnets in two crates

Beam	β	bunch gap t_{gap}	minimum delay $\frac{d_{crt1L-crt2R}}{\beta c} - (t_{gap} - 90 \text{ ns})$	possible delay $\frac{d_{crt1R-crt2R}}{\beta c}$	maximum delay $t_{gap} + (\frac{d_{crt1R-crt2L}}{\beta c} - 90 \text{ ns})$
H^+	0.982	184 ns	0 ns	69 ns	163 ns
U^{28+}	0.568	159 ns	61 ns	120 ns	189 ns
U^{73+}	0.872	104 ns	70 ns	78 ns	92 ns

According to the result, a constant firing delay is available for firing kicker magnets in two crate for all ion beams, e.g. 85 ns.

5.3.2 SIS100 Injection Kicker

Two bunches from SIS18 will be transferred into two SIS100 rf buckets in each B2B transfer. The SIS100 injection kicker must reach to the kicker flat-top during the bunch gap. For the instantaneous firing, all kicker magnets are fired only if the tail of the circulating bunch passes the rightmost kicker magnet. The “kicker passing time“ is defined as the time needed for the tail of a bunch to pass from the rightmost magnet to the leftmost kicker magnet. The rise time of the kicker magnet is shorter than 130 ns [53]. The distance from the rightmost to the leftmost kicker magnet $d_{crtL-crtR}$ is 3.79 m = $6 \times 0.22 \text{ m} + 5 \times 0.23 \text{ m}$. Two of ten buckets are always empty, so $t_{gap} = (2 + 0.25) \times T_{rf}^{SIS100}$. If the sum of the kicker passing time and rise time is shorter than the bunch gap, all kicker magnets could be fired instantaneous, see Fig. 5.15. Tab. 5.15 shows the sum of the kicker passing time and rise time for H^+ , U^{28+} and U^{73+} beams and the corresponding bunch gap.

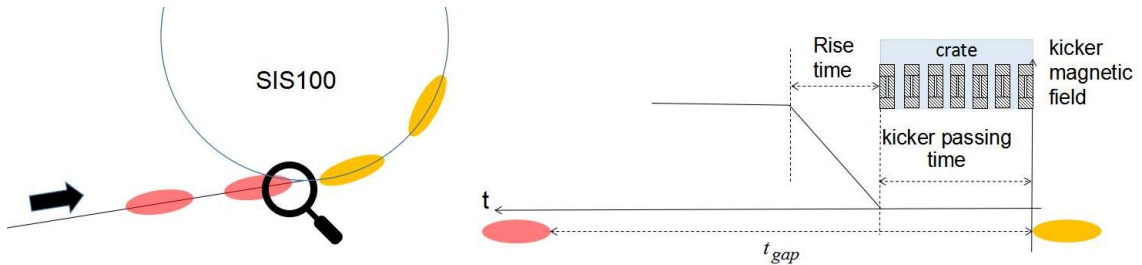


Figure 5.23: SIS100 injection kicker.

Yellow ellipse represents circulating bunches in SIS100 and red ones bunches to be injected. The head of the bunch is at the right side.

Table 5.15: The delay for firing SIS00 injection kicker

Beam	β	kicker passing time $\frac{d_{crtL-crtR}}{\beta c}$	Rise time	Sum $\frac{d_{crtL-crtR}}{\beta c} + 130 \text{ ns}$	bunch gap t_{gap}
H^+	0.982	3 ns	< 130 ns	133 ns	828 ns
U^{28+}	0.568	22 ns	< 130 ns	152 ns	1431 ns
U^{73+}	0.872	15 ns	< 130 ns	145 ns	932 ns

Tab. 5.15 shows that the sum of the kicker passing time and rise time is much shorter than the bunch gap, so the SIS100 kicker magnets could be fired instantaneous.

5.4 Test Setup for Data Collection, Merging and Redistribution

In this section, the test setup for the FAIR B2B transfer system is described, focusing mainly on the timing aspects.

5.4.1 Functionality of the Test Setup

Because some modules of the FAIR B2B transfer system are still under development, the test setup realizes partial functionality, mainly concentrated on the data collection, the data calculation and the data distribution. The detailed procedure of the partial functionality is

- After receiving CMD_B2B_START, both the B2B source and target SCUs collect the extrapolated phase equivalent data locally. The equivalence is a timestamp of the positive zero-crossing of the simulated phase measurement signal of the SIS18 and the SIS100.
- The B2B target SCU transfers the frame TGM_PHASE_TIME containing the timestamp to the B2B source SCU.
- After receiving the data, the B2B source SCU calculates the synchronization window.
- The B2B source SCU sends the frame TGM_SYNCH_WIN containing the start timestamp of the synchronization window to the WR network.
- After receiving the frame, the Trigger SCU produces a TTL output indicating the start of the synchronization window.

5.4.2 Test Setup

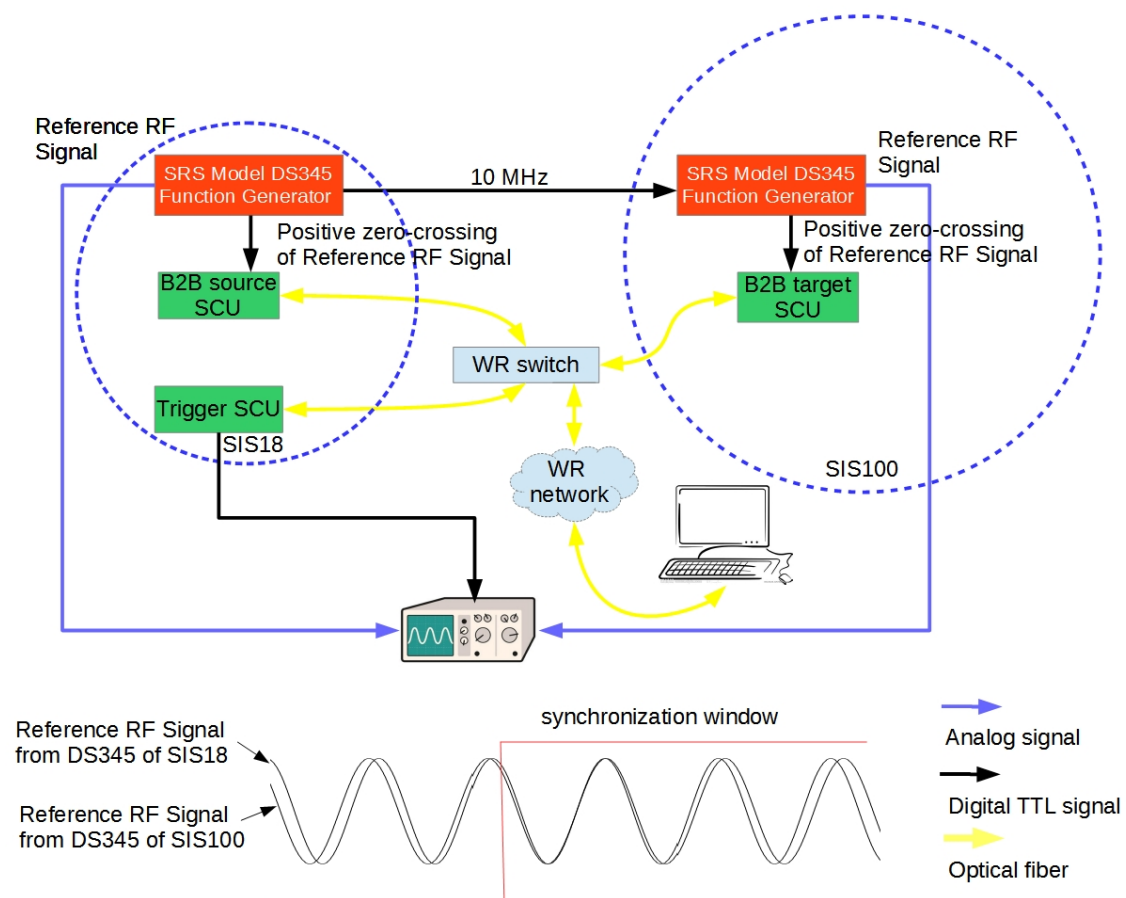


Figure 5.24: Schematic of the test setup.

Fig. 5.24 shows the schematic of the test setup. In this test setup, two SRS MODEL DS345 Synthesized Function Generators⁶ (short: DS345) are used to simulate the phase measurement signals of the SIS18 and that of the SIS100, which are with the frequency accuracy of ± 5 ppm (parts per million) of selected frequency. The DS345 of the SIS18 is synchronized to an internal 10 MHz clock, which works as an external reference clock for the DS345 of the SIS100. The B2B source SCU, the B2B target SCU and the Trigger SCU are connected to a WR switch, which connects to the timing network. A PC⁷ is used as a DM to produce the B2B start timing frame CMD_B2B_START. Besides, it monitors the status of the B2B transfer programs in all SCUs. The oscilloscope is used to monitor the alignment of two simulated phase measurement signals within the synchronization window provided by the Trigger SCU.

Fig. 5.25 shows the front view of the real test setup. The SIS18 DS345 produces 1.572 200 MHz sine wave and the SIS100 DS345 produces 1.572 000 MHz sine wave to the oscilloscope. The SIS18 DS345 produces a digital TTL signal for the B2B

⁶<http://www.thinksrs.com/downloads/PDFs/Manuals/DS345m.pdf>

⁷A Linux personal computer is installed with the standard TR tools and library.

<https://www-acc.gsi.de/wiki/Timing/TimingSystemNodesCurrentRelease>

5.4. Test Setup for Data Collection, Merging and Redistribution

source SCU, whose rising edges are aligned with the positive zero-crossings of the sine wave of 1.572 200 MHz and the SIS100 DS345 produces a digital TTL signal for the B2B target SCU, whose rising edges are synchronized to the positive zero-crossings of the sine wave of 1.572 000 MHz. So the beating frequency is 200 Hz and the beating period is 5 ms.

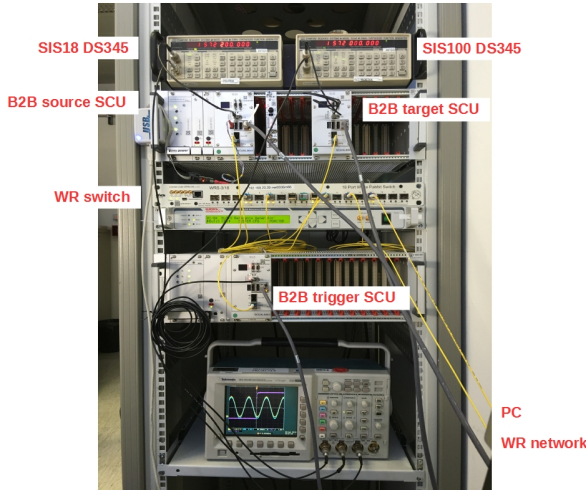


Figure 5.25: The front view of the test setup.

Compared with the final scenario, there are some difference of the test setup.

- The phase measurement signals will be produced by the Group DDS.
- The B2B source and target SCUs will get the phase of the phase measurement signals directly from the PAP modules.
- The B2B source SCU will transfer the required phase shift to the PSM for the phase shift and the phase correction to the Trigger SCUs.
- The B2B Trigger SCU will consider not only the synchronization window, but also the kicker delay compensation from the SM. Besides, it has several SCU slaves, which coordinate the correct B2B extraction and injection kicker with other systems, e.g. the MPS.

5.4.3 Firmware

The B2B source, B2B target and Trigger SCUs have different firmware running on their soft CPU, LM32⁸. The firmware are activated by the B2B start timing frame, CMD_B2B_START, which indicates the source and target synchrotrons of the B2B transfer.

- Firmware for the B2B source SCU

The firmware for the B2B source SCU is the core program of the B2B transfer system, see Fig. 5.26.

⁸LatticeMico32 is a 32-bit microprocessor soft core from Lattice Semiconductor optimized for field-programmable gate arrays (FPGAs).

5.4. Test Setup for Data Collection, Merging and Redistribution

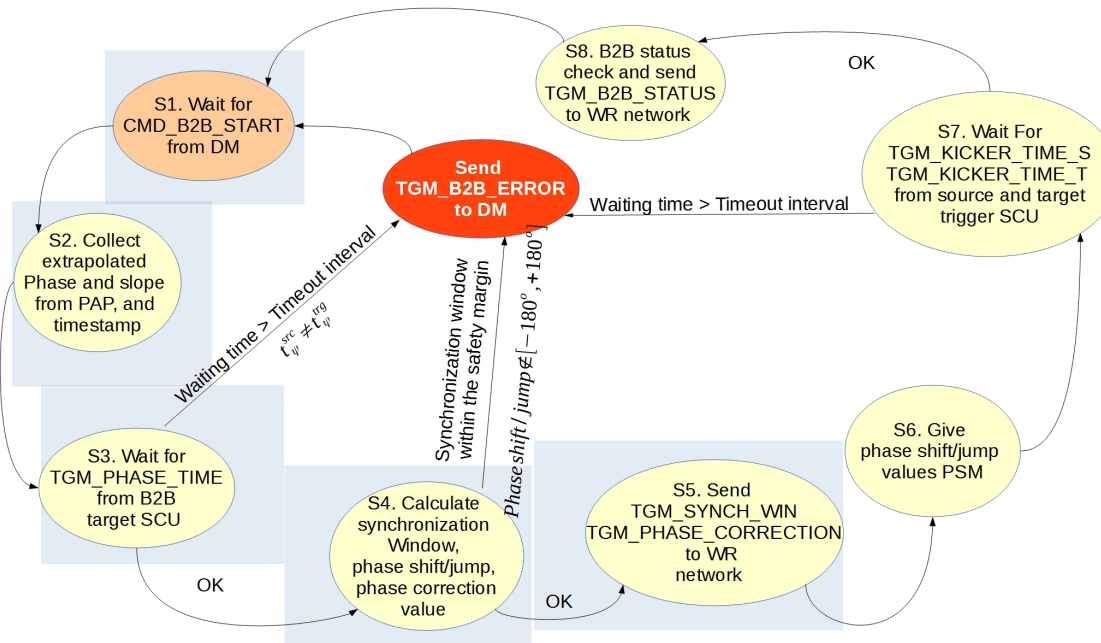


Figure 5.26: Flow chart of the firmware for the B2B source SCU.

“Step“ is represented as “S“ in the figure. The steps realized by the test setup are marked by the blue rectangle.

- Step 1. The program waits for the `CMD_START_B2B` timing frame.
- Step 2. When it receives the timing frame `CMD_START_B2B`, the program reads the extrapolated phase and the phase deviation slope from the PAP module, as well as the corresponding timestamp .
- Step 3. The program waits for the `TGM_PHASE_TIME` timing frame from the B2B target SCU, which contains the extrapolated phase, the corresponding timestamp and the slope of the phase deviation.
- Step 4. When the program receives the timing frame `TGM_PHASE_TIME` within a specified timeout interval, it checks whether the timestamp of the extrapolated phase of the target synchrotron equals to that of the source synchrotron. When they are equal, the program calculates the synchronization window, the phase shift/jump value and the phase correction value. When the program doesn't receive the timing frame `TGM_PHASE_TIME` within a specified timeout interval or two timestamp are not equal, it sends a timing frame `TGM_B2B_ERROR` to the WR network and goes back to the step 1, which indicates the timeout error of the frame. Besides, it checks whether the required phase shift is within the range of -180° to 180° and whether the start of the synchronization window is in the safety margin. If at least one of them is not correct, it sends a timing frame `TGM_B2B_ERROR` to the WR network and goes back to the step 1, which indicates the calculation error.
- Step 5. The program sends the timing frame `TGM_SYNCH_WIN` and `TGM_PHASE_CORRECTION` to the WR network. `TGM_SYNCH_WIN` indicates the start of the synchronization window and `TGM_PHASE_CORRECTION` is used for the Trigger

5.4. Test Setup for Data Collection, Merging and Redistribution

SCUs for the reproduction of the bucket indication signal.

- Step 6. The program gives the phase correction and phase shift/jump values to corresponding modules.
- Step 7. The program waits for the timing frame TGM_KICKER_TIME_S from the source Trigger SCU and TGM_KICKER_TIME_T from the target Trigger SCU, which contains the extraction/injection kicker trigger and firing timestamp. When it does not receive the timing frames within a specified timeout interval, it sends a timing frame TGM_B2B_ERROR to the WR network and goes back to the step 1, which indicates the timeout error of the frame.
- Step 8. When the program receives the timing frames mentioned in the step 7 within a specified timeout interval, it checks the B2B transfer status and sends TGM_B2B_STATUS to the WR network and goes to the step 1. The B2B transfer is successful, if all of the following checks are correct. Or the B2B transfer is failure.
 - * Trigger time < firing time of the extraction kicker of the source synchrotron
 - * Trigger time < firing time of the injection kicker of the target synchrotron
 - * Firing time of the extraction kicker < firing time of the injection kicker
- Firmware for the B2B target SCU

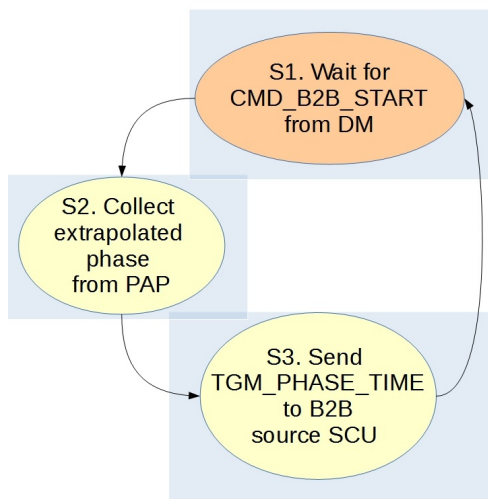


Figure 5.27: Flow chart of the firmware for the B2B target SCU.

“Step“ is represented as “S“ in the figure. The steps realized by the test setup are marked by the blue rectangle.

Fig. 5.27 shows the flow chart of the program of the B2B target SCU.

5.4. Test Setup for Data Collection, Merging and Redistribution

- Step 1. The program waits for the CMD_START_B2B timing frame.
- Step 2. When it receives the timing frame CMD_START_B2B, the program collects the extrapolated phase.
- Step 3. The program sends the TGM_PHASE_TIME timing frame to the B2B source SCU and goes back to the step 1.
- Firmware for the Trigger SCU

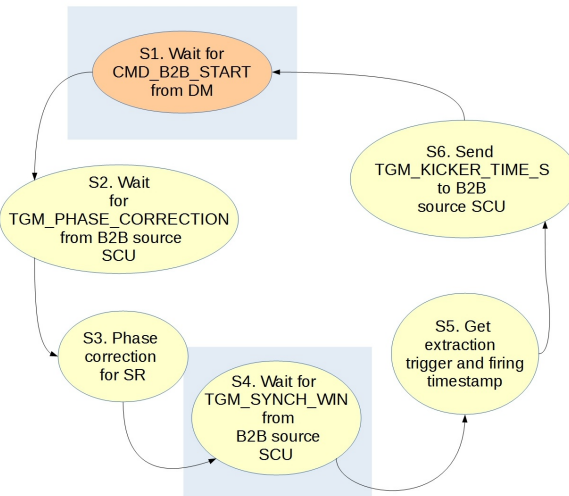


Figure 5.28: Flow chart of the firmware for the B2B Trigger SCU.

“Step“ is represented as “S“ in the figure. The steps realized by the test setup are marked by the blue rectangle.

Fig. 5.28 shows the flow chart of the program of the source Trigger SCU. For the target Trigger SCU, the flow chat is same only with the different name of the timing frame TGM_KICKER_TIME_T.

- Step 1. The program waits for the CMD_START_B2B timing frame.
- Step 2. The program waits for the TGM_PHASE_CORRECTION timing frame.
- Step 3. The program gives the phase correction value to the corresponding SR module for the bucket indication signal reproduction.
- Step 4. The program waits for the timing frame TGM_SYNCH_WIN to indicate the synchronization window for the kicker trigger.
- Step 5. After the beam extraction, the program collects the trigger and firing timestamp.
- Step 6. The program sends the TGM_KICKER_TIME_S timing frame to the B2B source SCU and goes back to the step 1.

5.4.4 Time Constraints

For the FAIR B2B transfer system, the time constraints are very important and strict. Because beam feedback loops are switched off before the B2B transfer, the

5.4. Test Setup for Data Collection, Merging and Redistribution

beam is stable only for a period of time. For FAIR, the upper bound B2B transfer time is 10 ms.

Fig. 5.29 shows the time constraint of the system. The `CMD_START_B2B` is executed at t_{B2B} . The PAP module needs 500 μ s for the phase extrapolation, so the B2B source and target SCUs collect the extrapolated phase and the slope from the PAP module at $t_{B2B} + 500 \mu\text{s}$. The upper bound latency of the timing frame `TGM_PHASE_TIME` transfer on the WR network from the B2B target SCU to the B2B source SCU is 500 μs , so the B2B source SCU receives the timing frame `TGM_PHASE_TIME` at around $t_{B2B} + 500 \mu\text{s} + 500 \mu\text{s} = t_{B2B} + 1 \text{ ms}$. After that, the B2B source SCU needs about 100 μs for the calculation, the sending of the timing frames `TGM_SYNCH_WIN` and `TGM_PHASE_CORRECTION` and the data transferring to the corresponding module. The timing frames `TGM_SYNCH_WIN` and `TGM_PHASE_CORRECTION` are sent by the B2B source SCU at around $t_{B2B} + 1 \text{ ms} + 100 \mu\text{s} = t_{B2B} + 1.1 \text{ ms}$. The upper bound latency of the timing frame transfer on the WR network from the B2B source SCU to the Trigger SCUs is 500 μs , so the Trigger SCUs receives `TGM_PHASE_CORRECTION` and `TGM_SYNCH_WIN` at around $t_{B2B} + 1.1 \text{ ms} + 500 \mu\text{s} = t_{B2B} + 1.6 \text{ ms}$. The start of the synchronization window must be later than $t_{B2B} + 1.1 \text{ ms} + 2 \times 500 \mu\text{s} = t_{B2B} + 2.1 \text{ ms}$. Two upper bound latency of the WR network are caused by the timing frame `TGM_SYNCH_WIN` transfer from the B2B source SCU back to the DM and further from the DM to the BI devices. After bunches are transferred into buckets, there is no hard real time requirement for the Trigger SCU to collect the trigger and firing timestamps and to send the timing frame `TGM_KICKER_TIME_S`, so 1 ms is used for the source Trigger SCU to do this task and the source Trigger SCU sends `TGM_KICKER_TIME_S` at around $t_{B2B} + 10 \text{ ms} + 1 \text{ ms} = t_{B2B} + 11 \text{ ms}$. The same time constraints is also for the target Trigger SCU. The B2B source SCU receives `TGM_KICKER_TIME_S` and `TGM_KICKER_TIME_T` from the WR network at around $t_{B2B} + 11 \text{ ms} + 500 \mu\text{s} = t_{B2B} + 11.5 \text{ ms}$. The B2B source SCU uses 100 μs to check the B2B transfer status and sends `TGM_B2B_STATUS` at around $t_{B2B} + 11.5 \text{ ms} + 100 \mu\text{s} = t_{B2B} + 11.6 \text{ ms}$. The BI devices receives the timing frame `TGM_B2B_STATUS` at around $t_{B2B} + 11.6 \text{ ms} + 2 \times 500 \mu\text{s} = t_{B2B} + 12.6 \text{ ms}$. $2 \times 500 \mu\text{s}$ is two upper bound latency of the WR network, which is caused by the timing frame `TGM_B2B_STATUS` transfer from the B2B source SCU back to the DM and further from the DM to the BI devices.

5.4. Test Setup for Data Collection, Merging and Redistribution

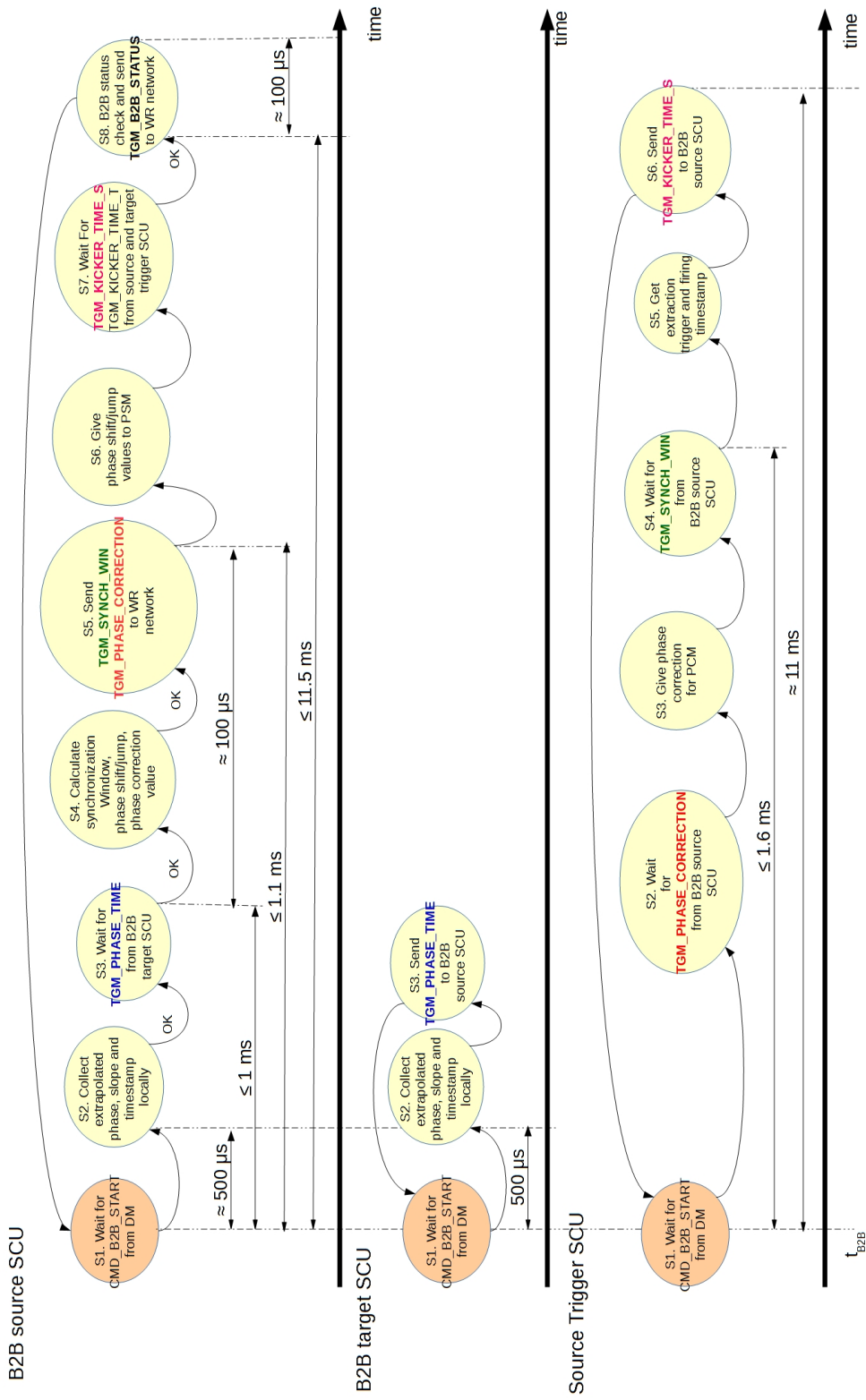


Figure 5.29: The time constraints of the B2B transfer system.

The sent and received timing frame pairs have the same color. (not drawn to accurate timescale)

5.4. Test Setup for Data Collection, Merging and Redistribution

5.4.5 Test Result

The steps with the blue rectangle in Fig. 5.29 are realized in this test setup. The test takes the U^{28+} B2B transfer from the SIS18 to the SIS100 with 200 Hz detuning on the SIS18 as an example. All timestamp are in the format of Greenwich Mean Time (GMT). The test result of the programs on the B2B source, B2B target and Trigger SCUs are shown as follows.

```
1 U28+ B2B transfer from SIS18 to SIS100 => B2B source SCU
2 -----
3
4 SIS18 phase measurement signal 1.572200MHz
5 SIS100 phase measurement signal 1.572000MHz
6 SIS18 period of phase measurement signal 636051(ps)
7 SIS100 period of phase measurement signal 636132(ps)
8
9 >>>>>>>>> Receive CMD_START_B2B from WR network
10 Timestamp of the SIS18 phase measurement signal (accuracy to 1ns}
11 GMT: Thu, Jan 8, 1970, 21:07:27.445405856
12
13 >>>>>>>>> Receive TGM_PHASE_TIME from WR network
14 Timestamp of the SIS100 phase measurement signal (accuracy to 1ns)
15 GMT: Thu, Jan 8, 1970, 21:07:27.445364560
16
17 Beating frequency: 200 Hz
18 Synchronization time: 4.622818 ms
19 The number of the period of SIS18 phase measurement signal for the
   synchronization: 7268
20 Start of the synchronization window: GMT: Thu, Jan 8, 1970,
   21:07:27.450028674
21
22 <<<<<<<<<<< Send TGM_SYNCH_WIN to WR network
```

```
1 U28+ B2B transfer from SIS18 to SIS100 => B2B target SCU
2 -----
3
4 >>>>>>>>> Receive CMD_START_B2B from WR network
5 Timestamp of the phase measurement signal from SIS100 (accuracy to 1ns)
6 GMT: Thu, Jan 8, 1970, 21:07:27.445364560
7
8 <<<<<<<<<<< Send TGM_PHASE_TIME to WR network
```

```
1 U28+ B2B transfer from SIS18 to SIS100 => Trigger SCU
2 -----
3
4 Waiting for timing frames...
5 >>>>>>>>>> Receive TGM_SYNCH_WIN from WR network
6 Event execution timestamp: GMT 1970-01-08 21:07:27.450028674
```

Chapter 6

Application of FAIR B2B Transfer System for FAIR Accelerators

For the FAIR B2B transfer system, both the phase shift and frequency beating methods are applicable. However, the phase shift method must be executed slowly enough to preserve the beam longitudinal emittance, which needs much longer time than the frequency beating method for the synchronization. Besides, many FAIR accelerator pairs are beating automatically due to the non-integer ratio of the circumference between two synchrotrons. So there is a preference for FAIR to use the frequency beating method. In this chapter all FAIR use cases with the frequency beating method will be discussed in details. Based on the circumference ratio, there are three scenarios of the B2B transfer for FAIR.

- The circumference ratio between the large and small synchrotrons is an integer.
 - The B2B transfer from the SIS18 to the SIS100
- The circumference ratio between the large and small synchrotrons is close to an integer.
 - The B2B transfer from the SIS18 to the ESR¹
 - The B2B transfer from the ESR² to the CRYRING
- The circumference ratio between the large and small synchrotrons is far away from an integer.
 - The B2B transfer from the CR to the HESR

Besides, FAIR has many use cases of B2B transfers that the extraction and injection beam have different energy because of targets installed between two synchrotrons (e.g. a Pbar, a FRS and a Super FRS). Due to the energy loss at the target, the beam revolution frequency ratio between the small and large synchrotrons is used instead of the circumference ratio between the large and small synchrotrons. The revolution frequency ratio takes the energy loss into consideration. For FAIR, there exists the following scenario.

¹Injection orbit

²Extraction orbit

6.1. Circumference Ratio is an Integer

- The revolution frequency ratio between the small and large synchrotrons is far away from an integer.
- The B2B transfer from the SIS100 to the CR via a Super FRS
- The B2B transfer from the SIS18 to the ESR via a FRS

Tab. 6.1 lists all FAIR use cases of the B2B transfer. m , n and κ are integers.

Table 6.1: List of the FAIR B2B transfer use cases

Circumference ratio	C^l/C^s	f_{rev}^s/f_{rev}^l	Use cases of FAIR accelerators
$C^l/C^s = \kappa$ an integer	5		U^{28+} B2B transfer from the SIS18 to the SIS100
	5		H^+ B2B transfer from the SIS18 to the SIS100
$C^l/C^s = \kappa + \lambda$ or $f_{rev}^s/f_{rev}^l = \kappa + \lambda$ close to an integer ($ \lambda \leq 0.005$)	2-0.003		h=4 B2B transfer from the SIS18 to the ESR
	2-0.003		h=1 B2B transfer from the SIS18 to the ESR
	2+0.003		B2B transfer from the ESR to the CRYRING
$C^l/C^s = m/n + \lambda$ or f_{rev}^s/f_{rev}^l $= m/n + \lambda$ far away from an integer ($ \lambda \leq 0.05$)	not applicable	4.8-0.039	H^+ B2B transfer from the SIS100 to the CR via a Pbar
	not applicable	4.4-0.0046	Rare isotope beams (RIB) B2B transfer from the SIS100 to the CR via a Super FRS
	2.6-0.003		B2B transfer from the CR to the HESR
	not applicable	1.8+0.036	B2B transfer from the SIS18 to the ESR via a FRS

6.1 Circumference Ratio is an Integer

When the circumference ratio of the large synchrotron to that of the small synchrotron is an integer, there exists the following relation between two cavity rf frequencies, see Chap. 2.

$$\frac{f_{rf}^l}{f_{rf}^s} = \frac{h^l}{h^s \cdot \kappa} \quad (6.1)$$

6.1. Circumference Ratio is an Integer

Two synchronization frequencies are

$$f_{syn}^l = \frac{f_{rf}^l}{h^l/Y} = Y f_{rev}^l \quad (6.2)$$

$$f_{syn}^s = \frac{f_{rf}^s}{h^s \kappa/Y} = \frac{Y}{\kappa} f_{rev}^s \quad (6.3)$$

Y is the GCD of h^l and $h^s \cdot \kappa$. More details, please see Sec. 2.2.1.

For the frequency beating method, two slightly different frequencies are chosen based on f_{syn}^l and f_{syn}^s by detuning Δf_{syn} either (or both) of rf systems. Generally the rf system of the source synchrotron is preferred to be detuned, which is easy to be achieved during or after the acceleration ramp.

The frequency of the bucket indication signal depends on the relation between f_{syn}^{trg} and f_{rev}^{trg} , see Chap. 4. When the large synchrotron is the target, there exists $f_{syn}^l = Y f_{rev}^l \geq f_{rev}^l$. The revolution period is Y times as long as the period of f_{syn}^l . The period of f_{syn}^l is not long enough to contain all buckets. So $f_{bucket} = f_{rev}^l$ and the length of the synchronization window $T_w = T_{rev}^l$ for this case. Tab. 6.2 shows the formulas for the frequency of the bucket indication signal f_{bucket} , the synchronization frequencies f_{syn}^X , the frequencies of two phase measurement signals f_{B2B}^X , the frequency of the synchronization reference signal f_{syn}^{REF} , the length of the synchronization window T_w and the bunch and bucket injection center mismatch $\Delta\phi_{rf}$ when the large synchrotron is the target.

Table 6.2: Parameters related to the B2B transfer when the circumference ratio is an integer and the large synchrotron is the target

Large synchrotron is target synchrotron	
f_{bucket}	f_{rev}^l
f_{syn}^X	$f_{syn}^s = \frac{f_{rf}^s}{h^s \kappa/Y}$ and $f_{syn}^l = \frac{f_{rf}^l}{h^l/Y}$
f_{B2B}^X	$f_{B2B}^s = \frac{f_{rev}^l}{f_{syn}^l} \cdot (f_{syn}^s + \Delta f_{syn}) = \frac{1}{\kappa} (f_{rev}^s + \frac{\kappa}{Y} \Delta f_{syn})$ and $f_{B2B}^l = f_{rev}^l$
f_{syn}^{REF}	$round(f_{rev}^l / 100 \text{ kHz}) \cdot 100 \text{ kHz}$
T_w	T_{rev}^l
$\Delta\phi_{rf}$	$\pm \frac{1}{2} \cdot 2\pi f_{syn}^s - f_{syn}^l \cdot T_w \cdot \frac{f_{rf}^l}{f_{syn}^l}$

When the small synchrotron is the target, the relation between $f_{syn}^s = \frac{Y}{\kappa} f_{rev}^s$ and f_{rev}^s is not fixed. If $f_{syn}^s \geq f_{rev}^s$, namely $\frac{Y}{\kappa} \geq 1$, the revolution period is $\frac{Y}{\kappa}$ times as long as the period of f_{syn}^s . Hence, $f_{bucket} = f_{rev}^s$ and $T_w = T_{rev}^s$ for this case. Oppositely, if $f_{syn}^s < f_{rev}^s$, namely $\frac{Y}{\kappa} < 1$, the period of f_{syn}^s is $\frac{\kappa}{Y}$ times as long as the revolution period. Hence, $f_{bucket} = f_{syn}^s$ and $T_w = T_{syn}^s$. Tab. 6.3 shows the formulas when the small synchrotron is the target.

6.1.1 Use Case of U^{28+} B2B Transfer from SIS18 to SIS100

The use case of the U^{28+} B2B transfer from the SIS18 to the SIS100 belongs to this scenario. Four batches of U^{28+} at 200 MeV/u are injected into continuous eight out

6.1. Circumference Ratio is an Integer

Table 6.3: Parameters related to the B2B transfer when the circumference ratio is an integer and the small synchrotron is the target

	Small synchrotron is target synchrotron	
Case	(1) $f_{syn}^s \geq f_{rev}^s (\frac{Y}{\kappa} \geq 1)$	(2) $f_{syn}^s < f_{rev}^s (\frac{Y}{\kappa} < 1)$
f_{bucket}	f_{rev}^s	f_{syn}^s
f_{syn}^X	$f_{syn}^s = \frac{f_{rf}^s}{h^s \kappa / Y}$ and $f_{syn}^l = \frac{f_{rf}^l}{h^l / Y}$	
f_{B2B}^X	$f_{B2B}^l = \frac{f_{rev}^s}{f_{syn}^s} \cdot (f_{syn}^l + \Delta f_{syn})$ $= \kappa(f_{rev}^l + \frac{1}{Y} \Delta f_{syn})$ and $f_{B2B}^s = f_{rev}^s$	$f_{B2B}^l = f_{syn}^l + \Delta f_{syn}$ $= Y(f_{rev}^l + \frac{1}{Y} \Delta f_{syn})$ and $f_{B2B}^s = f_{syn}^s = \frac{Y}{\kappa} f_{rev}^s$
f_{syn}^{REF}	$round(f_{rev}^s / 100 \text{ kHz}) \cdot 100 \text{ kHz}$	$round(f_{syn}^s / 100 \text{ kHz}) \cdot 100 \text{ kHz}$
T_w	T_{rev}^s	T_{syn}^s
$\Delta\phi_{rf}$	$\pm \frac{1}{2} \cdot 2\pi f_{syn}^s - f_{syn}^l \cdot T_w \cdot \frac{f_{rf}^s}{f_{syn}^s}$	

of ten buckets of the SIS100. Each batch consists of two bunches [38, 39]. The large synchrotron is the SIS100 and the small one the SIS18. $\kappa = 5$, $h^{SIS100} = 10$ and $h^{SIS18} = 2$. The GCD of $h^{SIS100} = 10$ and $h^{SIS18} \cdot \kappa = 2 \cdot 5 = 10$ is 10, namely $Y = 10$. Substituting these values into eq. 6.1, we get

$$\frac{f_{rf}^{SIS100}}{f_{rf}^{SIS18}} = \frac{h^{SIS100}}{h^{SIS18} \cdot \kappa} = \frac{10}{2 \cdot 5} = \frac{10}{10} \quad (6.4)$$

Because the SIS100 is the large synchrotron and the target, substituting h^X , κ , f_{rf}^X , f_{rev}^X and Y into formulas in Tab. 6.2, the parameters related to the U^{28+} B2B transfer from the SIS18 to the SIS100 is obtained, see Tab. 6.4. Here we assume that the SIS18 is detuned with 200 Hz for the synchronization frequency f_{syn}^{SIS18} .

Table 6.4: Parameters related to the U^{28+} B2B transfer from the SIS18 to the SIS100 with the frequency beating method

	Large synchrotron (SIS100) is target synchrotron
f_{bucket}	$f_{rev}^{SIS100} = 157.254 \text{ kHz}^3$
f_{syn}^X	$f_{syn}^{SIS18} = f_{rf}^{SIS18} = 1.572536 \text{ MHz}$ and $f_{syn}^{SIS100} = f_{rf}^{SIS100} = 1.572536 \text{ MHz}$
f_{B2B}^X	$f_{B2B}^{SIS18} = \frac{1}{5}(f_{rev}^{SIS18} + \frac{1}{2} \Delta f_{syn}) = 157.254 \text{ kHz} + 20 \text{ Hz}$ and $f_{B2B}^{SIS100} = 157.254 \text{ kHz}$
f_{syn}^{REF}	200 kHz
T_w	$T_{rev}^{SIS100} = 6.359 \mu\text{s}$
$\Delta\phi_{rf}$	$\pm 0.4^\circ$

³A Group DDS produces a given frequency with the mHz order of magnitude precision

6.1. Circumference Ratio is an Integer

The target time difference between the SIS18 and SIS100 rf systems equals to $t_{v_ext} + t_{v_inj} + t_{TOF}$, provided by the SM. The SIS100 revolution frequency works for the bucket indication. When the 1st and 2nd buckets are to be filled, $t_{pattern} = 0$. When the 3rd and 4th buckets are to be filled, $t_{pattern} = T_{rev}^{SIS18}$. When the 5th and 6th buckets are to be filled, $t_{pattern} = 2 \cdot T_{rev}^{SIS18}$. When the 7th and 8th buckets are to be filled, $t_{pattern} = 3 \cdot T_{rev}^{SIS18}$. Detailed parameters of the U^{28+} B2B transfer from the SIS18 to the SIS100, please see Appendix C.1.

6.1.2 Use Case of H^+ B2B Transfer from SIS18 to SIS100

Four batches of H^+ at 4 GeV/u are injected into continuous four out of ten buckets of the SIS100. Each batch consists of one bunch [38, 39]. The large synchrotron is the SIS100 and the small one the SIS18. $\kappa = 5$, $h^{SIS100} = 10$ and $h^{SIS18} = 1$. The GCD of $h^{SIS100} = 10$ and $h^{SIS18} \cdot \kappa = 1 \cdot 5$ is 5, namely $Y = 5$. Substituting these values into eq. 6.1, we get

$$\frac{f_{rf}^{SIS100}}{f_{rf}^{SIS18}} = \frac{h^{SIS100}}{h^{SIS18} \cdot \kappa} = \frac{10}{1 \cdot 5} = \frac{2}{1} \quad (6.5)$$

Because the SIS100 is the large synchrotron and the target, substituting h^X , κ , f_{rf}^X , f_{rev}^X and Y into formulas in Tab. 6.2, the parameters related to the H^+ B2B transfer from the SIS18 to the SIS100 is obtained, see Tab. 6.5. Here we assume that the SIS18 is detuned with 200 Hz for the synchronization frequency f_{syn}^{SIS18} .

Table 6.5: Parameters related to the H^+ B2B transfer from the SIS18 to the SIS100 with the frequency beating method

	Large synchrotron (SIS100) is target synchrotron
f_{bucket}	$f_{rev}^{SIS100} = 271.872$ kHz
f_{syn}^X	$f_{syn}^{SIS18} = f_{rf}^{SIS18} = 1.359\,358$ MHz and $f_{syn}^{SIS100} = f_{rf}^{SIS100}/2 = 1.359\,358$ MHz
f_{B2B}^X	$f_{B2B}^{SIS18} = \frac{1}{5}(f_{rev}^{SIS18} + \Delta f_{syn}) = 271.872$ kHz + 40 Hz and $f_{B2B}^{SIS100} = 271.872$ kHz
f_{syn}^{REF}	300 kHz
T_w	$T_{rev}^{SIS100} = 3.678$ μ s
$\Delta\phi_{rf}$	$\pm 0.4^\circ$

The SIS100 revolution frequency works for the bucket indication. In order to inject into the odd and even number buckets, there are two scenarios of the target time difference between the SIS18 and SIS100 rf systems.

- Injection into odd number buckets

The target time difference between the SIS18 and SIS100 rf systems equals to $t_{v_ext} + t_{v_inj} + t_{TOF}$. When the 1st bucket is to be filled, $t_{pattern}=0$. When the 3rd bucket is to be filled, $t_{pattern} = 1 \cdot T_{rev}^{SIS18}$.

6.2. Circumference Ratio is close to an Integer

- Injection into even number buckets

The target time difference between the SIS18 and SIS100 rf systems equals to $t_{v_ext} + t_{v_inj} + t_{TOF} - T_{rf}^{SIS100}$. When the 2nd bucket is to be filled, $t_{pattern} = 0$. When the 4th bucket is to be filled, $t_{pattern} = 1 \cdot T_{rev}^{SIS18}$.

Detailed parameters of the H^+ B2B transfer from the SIS18 to the SIS100, please see Appendix C.1.

6.2 Circumference Ratio is close to an Integer

When the circumference ratio of the large synchrotron to that of the small synchrotron is very close to an integer, there exists the relation between two cavity rf frequencies, see Chap. 2.

$$\frac{f_{rf}^l}{f_{rf}^s} = \frac{h^l}{h^s \cdot (\kappa + \lambda)} = \frac{h^l}{h^s \cdot \kappa + h^s \cdot \lambda} \quad (6.6)$$

Besides, it is also grouped to this scenario, that the revolution frequency ratio between the small and large synchrotrons is close to an integer when the beam passes a target (e.g. a FRS, a Pbar) between two synchrotrons. The ratio between two revolution frequencies can be expressed as

$$\frac{f_{rev}^s}{f_{rev}^l} = \kappa + \lambda \quad (6.7)$$

The relation between two cavity rf frequencies is same as eq. 6.6. Two synchronization frequencies are

$$f_{syn}^l = \frac{f_{rf}^l}{h^l/Y} = Y f_{rev}^l \quad (6.8)$$

$$f_{syn}^s = \frac{f_{rf}^s}{h^s \kappa / Y} = \frac{Y}{\kappa} f_{rev}^s \quad (6.9)$$

Y is the GCD of h^l and $h^s \cdot \kappa$.

Two synchronization frequencies are beating automatically. The choice of the frequency for the bucket indication signal and the calculation of the synchronization window are similar as that of the integral circumference ratio scenario, see Sec. 6.1. Tab. 6.6 shows the formulas related to the B2B transfer when the large synchrotron is the target and Tab. 6.7 shows the formulas when the small synchrotron is the target.

6.2.1 Use Case of $h=4$ B2B Transfer from SIS18 to ESR

Continuous two of four bunches are injected into two buckets of the injection orbit of the ESR [54]. The beam is accumulated in the ESR. The large synchrotron is the SIS18 and the small one is the ESR. $h^{SIS18} = 4$ and $h^{ESR} = 2$. The circumference ratio between the SIS18 and the ESR is

$$\frac{C^l}{C^s} = \kappa + \lambda = 2 - 0.003 \quad (6.10)$$

6.2. Circumference Ratio is close to an Integer

Table 6.6: Parameters related to the B2B transfer when the circumference ratio is close to an integer and the large synchrotron is the target

	Large synchrotron is target synchrotron
f_{bucket}	f_{rev}^l
f_{syn}^X	$f_{syn}^s = \frac{f_{rf}^s}{(h^s \cdot \kappa)/Y}$ and $f_{syn}^l = \frac{f_{rf}^l}{h^l/Y}$
f_{B2B}^X	$f_{B2B}^s = \frac{f_{rev}^l}{f_{syn}^l} \cdot f_{syn}^s = \frac{1}{\kappa} f_{rev}^s$ and $f_{B2B}^l = f_{rev}^l$
f_{syn}^{REF}	$round(f_{rev}^l/100 \text{ kHz}) \cdot 100 \text{ kHz}$
Δf	$ f_{syn}^s - f_{syn}^l $
T_w	T_{rev}^l
$\Delta\phi_{rf}$	$\pm \frac{1}{2} \cdot 2\pi f_{syn}^s - f_{syn}^l \cdot T_w \cdot \frac{f_{rf}^l}{f_{syn}^s}$

Table 6.7: Parameters related to the B2B transfer when the circumference ratio is close to an integer and the small synchrotron is the target

	Small synchrotron is target synchrotron	
Case	(1) $f_{syn}^s \geq f_{rev}^s (\frac{Y}{\kappa} \geq 1)$	(2) $f_{syn}^s < f_{rev}^s (\frac{Y}{\kappa} < 1)$
f_{bucket}	f_{rev}^s	f_{syn}^s
f_{syn}^X	$f_{syn}^s = \frac{f_{rf}^s}{(h^s \cdot \kappa)/Y}$ and $f_{syn}^l = \frac{f_{rf}^l}{h^l/Y}$	
f_{B2B}^X	$f_{B2B}^l = \frac{f_{rev}^s}{f_{syn}^s} \cdot f_{syn}^l = \kappa f_{rev}^l$ and $f_{B2B}^s = f_{rev}^s$	$f_{B2B}^l = f_{syn}^l = Y f_{rev}^l$ and $f_{B2B}^s = f_{syn}^s = \frac{Y}{\kappa} f_{rev}^s$
f_{syn}^{REF}	$round(f_{rev}^s/100 \text{ kHz}) \cdot 100 \text{ kHz}$	$round(f_{syn}^s/100 \text{ kHz}) \cdot 100 \text{ kHz}$
Δf	$ f_{syn}^s - f_{syn}^l $	
T_w	T_{rev}^s	T_{syn}^s
$\Delta\phi_{rf}$	$\pm \frac{1}{2} \cdot 2\pi f_{syn}^s - f_{syn}^l \cdot T_w \cdot \frac{f_{rf}^s}{f_{syn}^s}$	

The GCD of $h^{SIS18} = 4$ and $h^{ESR} \cdot \kappa = 2 \cdot 2 = 2$ is 4, namely $Y = 4$. Substituting h^{SIS18} , h^{ESR} , κ and λ into eq. 6.6, we get

$$\frac{f_{rf}^{SIS18}}{f_{rf}^{ESR}} = \frac{h^{SIS18}}{h^{ESR} \cdot (\kappa + \lambda)} = \frac{4}{2 \cdot (2 - 0.003)} \quad (6.11)$$

The ESR is the small synchrotron and the target and there exists $Y/\kappa > 1$, so substituting h^X , κ , λ , f_{rf}^X and Y into formulas of the case (1) in Tab. 6.7, the parameters related to the $h=4$ B2B transfer from the SIS18 to the ESR is obtained, see Tab. 6.8. Here we use the 30 MeV/u heavy ion B2B transfer as an example.

Detailed parameters of the $h = 4$ B2B transfer from the SIS18 to the ESR, please see Appendix C.2. The target time difference between the SIS18 and ESR rf systems depends on the accumulation method.

6.2. Circumference Ratio is close to an Integer

Table 6.8: Parameters related to the h=4 B2B transfer from the SIS18 to the ESR with the frequency beating method

	Small synchrotron (ESR) is target synchrotron
f_{bucket}	$f_{rev}^{ESR} = 685.651 \text{ kHz}$
f_{syn}^X	$f_{syn}^{SIS18} = f_{rf}^{SIS18} = 1.373\,201 \text{ MHz}$ and $f_{syn}^{ESR} = f_{rf}^{ESR} = 1.371\,302 \text{ MHz}$
f_{B2B}^X	$f_{B2B}^{SIS18} = 2f_{rev}^{SIS18} = 686.601 \text{ kHz}$ and $f_{B2B}^{ESR} = f_{rev}^{ESR} = 685.651 \text{ kHz}$
f_{syn}^{REF}	700 kHz
Δf	1899 Hz
T_w	$T_{rev}^{ESR} = 1.456 \mu\text{s}$
$\Delta\phi_{rf}$	$\pm 0.5^\circ$

6.2.2 Use Case of h=1 B2B Transfer from SIS18 to ESR

One bunch is injected into one bucket of the injection orbit of the ESR. The beam is accumulated in the ESR. The large synchrotron is the SIS18 and the small one is the ESR. $h^{SIS18} = 1$ and $h^{ESR} = 1$. The circumference ratio between the SIS18 and the ESR is

$$\frac{C^l}{C^s} = \kappa + \lambda = 2 - 0.003 \quad (6.12)$$

The GCD of $h^{SIS18} = 1$ and $h^{ESR} \cdot \kappa = 1 \cdot 2 = 2$ is 1, namely $Y = 1$. Substituting h^{SIS18} , h^{ESR} , κ and λ into eq. 6.6, we get

$$\frac{f_{rf}^{SIS18}}{f_{rf}^{ESR}} = \frac{h^l}{h^s \cdot (\kappa + \lambda)} = \frac{1}{1 \cdot (2 - 0.003)} \quad (6.13)$$

The ESR is the target and there exists $Y/\kappa < 1$, so substituting h^X , κ , λ , f_{rf}^X and Y into formulas of the case (2) in Tab. 6.7, the parameters related to the h=1 B2B transfer from the SIS18 to the ESR is obtained, see Tab. 6.9. Here we use the 400 MeV/u proton B2B transfer as an example.

Table 6.9: Parameters related to the h=1 B2B transfer from the SIS18 to the ESR with the frequency beating method

	Small synchrotron (ESR) is target synchrotron
f_{bucket}	$f_{syn}^{ESR} = 988.388 \text{ kHz}$
f_{syn}^X	$f_{syn}^{SIS18} = f_{rf}^{SIS18} = 989.756 \text{ kHz}$ and $f_{syn}^{ESR} = f_{rf}^{ESR}/2 = 988.388 \text{ kHz}$
f_{B2B}^X	$f_{B2B}^{SIS18} = f_{rev}^{SIS18} = 989.756 \text{ kHz}$ and $f_{B2B}^{ESR} = f_{rev}^{ESR}/2 = 988.388 \text{ kHz}$
f_{syn}^{REF}	1 MHz
Δf	1368 Hz
T_w	$T_{syn}^{ESR} = 1.017 \mu\text{s}$
$\Delta\phi_{rf}$	$\pm 0.5^\circ$

Detailed parameters of the $h = 1$ B2B transfer from the SIS18 to the ESR, please see Appendix C.2. The target time difference between the SIS18 and ESR rf systems depends on the accumulation method.

6.2.3 Use Case of B2B transfer from ESR to CRYRING

Only one bunch is injected into one bucket of the CRYRING [16, 55]. The large synchrotron is the SIS18 and the small one is the CRYRING. $h^{ESR} = 1$ and $h^{CRYRING} = 1$. The circumference ratio between the ESR and the CRYRING is

$$\frac{C^l}{C^s} = \kappa + \lambda = 2 + 0.003 \quad (6.14)$$

The GCD of $h^{ESR} = 1$ and $h^{CRYRING} \cdot \kappa = 1 \cdot 2$ is 1, namely $Y = 1$. Substituting h^{ESR} , $h^{CRYRING}$, κ and λ into eq. 6.6, we get

$$\frac{f_{rf}^{ESR}}{f_{rf}^{CRYRING}} = \frac{h^l}{h^s \cdot (\kappa + \lambda)} = \frac{1}{1 \cdot (2 + 0.003)} \quad (6.15)$$

The CRYRING is the target and there exists $Y/\kappa < 1$, so substituting h^X , κ , λ , f_{rf}^X and Y into formulas of the case (2) in Tab. 6.7, the parameters related to the B2B transfer from the ESR to the CRYRING is obtained, see Tab. 6.10. Here we use the 30 MeV/u proton B2B transfer as an example.

Table 6.10: Parameters related to the B2B transfer from the ESR to the CRYRING with the frequency beating method

	Small synchrotron (CRYRING) is target synchrotron
f_{bucket}	$f_{syn}^{CRYRING} = 686.600 \text{ kHz}$
f_{syn}^X	$f_{syn}^{ESR} = f_{rf}^{ESR} = 685.651 \text{ kHz}$ and $f_{syn}^{CRYRING} = f_{rf}^{CRYRING}/2 = 686.600 \text{ kHz}$
f_{B2B}^X	$f_{B2B}^{ESR} = f_{rev}^{ESR} = 0.685\,651 \text{ MHz}$ and $f_{B2B}^{CRYRING} = f_{rev}^{CRYRING}/2 = 0.686\,600 \text{ MHz}$
f_{syn}^{REF}	700 kHz
Δf	949 Hz
T_w	$T_{syn}^{CRYRING} = 1.456 \mu\text{s}$
$\Delta\phi_{rf}$	$\pm 0.5^\circ$

The CRYRING synchronization frequency works for the bucket indication. The target time difference between the ESR and CRYRING rf systems equals to $t_{v_ext} + t_{v_inj} + t_{TOF}$. Detailed parameters of the B2B transfer from the ESR to the CRYRING, please see Appendix C.4.

6.3 Circumference Ratio is far away from an Integer

When the circumference ratio of the large synchrotron to that of the small synchrotron is far away from an integer, there exists the relation between two cavity rf

6.3. Circumference Ratio is far away from an Integer

frequencies, see Chap. 2.

$$\frac{f_{rf}^l}{f_{rf}^s} = \frac{h^l \cdot n}{h^s \cdot m + h^s \cdot \lambda \cdot n} \quad (6.16)$$

Besides, it is also grouped to this scenario, that the revolution frequency ratio between the small and large synchrotrons is far away from an integer when the beam passes a target between two synchrotrons. The revolution frequency ratio can be expressed as

$$\frac{f_{rev}^s}{f_{rev}^l} = \frac{m}{n} + \lambda \quad (6.17)$$

The relation between two cavity rf frequencies is same as eq. 6.16. Two synchronization frequencies are

$$f_{syn}^l = \frac{f_{rf}^l}{h^l n / Y} = \frac{Y}{n} f_{rev}^l \quad (6.18)$$

$$f_{syn}^s = \frac{f_{rf}^s}{h^s m / Y} = \frac{Y}{m} f_{rev}^s \quad (6.19)$$

Y is the GCD of $h^l \cdot n$ and $h^s \cdot m$.

Two synchronization frequencies are beating automatically. When the large synchrotron is the target, the frequency of the bucket indication signal depends on the relation between f_{syn}^l and f_{rev}^l . When $f_{syn}^l \geq f_{rev}^l$, namely $\frac{Y}{n} \geq 1$, $f_{bucket} = f_{rev}^s$. When $f_{syn}^l < f_{rev}^l$, $f_{bucket} = f_{syn}^l$. Tab. 6.11 shows the formulas related to the B2B transfer when the large synchrotron is the target.

Table 6.11: Parameters related to the B2B transfer when the circumference ratio is far away from an integer and the large synchrotron is the target

	Large synchrotron is target synchrotron	
Case	(1) $f_{syn}^l \geq f_{rev}^l$ ($\frac{Y}{n} \geq 1$)	(2) $f_{syn}^l < f_{rev}^l$ ($\frac{Y}{n} < 1$)
f_{bucket}	f_{rev}^l	f_{syn}^l
f_{syn}^X	$f_{syn}^s = \frac{f_{rf}^s}{(h^s \cdot m) / Y}$ and $f_{syn}^l = \frac{f_{rf}^l}{(h^l \cdot n) / Y}$	
f_{B2B}^X	$f_{B2B}^s = \frac{f_{rev}^s}{f_{syn}^l} \cdot f_{syn}^s = \frac{n}{m} f_{rev}^s$ and $f_{B2B}^l = f_{rev}^l$	$f_{B2B}^s = f_{syn}^s = \frac{Y}{m} f_{rev}^s$ and $f_{B2B}^l = f_{syn}^l = \frac{Y}{n} f_{rev}^l$
f_{syn}^{REF}	$round(f_{rev}^l / 100 \text{ kHz}) \cdot 100 \text{ kHz}$	$round(f_{syn}^l / 100 \text{ kHz}) \cdot 100 \text{ kHz}$
Δf	$ f_{syn}^l - f_{syn}^s $	
T_w	T_{rev}^l	T_{syn}^l
$\Delta\phi_{rf}$	$\pm \frac{1}{2} \cdot 2\pi f_{syn}^s - f_{syn}^l \cdot T_w \cdot \frac{f_{rf}^l}{f_{syn}^l}$	

When the small synchrotron is the target, the frequency of the bucket indication signal depends on the relation between f_{syn}^s and f_{rev}^s . When $f_{syn}^s \geq f_{rev}^s$, namely $\frac{Y}{m} \geq 1$, $f_{bucket} = f_{rev}^s$. When $f_{syn}^s < f_{rev}^s$, $f_{bucket} = f_{syn}^s$. Tab. 6.12 shows the formulas related to the B2B transfer when the small synchrotron is the target.

6.3. Circumference Ratio is far away from an Integer

Table 6.12: Parameters related to the B2B transfer when the circumference ratio is far away from an integer and the small synchrotron is the target

	Small synchrotron is target synchrotron	
Case	(1) $f_{syn}^s \geq f_{rev}^s$ ($\frac{Y}{m} \geq 1$)	(2) $f_{syn}^s < f_{rev}^s$ ($\frac{Y}{m} < 1$)
f_{bucket}	f_{rev}^s	f_{syn}^s
f_{syn}^X	$f_{syn}^s = \frac{f_{rf}^s}{(h^s \cdot m)/Y}$ and $f_{syn}^l = \frac{f_{rf}^l}{(h^l \cdot n)/Y}$	
f_{B2B}^X	$f_{B2B}^s = f_{rev}^s$ and $f_{B2B}^l = \frac{f_{rev}^s}{f_{syn}^s} \cdot f_{syn}^l = \frac{m}{n} f_{rev}^l$	$f_{B2B}^s = f_{syn}^s = \frac{Y}{m} f_{rev}^s$ and $f_{B2B}^l = f_{syn}^l = \frac{Y}{n} f_{rev}^l$
f_{syn}^{REF}	$round(f_{rev}^s / 100 \text{ kHz}) \cdot 100 \text{ kHz}$	$round(f_{syn}^s / 100 \text{ kHz}) \cdot 100 \text{ kHz}$
Δf	$ f_{syn}^s - f_{syn}^l $	
T_w	T_{rev}^s	T_{syn}^s
$\Delta\phi_{rf}$	$\pm \frac{1}{2} \cdot 2\pi f_{syn}^s - f_{syn}^l \cdot T_w \cdot \frac{f_{rf}^s}{f_{syn}^s}$	

6.3.1 Use Case of H^+ B2B Transfer from SIS100 to CR

Only one out of five bunches of proton is extracted from the SIS100 and goes to a Pbar, then antiprotons are produced and injected into one bucket of the CR [54]. The large synchrotron is the SIS100 and the small one is the CR, $h^{SIS100} = 5$ and $h^{CR} = 1$. Here we take an example, that the proton energy before the Pbar is 28.8 GeV/u and the antiproton energy after the Pbar is 3 GeV/u. Substituting the extraction and injection revolution frequencies into eq. 6.17, we get

$$\frac{f_{rev}^{CR}}{f_{rev}^{SIS100}} = 4.8 - 0.039 = \frac{m}{n} + \lambda = \frac{24}{5} - 0.039 \quad (6.20)$$

The GCD of $h^{SIS100} \cdot n = 5 \cdot 5 = 25$ and $h^{CR} \cdot m = 1 \cdot 24 = 24$ is 1, namely $Y = 1$. Substituting h^{SIS100} , h^{CR} , m, n and λ into eq. 6.16, we get

$$\frac{f_{rf}^{SIS100}}{f_{rf}^{CR}} = \frac{h^{SIS100} \cdot n}{h^{CR} \cdot m + h^{CR} \cdot \lambda \cdot n} = \frac{5 \cdot 5}{1 \cdot 24 - 1 \cdot 0.039 \cdot 5} \quad (6.21)$$

The CR is the small synchrotron and the target and there exists $\frac{Y}{m} = 1/24 < 1$, so substituting h^X , m, n, λ , f_{rf}^X and Y into formulas of the case (2) in Tab. 6.12, the parameters related to the H^+ B2B transfer from the SIS100 to the CR is obtained, see Tab. 6.13.

There exists an inevitable big bunch-to-bucket injection center mismatch with the frequency beating method. Other B2B injection mechanism should be used for the transfer (e.g. the phase jump for the CR), which is beyond the scope of this dissertation. Detailed parameters of the H^+ B2B transfer from the SIS100 to the CR , please see Appendix C.6.

6.3.2 Use Case of RIB B2B Transfer from SIS100 to CR

Only one out of two bunches is extracted from the SIS100 and goes to a Super FRS, then the RIB is produced and injected into one bucket of the CR. The large

6.3. Circumference Ratio is far away from an Integer

Table 6.13: Parameters related to the H^+ B2B transfer from the SIS100 to the CR with the frequency beating method

	Small synchrotron (CR) is target synchrotron
f_{bucket}	$f_{syn}^{CR} = 54.866 \text{ kHz}$
f_{syn}^X	$f_{syn}^{SIS100} = f_{rf}^{SIS100}/25 = 55.316 \text{ kHz}$ and $f_{syn}^{CR} = f_{rf}^{CR}/24 = 54.866 \text{ kHz}$
f_{B2B}^X	$f_{B2B}^{SIS100} = f_{rev}^{SIS100}/5 = 55.316 \text{ kHz}$ and $f_{B2B}^{CR} = f_{rev}^{CR}/24 = 54.866 \text{ kHz}$
f_{syn}^{REF}	100 kHz
Δf	450 Hz
T_w	$T_{syn}^{CR} = 18.226 \mu\text{s}$
$\Delta\phi_{rf}$	$\pm 35.5^\circ$

synchrotron is the SIS100 and the small one is the CR. $h^{SIS100} = 2$ and $h^{CR} = 1$. Here we take an example, that the energy of the heavy ion beam before the Super FRS is 1.5 GeV/u and the RIB energy after the Super FRS is 740 MeV/u. Substituting the extraction and injection revolution frequencies into eq. 6.17, we get

$$\frac{f_{rev}^{CR}}{f_{rev}^{SIS100}} = 4.4 - 0.0046 = \frac{m}{n} + \lambda = \frac{22}{5} - 0.0046 \quad (6.22)$$

Substituting h^{SIS100} , h^{CR} , m, n and λ into eq. 6.16, we get

$$\frac{f_{rf}^{SIS100}}{f_{rf}^{CR}} = \frac{h^{SIS100} \cdot n}{h^{CR} \cdot m + h^{CR} \cdot \lambda \cdot n} = \frac{2 \cdot 5}{1 \cdot 22 - 1 \cdot 0.0046 \cdot 5} \quad (6.23)$$

The GCD of $h^{SIS100} \cdot n = 2 \cdot 5 = 10$ and $h^{CR} \cdot m = 1 \cdot 22 = 22$ is 2, namely $Y = 2$. the CR is the small synchrotron and the target and there exists $\frac{Y}{m} = 1/11 < 1$, so substituting h^X , m, n, λ , f_{rf}^X and Y into formulas of the case (2) in Tab. 6.12, the parameters related the RIB B2B transfer from the SIS100 to the CR is obtained, see Tab. 6.14.

Table 6.14: Parameters related to the RIB B2B transfer from the SIS100 to the CR with the frequency beating method

	Small synchrotron (CR) is target synchrotron
f_{bucket}	$f_{syn}^{CR} = 102.218 \text{ kHz}$
f_{syn}^X	$f_{syn}^{SIS100} = f_{rf}^{SIS100}/5 = 102.326 \text{ kHz}$ and $f_{syn}^{CR} = f_{rf}^{CR}/11 = 102.218 \text{ kHz}$
f_{B2B}^X	$f_{B2B}^{SIS100} = 2f_{rev}^{SIS100}/5 = 102.326 \text{ kHz}$ and $f_{B2B}^{CR} = f_{rev}^{CR}/11 = 102.218 \text{ kHz}$
f_{syn}^{REF}	100 kHz
Δf	108 Hz
T_w	$T_{syn}^{CR} = 9.779 \mu\text{s}$
$\Delta\phi_{rf}$	$\pm 2.1^\circ$

Detailed parameters of RIB B2B transfer from the SIS100 to the CR, please see Appendix C.6.

6.3.3 Use Case of B2B Transfer from CR to HESR

One bunch of the CR is injected into one bucket of the HESR. The beam is accumulated in the HESR [15]. The large synchrotron is the HESR and the small one is the CR. $h^{HESR} = 1$ and $h^{CR} = 1$. The circumference ratio between the HESR and the CR is

$$\frac{C^{HESR}}{C^{CR}} = 2.6 - 0.003 = \frac{m}{n} + \lambda = \frac{13}{5} - 0.003 \quad (6.24)$$

The GCD of $h^{HESR} \cdot n = 1 \cdot 5 = 5$ and $h^{CR} \cdot m = 1 \cdot 13 = 13$ is 1, namely $Y = 1$. Substituting h^{HESR} , h^{CR} , m, n and λ into eq. 6.16, we get

$$\frac{f_{rf}^{HESR}}{f_{rf}^{CR}} = \frac{h^{HESR} \cdot n}{h^{CR} \cdot m + h^{HESR} \cdot \lambda \cdot n} = \frac{1 \cdot 5}{1 \cdot 13 - 1 \cdot 0.003 \cdot 5} \quad (6.25)$$

The HESR is the large synchrotron and the target and there exists $\frac{Y}{n} = 1/5 < 1$, so substituting h^X , m , n , λ , f_{rf}^X and Y into formulas of the case (2) in Tab. 6.11, the parameters related to the B2B transfer from the CR to the HESR is obtained. Tab. 6.15 shows parameters of two operations, the antiproton and RIB B2B transfer.

Table 6.15: Parameters related to the B2B transfer from the CR to the HESR with the frequency beating method

	Larger synchrotron (HESR) is target synchrotron
	3 GeV/u antiproton
f_{bucket}	$f_{syn}^{HESR} = 101.426 \text{ kHz}$
f_{syn}^X	$f_{syn}^{CR} = \frac{f_{rf}^{CR}}{13} = 101.290 \text{ kHz}$ and $f_{syn}^{HESR} = \frac{f_{rf}^{HESR}}{5} = 101.426 \text{ kHz}$
f_{B2B}^X	$f_{B2B}^{CR} = \frac{f_{rev}^{CR}}{13} = 101.290 \text{ kHz}$ and $f_{B2B}^{HESR} = \frac{f_{rev}^{HESR}}{5} = 101.426 \text{ kHz}$
f_{syn}^{REF}	100 kHz
Δf	136 Hz
T_w	$T_{syn}^{HESR} = 9.860 \mu\text{s}$
$\Delta\phi_{rf}$	$\pm 1.2^\circ$
	740 MeV/u RIB
f_{bucket}	$f_{syn}^{HESR} = 86.608 \text{ kHz}$
f_{syn}^X	$f_{syn}^{CR} = f_{rf}^{CR}/13 = 86.493 \text{ kHz}$ and $f_{syn}^{HESR} = f_{rf}^{HESR}/5 = 86.608 \text{ kHz}$
f_{B2B}^X	$f_{B2B}^{CR} = f_{rev}^{CR}/13 = 86.493 \text{ kHz}$ and $f_{B2B}^{HESR} = f_{rev}^{HESR}/5 = 86.608 \text{ kHz}$
f_{syn}^{REF}	100 kHz
Δf	113 Hz
T_w	$T_{syn}^{HESR} = 11.545 \mu\text{s}$
$\Delta\phi_{rf}$	$\pm 1.2^\circ$

The target time difference between two rf systems depends on the accumulation method. Detailed parameter about the B2B transfer from the CR to the HESR, please see Appendix C.5.

6.3.4 Use Case of B2B Transfer from SIS18 to ESR via a FRS

Only one bunch is extracted from the SIS18 and goes to a FRS, then a RIB is produced and injected into one bucket of the ESR. The large synchrotron is the SIS18 and the small one is the ESR. $h^{SIS18} = 1$ and $h^{ESR} = 1$. Here we take an applied case as an example, that the energy of the heavy ion beam before the FRS is 550 MeV/u and the RIB energy after the FRS is 400 MeV/u. Substituting the extraction and injection revolution frequencies into eq. 6.17, we get

$$\frac{f_{rev}^{ESR}}{f_{rev}^{SIS18}} = 1.8 + 0.036 = \frac{m}{n} + \lambda = \frac{9}{5} + 0.036 \quad (6.26)$$

Substituting h^{SIS18} , h^{ESR} , m, n and λ into eq. 6.16, we get

$$\frac{f_{rf}^{SIS18}}{f_{rf}^{ESR}} = \frac{h^{SIS18} \cdot n}{h^s \cdot m + h^{ESR} \cdot \lambda \cdot n} = \frac{1 \cdot 5}{1 \cdot 9 + 1 \cdot 0.036 \cdot 5} \quad (6.27)$$

The GCD of $h^{SIS18} \cdot n = 1 \cdot 5 = 5$ and $h^s \cdot m = 1 \cdot 9 = 9$ is 1, namely $Y = 1$. The ESR is the small synchrotron and the target and there exists $\frac{Y}{m} = 1/9 < 1$, so substituting h^X , m , n , λ , f_{rf}^X and Y into formulas of the case (2) in Tab. 6.12, the parameters related to the B2B transfer from the SIS18 to the ESR via a FRS is obtained, see Tab. 6.16.

Table 6.16: Parameters related to the B2B transfer from the SIS18 to the ESR via a FRS with the frequency beating method

	Small synchrotron (ESR) is target synchrotron
f_{bucket}	$f_{syn}^{ESR} = 219.642$ kHz
f_{syn}^X	$f_{syn}^{SIS18} = f_{rf}^{SIS18}/5 = 215.393$ kHz and $f_{syn}^{ESR} = f_{rf}^{ESR}/9 = 219.642$ kHz
f_{B2B}^X	$f_{B2B}^{SIS18} = f_{rev}^{SIS18}/5 = 215.393$ kHz and $f_{B2B}^{ESR} = f_{rev}^{ESR}/9 = 219.642$ kHz
f_{syn}^{REF}	200 kHz
Δf	4249 Hz
T_w	$T_{syn}^{ESR} = 4.553$ μ s
$\Delta\phi_{rf}$	$\pm 31.2^\circ$

There exists an inevitable big bunch-to-bucket injection center mismatch with the frequency beating method. Other B2B injection mechanism should be used for the transfer (e.g. the phase jump for the ESR or the coasting beam injection), which is beyond the scope of this dissertation. More parameters about the B2B transfer from the SIS18 to the ESR via a FRS, please see Appendix C.3.

6.4 Summary of Formulas related to B2B Transfer

In this section, all the formulas are summarized. Tab. 6.17 summarizes the formulas related to the B2B transfer when the large synchrotron is the target. Tab. 6.18

6.4. Summary of Formulas related to B2B Transfer

summarizes the formulas when the small synchrotron is the target and the revolution period is longer than the period of the synchronization frequency of the target synchrotron. Tab. 6.19 summarizes the formulas when the small synchrotron is the target and the revolution period is shorter than the period of the synchronization frequency of the target synchrotron.

6.4. Summary of Formulas related to the B2B Transfer

Table 6.17: Summary of the formulas related to the B2B transfer when the large synchrotron is the target

Circumference ratio	Cavity rf frequency ratio f_{rf}^l/f_{rf}^s	Bucket indication signal f_{bucket}	Synchronization frequencies f_{syn}^X $f_{syn}^s = \frac{f_{rf}^s}{(h^s \cdot \kappa) / Y}$	phase measurement signal f_{B2B}^X
$C^l/C^s = \kappa$ Integer	$\frac{h^l}{h^s \cdot \kappa}$ $Y = \text{GCD}(h^l, h^s \cdot \kappa)$	f_{rev}^l	$f_{syn}^s = \frac{f_{rf}^l}{h^l / Y}$ and $f_{syn}^l = \frac{f_{rf}^l}{h^l / Y}$	$f_{B2B}^s = \frac{f_{rev}^l}{f_{syn}^s} \cdot (f_{syn}^s + \Delta f_{syn})$ and $f_{B2B}^l = f_{rev}^l$
$C^l/C^s = \kappa + \lambda$ or $f_{rev}^s/f_{rev}^l = \kappa + \lambda$ close to integer	$\frac{h^l}{h^s \cdot (\kappa + \lambda)}$ $Y = \text{GCD}(h^l, h^s \cdot \kappa)$	f_{rev}^l	$\Delta f = \Delta f_{syn}$ $f_{syn}^s = \frac{f_{rf}^s}{h^s / Y}$ and $f_{syn}^l = \frac{f_{rf}^s}{(h^s \cdot \kappa) / Y}$	$f_{B2B}^s = \frac{f_{rev}^l}{f_{syn}^s} \cdot f_{syn}^s$ and $f_{B2B}^l = f_{rev}^l$
$C^l/C^s = m/n + \lambda$ or $f_{rev}^s/f_{rev}^l = m/n + \lambda$ far away from integer	$\frac{h^l}{h^s \cdot (m/n + \lambda)}$ $Y = \text{GCD}(h^l \cdot n, h^s \cdot m)$		$\Delta f = f_{syn}^l - f_{syn}^s $ $f_{syn}^s = \frac{f_{rf}^l}{(h^l \cdot n) / Y}$ and $f_{syn}^l = \frac{f_{rf}^s}{(h^s \cdot m) / Y}$	$f_{B2B}^s = \frac{f_{rev}^l}{f_{syn}^s} \cdot f_{syn}^s$ and $f_{B2B}^l = f_{rev}^l$
<i>Note:</i> $f_{syn}^{REF} = round(f_{bucket}/100 \text{ kHz}) \cdot 100 \text{ kHz}$, $T_w = 1/f_{bucket}$ and $\Delta \phi_{rf} = \pm \frac{1}{2} \cdot 2\pi f_{syn}^s - f_{syn}^l \cdot T_w \cdot \frac{f_{rf}^l}{f_{syn}^l}$				

6.4. Summary of Formulas related to B2B Transfer

Table 6.18: Summary of the formulas related to the B2B transfer when the small synchrotron is the target and the revolution period is longer than the period of the synchronization frequency of the target synchrotron

Circumference ratio	Cavity rf frequency ratio f_{rf}^l/f_{rf}^s	Bucket indication signal f_{bucket}	Synchronization frequencies f_{syn}^X	phase measurement signal f_{B2B}^X
$C^l/C^s = \kappa$ Integer	$\frac{h^l}{h^s \cdot \kappa}$	$Y/\kappa \geq 1, f_{rev}^s$	$f_{syn}^l = \frac{f_{rf}^l}{h^l/Y}$ and $f_{syn}^s = \frac{f_{rf}^s}{(h^s \cdot \kappa)/Y}$	$f_{B2B}^l = \frac{f_{rev}^s}{f_{syn}^s} \cdot (f_{syn}^l + \Delta f_{syn})$ and $f_{B2B}^s = f_{rev}^s$
$C^l/C^s = \kappa + \lambda$ or $frev^s/frev^l = \kappa + \lambda$ close to integer	$\frac{h^l}{h^s \cdot (\kappa + \lambda)}$	$Y/\kappa \geq 1, f_{rev}^s$	$\Delta f = \Delta f_{syn}$	$f_{B2B}^l = \frac{f_{rev}^s}{f_{syn}^s} \cdot f_{syn}^l$ and $f_{B2B}^s = f_{rev}^s$
$C^l/C^s = m/n + \lambda$ or $frev^s/frev^l = m/n + \lambda$ far away from integer	$\frac{h^l}{h^s \cdot (m/n + \lambda)}$	$Y/m \geq 1, f_{rev}^s$	$\Delta f = f_{syn}^l - f_{syn}^s $	$f_{B2B}^l = \frac{f_{rev}^s}{f_{syn}^s} \cdot \frac{f_{rf}^l}{(h^l \cdot n)/Y}$ and $f_{B2B}^s = \frac{f_{rev}^s}{f_{syn}^s} \cdot \frac{f_{rf}^s}{(h^s \cdot m)/Y}$ $f_{B2B}^s = f_{rev}^s$

Note: $f_{syn}^{REF} = round(f_{bucket}/100\text{ kHz}) \cdot 100\text{ kHz}$, $T_w = 1/f_{bucket}$ and $\Delta\phi_{rf} = \pm \frac{1}{2} \cdot 2\pi |f_{syn}^s - f_{syn}^l| \cdot T_w \cdot \frac{f_{rf}}{f_{syn}^s}$

Table 6.19: Summary of the formulas related to the B2B transfer when the small synchrotron is the target and the revolution period is shorter than the period of the synchronization frequency of the target synchrotron

Circumference ratio	Cavity rf frequency ratio f_{rf}^l/f_{rf}^s	Bucket indication signal f_{bucket}	Synchronization frequencies f_{syn}^X	phase measurement signal f_{B2B}^X
$C^l/C^s = \kappa$ Integer	$\frac{h^l}{h^s \cdot \kappa}$ $Y = GCD(h^l, h^s \kappa)$	$Y/\kappa < 1, f_{syn}^s$	$f_{syn}^l = \frac{f_{rf}^l}{h^l/Y}$ and $f_{syn}^s = \frac{f_{rf}^s}{(h^s \cdot \kappa)/Y}$	$f_{B2B}^l = f_{syn}^l + \Delta f_{syn}$ and $f_{B2B}^s = f_{syn}^s$
$C^l/C^s = \kappa + \lambda$ or $frev^s/frev^l = \kappa + \lambda$ close to integer	$\frac{h^l}{h^s \cdot (\kappa + \lambda)}$ $Y = GCD(h^l, h^s \kappa)$	$Y/\kappa < 1, f_{syn}^s$	$\Delta f = \Delta f_{syn}$ $f_{syn}^l = \frac{f_{rf}^l}{h^l/Y}$ and $f_{syn}^s = \frac{f_{rf}^s}{(h^s \cdot \kappa)/Y}$	$f_{B2B}^l = f_{syn}^l$ and $f_{B2B}^s = f_{syn}^s$
$C^l/C^s = m/n + \lambda$ or $frev^s/frev^l = m/n + \lambda$ far away from integer	$\frac{h^l}{h^s \cdot (m/n + \lambda)}$ $Y = GCD(h^l n, h^s m)$	$Y/m < 1, f_{syn}^s$	$\Delta f = f_{syn}^l - f_{syn}^s $ $f_{syn}^l = \frac{f_{rf}^l}{(h^l \cdot n)/Y}$ and $f_{syn}^s = \frac{f_{rf}^s}{(h^s \cdot m)/Y}$	$f_{B2B}^l = f_{syn}^l$ and $f_{B2B}^s = f_{syn}^s$

Note: $f_{syn}^{REF} = round(f_{bucket}/100\text{kHz}) \cdot 100\text{kHz}$, $T_w = 1/f_{bucket}$ and $\Delta\phi_{rf} = \pm\frac{1}{2} \cdot 2\pi |f_{syn}^s - f_{syn}^l| \cdot T_w \cdot \frac{f_{rf}^s}{f_{syn}^s}$

Chapter 7

Conclusion and Outlook

For many large scale accelerator facilities, it is inevitable to transfer bunched beam from one ring accelerator to another to gain high energy, high intensity and high quality beam. Without the proper transfer, the beam will be subject to various disturbances and even beam loss. Hence, the proper bunch-to-bucket transfer between two accelerators is of great importance.

FAIR, Facility for Antiproton and Ion Research, is a new international accelerator facility under construction at GSI Helmholtz center for Heavy Ion Research GmbH, aiming at providing high-energy beams of ions from antiproton to uranium with high intensities. The existing GSI accelerator includes the SIS18 and the ESR. The new FAIR accelerator complex with storage rings consists of the SIS100, the SIS300, the Collector Ring (CR), the Recycled Experimental Storage Ring (RESR), the New Experimental Storage Ring (NESR) and the High Energy Storage Ring (HESR). Although the existing GSI control system realizes the B2B transfer from the SIS18 to the ESR and from the ESR back to the SIS18, it is not applicable for the new FAIR accelerator complex due to the FAIR existing infrastructures, (e.g. the FAIR control system and the LLRF system) and unique FAIR demands (e.g. MPS). Hence, the development of the FAIR B2B transfer system is imperative. The FAIR B2B transfer system focuses first of all on the transfer from the SIS18 to the SIS100, but it will be firstly tested for the transfer from the SIS18 to the ESR and further to the CRYRING.

The FAIR B2B transfer system is introduced in this work at hand from the functional point of view. For the B2B transfer, there is a “B2B transfer master”, which is responsible for the data collection of two synchrotrons, the data calculation, the data redistribution and the B2B transfer status check. The data of the source and target synchrotron must be transferred to the “B2B transfer master” via the deterministic WR network in the format of the timing frame. For FAIR use cases, the source synchrotron works as the “B2B transfer master”. The phase difference between two rf systems of two synchrotrons is obtained with the help of a shared reference signal at two synchrotrons. The source synchrotron is responsible for the calculation of the start of the synchronization window, the phase correction and the required phase shift (only for phase shift method). The extraction and injection kicker firing is based on the bucket indication signal marker within the synchronization window plus a specified delay. In addition, this work presents how all FAIR use cases apply the FAIR B2B transfer system and how precise the bunch-to-bucket transfer is achieved with the system.

The FAIR B2B transfer system supports both the phase shift and frequency beating methods. It is more flexible. It supports several B2B transfers running at the same time, e.g. the B2B transfer from the SIS18 to the SIS100 and the B2B transfer from the ESR to the CRYRING. It is capable to transfer different species beam from one machine cycle to another without the operator's configuration. It is capable to transfer the beam between two synchrotrons via a FRS, Pbar or Super FRS. It can achieve various complex bucket pattern. What is more, the FAIR B2B transfer system coordinates with the MPS system, which protects SIS100/SIS300 from unacceptable failure or situation. For most FAIR use cases, it achieves the B2B transfer with the bunch-to-bucket injection center mismatch less than $\pm 1^\circ$ and within a upper bound B2B transfer time.

In addition, the beam dynamic of the U^{28+} B2B transfer from SIS18 to SIS100 is simulated for two synchronization methods, the phase shift and frequency beating method. This work explains the timing constraints of the system, the calculation of the synchronization window and presents the usage of the WR network for the B2B transfer system. Further, the SIS18 extraction and SIS100 injection kickers are analyzed for the different triggering possibilities.

This work presents a test setup for the system, achieving the phase collection of two synchrotrons locally, the phase transfer from the target synchrotron to the source synchrotron, the calculation of the synchronization window at the source synchrotron, the redistribution of the start of the synchronization window to the WR network, the production of the synchronization window at the source/target synchrotron.

Although the B2B transfer system for FAIR is flexible and with high compatibility, there still exists several improvement.

In order to reduce the synchronization time, the synchronization process could be started during the acceleration. The phase difference between two Reference RF Signals of the source and target synchrotrons at the flattop could be predicted by comparison the phases of these two signals at any time during the acceleration. Once the phase difference at the flattop is predicted, the synchronization process can be carried out:

- Phase shift method

First, the radial loop must be turned off. At some time during the acceleration, the phases difference between the source and target synchrotrons are obtained with the help of the Synchronization Reference Signal, and the phase difference at the flattop is picked up from the look-up table. Then, a rf frequency modulation is superposed on the initial frequency pattern. The integration of the rf frequency modulation equals to the required phase difference. With this new frequency pattern, the phase difference at the flattop will be the required phase difference when the cavity rf frequency of the source and target synchrotrons reach the flattop.

- Frequency beating method

The radial loop keeps on. At some time during the acceleration, the phases difference between the source and target synchrotrons are obtained. Then, a frequency detune is superposed on the initial frequency pattern. With this new frequency pattern, the synchronization window will be calculated.

Appendix A

FAIR B2B Transfer related Timing Frames

APPENDIX A. FAIR B2B TRANSFER RELATED TIMING FRAMES

Table A.1: B2B timing frames

No	Frame Name	Event ID	Priority	Source	Destination
1	CMD_START_B2B		7	DM	Source and B2B target SCU
2	TGM_PHASE_TIME		6	B2B target SCU	B2B source SCU
3	TGM_SYNCH_WIN		6	B2B source SCU	DM, source and target Trigger SCUs
4	CMD_SYNCH_WIN		7	DM	Beam Instrumentation (BI)
5	TGM_PHASE_JUMP		6	B2B source SCU	B2B target SCU
6	TGM_PHASE_CORRECTION		6	B2B source SCU	Source Trigger SCU
7	TGM_KICKER_TRIGGER_TIME_S		6	Source Trigger SCU	B2B source SCU
8	TGM_KICKER_TRIGGER_TIME_T		6	Target Trigger SCU	B2B source SCU
9	TGM_B2B_STATUS		6	B2B source SCU	DM
10	CMD_B2B_STATUS		7	DM	BI
No	Content	Description			
1	64 bits timestamp	Begin of the B2B transfer process			
2	16 bits phase advance and 64 bits stop	Transfer of the phase advance and the stop			
3	64 bits timestamp	Indication the start of the synchronization window			
4	64 bits timestamp	Indication the start of the synchronization window			
5	16 bits the expected jumped phase	Indication the jumped phase for the empty target machine			
6	16 bits phase correction	Target revolution frequency reproduction			
7	2 × 64 bits timestamp	Timestamps of trigger and firing of extraction kicker			
8	2 × 64 bits timestamp	Timestamps of trigger and firing of injection kicker			
9	64 bits timestamp + 1 bit	The actual beam extraction time and the status of the B2B system			
10	64 bits timestamp + 1 bit	The actual beam extraction time and the status of the B2B system			

Appendix B

Timing Frames Transfer for FAIR B2B Transfer System

APPENDIX B. TIMING FRAMES TRANSFER FOR FAIR B2B TRANSFER SYSTEM

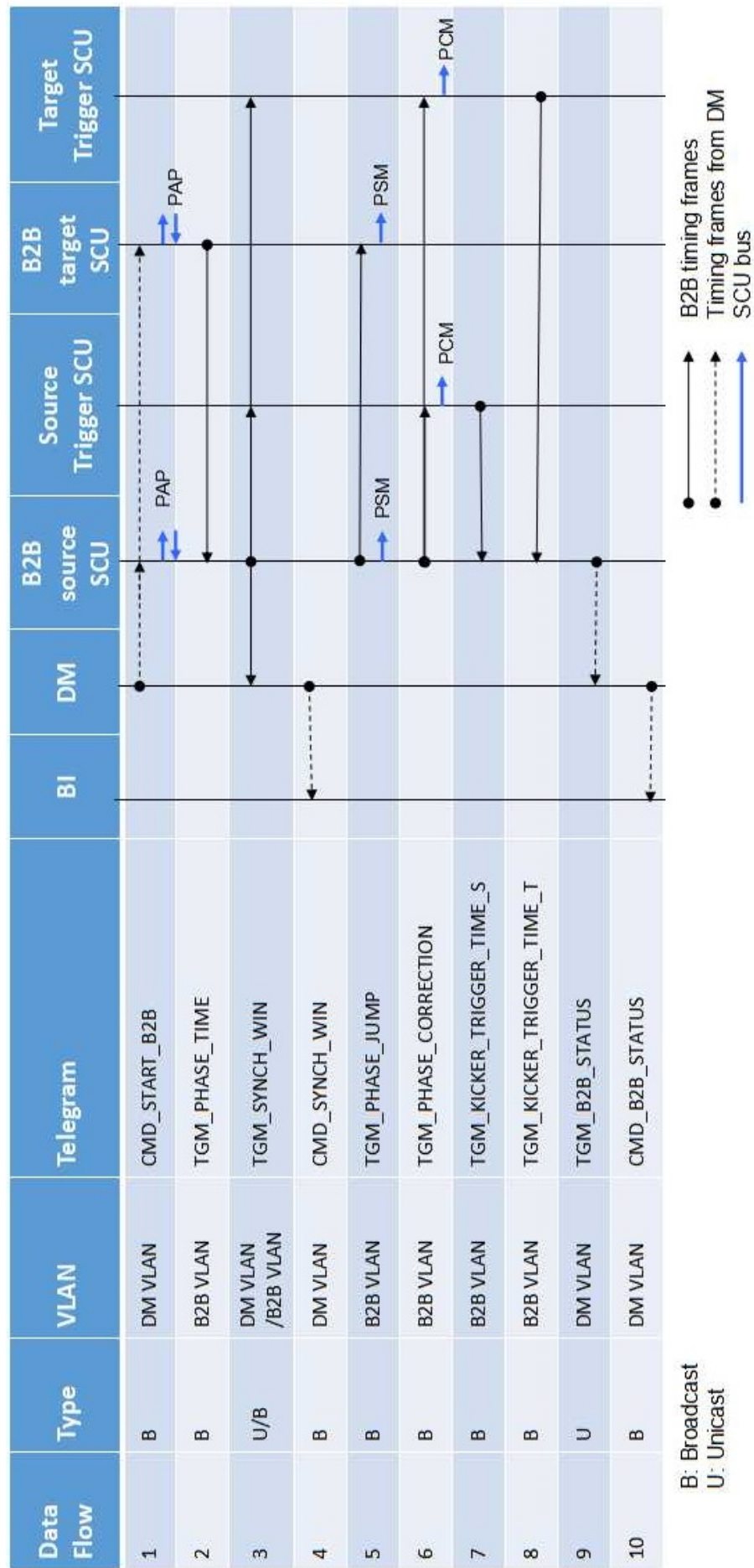


Figure B.1: Timing frames transfer for the B2B transfer

Appendix C

Parameters of FAIR Use Cases

C.1 Parameters related to the B2B transfer from SIS18 to SIS100

		Proton		Heavy Ion U^{28+}	
	Unit	SIS18 Ext	SIS100 Inj	SIS18 Ext	SIS100 Inj
Design orbit	m	216.72	1083.6	216.72	1083.6
$C_{SIS18} : C_{SIS100}$		5		5	
Ext kinetic energy	MeV/u	4000		200	
Inj kinetic energy	MeV/u		4000		200
h		1	10(1×4)	2	10(2×4)
f_{rf}	MHz	1.359358	2.718715	1.572536	1.572536
T_{rf}	μs	0.736	0.368	0.636	0.636
f_{rev}	MHz	1.359358	0.271872	0.786268	0.157254
T_{rev}	μs	0.736	3.678	1.272	6.359
Max $\Delta p/p$		±0.008	±0.01	±0.008	±0.01
$\Delta R/R$		$\pm 0.8 \times 10^{-4}$		$\pm 2.4 \times 10^{-4}$	
$\eta = \frac{1}{\gamma^2} - \alpha_p$		0.026		0.647	
γ_t		10		5.8	
α_p		0.010		0.030	
β		0.982	0.982	0.568	0.568
γ		5.294	5.294	1.215	1.215
Q_x		4.17		4.17	
Q_y		3.4		3.4	
Q'_x		-7.5		-6.5	
Q'_y		-4.4		-4.1	
		Injection four times		Injection four times	

Table C.1: Parameters related to the B2B transfer from SIS18 to SIS100

C.2 Parameters related to the B2B transfer from SIS18 to ESR

		Proton/Heavy Ion		Heavy Ion	
	Unit	SIS18 Ext	ESR Inj	SIS18 Ext	ESR Inj
Design orbit	m	216.72	108.36	216.72	108.36
Inj orbit	m		108.36 +0.15		108.36 +0.15
$C_{SIS18} : C_{ESR}$		1.997		1.997	
Ext kinetic energy	MeV/u	550		30	
Inj kinetic energy	MeV/u		400		30
h		1	1	4	2
f_{rf}	MHz	0.989756	1.976777	1.373201	1.371302
T_{rf}	μs	1.010	0.506	0.728	0.879
f_{rev}	MHz	0.989756	1.976777	0.343300	0.685651
T_{rev}	μs	1.010	0.506	2.913	1.458
$\Delta p/p$ compared with design orbit			1%		1%
$\Delta R/R$			0.138%		0.138%
$\eta = \frac{1}{\gamma^2} - \alpha_p$		0.480	0.310	0.909	0.759
γ_t		10	2.357	5.8	2.357
α_p		0.010	0.18	0.030	0.18
β		0.715	0.715	0.248	0.248
γ		1.429	1.429	1.032	1.032
		Accumulation beam in injection orbit		Accumulation beam in injection orbit	

Table C.2: Parameters related to the B2B transfer from SIS18 to ESR

C.3 Parameters related to the B2B transfer from SIS18 to ESR via FRS

		Heavy Ion Beam	Rare Isotope Beam
	Unit	SIS18 Ext	ESR Inj
Design orbit	m	216.72	108.36
Inj orbit	m		108.36 +0.15
$C_{SIS18} : C_{ESR}$		1.997	
Ext kinetic energy	MeV/u	400	
Inj kinetic energy	MeV/u		400
h		1	1
f_{rf}	MHz	1.076965	1.976777
T_{rf}	μs	0.929	0.506
f_{rev}	MHz	1.076965	1.976777
T_{rev}	μs	0.929	0.506
$\Delta p/p$ compared with design orbit			1%
$\Delta R/R$			0.138%
$\eta = \frac{1}{\gamma^2} - \alpha_p$		0.366	0.310
γ_t		5.8	2.357
α_p		0.030	0.18
β		0.778	0.715
γ		1.590	1.429
		One time injection	

Table C.3: Parameters related to the B2B transfer from SIS18 to ESR via FRS

C.4 Parameters related to the B2B transfer from ESR to CRYRING

		Proton/Antiproton		Heavy Ion	
	Unit	ESR Ext	CRYRING Inj	ESR Ext	CRYRING Inj
Design orbit	m	108.36	54.18	108.36	54.18
Ext orbit	m	108.36 +0.15		108.36 +0.15	
$C_{ESR} : C_{CRYRING}$		2.003		2.003	
Ext kinetic energy	MeV/u	30		4-10	
Inj kinetic energy	MeV/u		30		4-10
h		1	1	1	1
f_{rf}	MHz	0.685651	1.373200	0.254354- 0.400885	0.509507- 0.802879
T_{rf}	μs	1.458	0.728	3.932- 2.494	1.963- 1.246
f_{rev}	MHz	0.685651	1.373200	0.254354- 0.400885	0.509507- 0.802879
T_{rev}	μs	1.458	0.728	3.932- 2.494	1.963- 1.246
$\eta = \frac{1}{\gamma^2} - \alpha_p$		0.759		0.798-0.812	
γ_t		2.357		2.357	
α_p		0.18		0.18	
β		0.248	0.248	0.092-0.145	0.092-0.145
γ		1.032	1.032	1.004-1.011	1.004-1.011
		One time injection		One time injection	

C.5 Parameters related to the B2B transfer from CR to HESR

		Proton→ Antiproton		Heavy Ion→ RIB	
	Unit	CR Ext	HESR Inj	CR Ext	HESR Inj
Design orbit	m	221.45	575	221.45	575
$C_{HESR} : C_{CR}$		2.597		2.597	
Ext kinetic energy	GeV/u	3		0.74	
Inj kinetic energy	GeV/u		3		0.74
h		1	1	1	1
f_{rf}	MHz	1.316775	0.507131	1.124408	0.433043
T_{rf}	μs	0.759	1.972	0.889	2.309
f_{rev}	MHz	1.316775	0.507131	1.124408	0.433043
T_{rev}	μs	0.759	1.972	0.889	2.309
Max $\Delta p/p$		±3%		±1.5%	
$\eta = \frac{1}{\gamma^2} - \alpha_p$		-0.011		0.178	
γ_t		3.85		2.711	
α_p		0.067			
β		0.972	0.972	0.830	0.830
γ		4.221	4.221	1.794	1.794
		100 times Injection per 10 seconds		100 times Injection per 10 seconds	

Table C.5: Parameters related to the B2B transfer from CR to HESR

C.6 Parameters related to the B2B transfer from SIS100 to CR

		Proton→ Antiproton		Heavy Ion→ RIB	
	Unit	SIS100 Ext	CR Inj	SIS100 Ext	CR Inj
Design orbit	m	1083.6	221.45	1083.6	221.45
$C_{SIS100} : C_{CR}$		4.893		4.893	
Ext kinetic energy	GeV/u	28.8		1.5	
Inj kinetic energy	GeV/u		3		0.74
h		5(1 bunch)	1	2(1 bunch)	1
f_{rf}	MHz	1.382889	1.316778	0.511628	1.124408
T_{rf}	μs	0.723	0.759	1.955	0.889
f_{rev}	MHz	0.276578	1.316778	0.255814	1.124408
T_{rev}	μs	3.616	0.759	3.909	0.889
Max $\Delta p/p$		±3%		±1.5%	
β		0.999	0.972	0.924	0.830
γ		31.918	4.221	2.610	1.794
		One time injection		One time injection	

Table C.6: Parameters related to the B2B transfer from SIS100 to CR

Appendix D

Parameters of FAIR B2B Transfer System from Settings Management

Table D.1: Parameters for the B2B transfer provided by SM

Parameter	Destination	Usage
f_{syn}^X	B2B source SCU	Start of synchronization window calculation
f_{syn}^{REF}	B2B source SCU	Phase advance extrapolation for PCM
Frequency of bucket indication signal	B2B source SCU⇒SR B2B target SCU⇒SR Trigger SCU⇒SR	Bucket label signal production
t_{delay}	Delay compensation for TOF, all propagation and kicker preparation	
Extraction kicker delay compensation	B2B source SCU	Start of synchronization window calculation
Injection kicker delay compensation	Trigger SCU⇒TD	Extraction kicker trigger signal production
Emergency kicker delay compensation	Trigger SCU⇒TD	Injection kicker trigger signal production
Target time	Trigger SCU⇒TD	Emergency kicker trigger signal production
$t_{diff-sync}$	B2B source SCU	Start of synchronization window calculation or phase correction calculation for PCM
Δf	B2B source SCU	Start of synchronization window calculation
T	Duration of rf frequency modulation for the phase shift method	Start of synchronization window calculation and rf frequency modulation profile with certain duration T production
$\Delta f_{rf}, \Delta \dot{f}_{rf}$ and $\Delta \ddot{f}_{rf}$	B2B source SCU⇒PSM	Adiabatical rf frequency modulation profile production

Appendix E

Parameters of kicker magnets

Table E.1: Parameters of kicker magnets

Kicker	Units	Preparation time	Kicker rise time	Kicker fall time
SIS18 extraction kicker	9	5 us	90 ns	arbitrary
SIS100 injection kicker	6	5 us	130 ns	$\frac{1}{4}T_{rev}$
SIS100 extraction/ emergency kicker	8	10 us	750 ns	arbitrary
CR injection/ extraction kicker	9		320 ns	
ESR injection kicker	3		90 ns	

Bibliography

- [1] Particle accelerator. URL https://en.wikipedia.org/wiki/Particle_accelerator.
- [2] P. Møller. Beam-residual gas interactions. Technical report, CERN, 1999. URL <http://cds.cern.ch/record/455561/files/p155.ps.gz>.
- [3] Thibault Ferrand, Harald Klingbeil, and Heiko Damerau. Synchronization of Synchrotrons for bunch-to-bucket Transfers. Technical report, 2015. URL <http://cds.cern.ch/record/2053285>.
- [4] J-PARC. URL <https://www.kek.jp/en/Facility/ACCL/J-PARC/>.
- [5] Brookhaven National Laboratory. URL https://en.wikipedia.org/wiki/Particle_physics.
- [6] Fermi National Accelerator Laboratory. URL <http://www.fnal.gov/pub/science/particle-accelerators/accelerator-complex.html>.
- [7] Institute of Modern Physics of the Chinese Academy of Sciences. URL http://english.imp.cas.cn/au/bi/201312/t20131231_115141.html.
- [8] Kaidi Man, Yizhen Guo, Guozhu Cai, Sengli Yang, and Shoujin Wang. Survey and Alignment of HIRFL-CSR at IMP. In Proc. IWAA2002, 2002. URL http://www-group.slac.stanford.edu/met/IWAA/TOC_S/PAPERS/KMan02.pdf.
- [9] Jürgen Eschke. International Facility for Antiproton and Ion Research (FAIR) at GSI, Darmstadt. Journal of Physics G: Nuclear and Particle Physics, 31(6):S967, 2005. URL <http://iopscience.iop.org/article/10.1088/0954-3899/31/6/041/meta>.
- [10] FAIR - Facility for Antiproton and Ion Research, May 2011. URL <https://www.gsi.de//forschungbeschleuniger/fair.htm>.
- [11] P. Spiller and G. Franchetti. The FAIR accelerator project at GSI. Nuclear Instruments and Methods in Physics Research Section A, 561(2):305–309, 2006. URL <http://www.sciencedirect.com/science/article/pii/S0168900206000507>.
- [12] M. Steck, R. Bär, U. Blell, C. Dimopoulou, A. Dolinskii, P. Forck, B. Franzke, O. Gorda, V. Gostishchev, U. Jandewerth, and others. Advanced Design of the FAIR Storage Ring Complex. In In Proc. of EPAC, 2008. URL <https://accelconf.web.cern.ch/AccelConf/PAC2009/papers/fr1gri03.pdf>.

BIBLIOGRAPHY

- [13] Fritz Nolden, K. Beckert, P. Beller, U. Blell, C. Dimopoulou, A. Dolinskii, U. Laier, G. Moritz, C. Muehle, I. Nesmiyan, and others. The Collector Ring CR of the FAIR project. *Proc. EPAC*, 3(1):5, 2006. URL <http://accelconf.web.cern.ch/AccelConf/e06/PAPERS/MOPCH077.PDF>.
- [14] T. Abe, I. Adachi, K. Adamczyk, S. Ahn, H. Aihara, K. Akai, M. Aloisio, L. Andricek, K. Aoki, Y. Arai, and others. Technical design report Collector Ring. *KEK Report*, 2010. URL <http://arxiv.org/abs/1011.0352>.
- [15] R. Toelle, K. Bongardt, J. Dietrich, F. Esser, O. Felden, R. Greven, G. Hansen, F. Klehr, A. Lehrach, B. Lorentz, and others. HESR at FAIR: Status of technical planning. 2007. URL <http://epaper.kek.jp/p07/PAPERS/TUPAN024.PDF>.
- [16] M. Lestinsky, A. Bräuning-Demian, H. Aakan Danared, M. Engström, W. Enders, S. Fedotova, B. Franzke, A. Heinz, F. Herfurth, A. Källberg, and others. CRYRING@ ESR: present status and future research. *Physica Scripta*, 2015 (T166):014075, 2015. URL <http://iopscience.iop.org/article/10.1088/0031-8949/2015/T166/014075/meta>.
- [17] M. Lestinsky and others. CRYRING@ ESR: A study group report. *GSI and FAIR Report*, 2012.
- [18] S Y Lee. *Accelerator Physics*. WORLD SCIENTIFIC, Singapore, 3 edition, November 2011. ISBN 978-981-4374-94-1 978-981-4374-95-8. URL <http://www.worldscientific.com/worldscibooks/10.1142/8335>.
- [19] Harms Barletta. Overview on Magnetic fields. URL http://uspas.fnal.gov/materials/12MSU/xverse_dynamics.pdf.
- [20] R Garoby. Timing aspect of bunch transfer between circular machines. State of the art in the PS complex, PS/RF. Technical report, Note 84-6, 17 December 84, 1984.
- [21] Jochen Michael Grieser. *Beam phase feedback in a heavy-ion synchrotron with dual-harmonic cavity system*. PhD thesis, Technical University Darmstadt, 2015. URL <http://tuprints.ulb.tu-darmstadt.de/4634/>.
- [22] K. Gross, U. Hartel, U. Laier, D. Lens, K. P. Ningel, S. Schäfer, B. Zipfel, and H. Klingbeil. Bunch-by-Bunch Longitudinal RF Feedback for Beam Stabilization at FAIR. In *Proc. of IPAC*, 2015. URL <http://accelconf.web.cern.ch/AccelConf/IPAC2015/papers/mopha021.pdf>.
- [23] Eizi Ezura, Masahito YOSHII, Fumihiko TAMURA, and Alexander SCHNASE. Beam-Dynamics View of RF Phase Adjustment for Synchronizing J-PARC RCS with MR or MLF, 2008. URL <http://ccdb5fs.kek.jp/tiff/2008/0826/0826001.pdf>.
- [24] Ralph J. Steinhagen. Tune and chromaticity diagnostics, 2008. URL https://www.researchgate.net/profile/Ralph_Steinhagen/publication/261961271_Tune_and_Chromaticity_Diagnostics/links/02e7e5360c028adac1000000.pdf.

BIBLIOGRAPHY

- [25] B. J. Holzer. Introduction to transverse beam dynamics. CERN Yellow Report, 2013. URL <http://arxiv.org/abs/1404.0923>.
- [26] Isfried Petzenhauser, Leif Baandrup, Henning Bach, Udo Blell, Guido Blokesch, Nils Hauge, Kim Laurberg, Michael Osemann, and Peter Spiller. Concept and Design of the Injection Kicker System for the FAIR SIS100 Synchrotron. In IPAC, pages 3582–3584, Busan, Korea,, 2016. JACOW, Geneva, Switzerland.
- [27] Blell Udo. Injection and Extraction Components of SIS 100 / 300, 2014.
- [28] T. Hoffmann. FESA—The front-End Software architecture at FAIR. PCaPAC08, 2008. URL <http://accelconf.web.cern.ch/AccelConf/pc08/papers/wep007.pdf>.
- [29] Ralf Huhmann, Ralph C. Bär, Dietrich Hans Beck, Jutta Fitzek, Günther Fröhlich, Ludwig Hechler, Udo Krause, and Matthias Thieme. The FAIR control system—System architecture and first implementations. ICALEPCS, 2013. URL <http://epaper.kek.jp/ICALEPCS2013/papers/moppc097.pdf>.
- [30] Peter Moritz. BuTiS—Development of a Bunchphase Timing System. GSI Scientific Report, 2006. URL <http://citeseerx.ist.psu.edu/viewdoc/download?doi=10.1.1.162.1765&rep=rep1&type=pdf>.
- [31] B. Zipfel, P. Moritz, and others. Recent Progress on the Technical Realization of the Bunch Phase Timing System BuTiS. Proc. IPAC, pages 418–420, 2011. URL <http://accelconf.web.cern.ch/accelconf/ipac2011/papers/mopc145.pdf>.
- [32] Dietrich Beck, R. Bar, Mathias Kreider, Cesar Prados, Stefan Rauch, Wesley Terpstra, and Marcus Zweig. The new White Rabbit based timing system for the FAIR facility. PCaPAC, 2012. URL <http://accelconf.web.cern.ch/Accelconf/pcapac2012/papers/fria01.pdf>.
- [33] Dietrich Beck, Mathias Kreider, Cesar Prados, Wesley Terpstra, Stefan Rauch, and Marcus Zweig. The General Machine Timing System for FAIR and GSI. URL https://www-acc.gsi.de/wiki/pub/Timing/TimingSystemDocuments/GMT_Description_v3-1.pdf.
- [34] Dietrich Beck. Timing Messages of GMT system for FAIR, 2015. URL <https://www-acc.gsi.de/wiki/Timing/TimingSystemEvent>.
- [35] Harald Klingbeil, Ulrich Laier, Klaus-Peter Ningel, Stefan Schäfer, Christof Thielmann, and Bernhard Zipfel. New digital low-level rf system for heavy-ion synchrotrons. Physical Review Special Topics - Accelerators and Beams, 14(10), October 2011. ISSN 1098-4402. doi: 10.1103/PhysRevSTAB.14.102802. URL <http://link.aps.org/doi/10.1103/PhysRevSTAB.14.102802>.
- [36] P. Baudrenghien. Low-level RF. 13(14):15, 2010. URL <https://cas.web.cern.ch/cas/Denmark-2010/Writeups/Baudrenghien.docx>.
- [37] Marko Mandakovic. FAIR Fast Beam Abort System. URL https://fair-wiki.gsi.de/foswiki/pub/FC2WG/FairC2WGMinutes/20151021_Fast_Beam_Abort_System_Mandakovic.pdf.

BIBLIOGRAPHY

- [38] H. Liebermann and D. Ondreka. FAIR and GSI Reference Cycles for SIS18, 2013.
- [39] H. Liebermann and D. Ondreka. SIS100 Cycles, 2013.
- [40] J. Bai, T. Ferrand, D. Beck, R. Bär, O. Kester, D. Ondreka, C. Prados, and W. Terpstra. BUNCH TO BUCKET TRANSFER SYSTEM FOR FAIR. In ICALEPCS, 2015. URL <http://icalepcs.synchrotron.org.au/papers/wepgf119.pdf>.
- [41] T. Ferrand and J. Bai. System Simulation of Bunch-to-Bucket Transfer Between Synchrotrons. GSI Scientific Report, 2014. URL <http://repository.gsi.de/record/184160/files/FG-GENERAL-28.pdf>.
- [42] T. Ferrand and J. Bai. SYSTEM DESIGN FOR A DETERMINISTIC BUNCH-TO-BUCKET TRANSFER. In IPAC, 2015. URL <http://accelconf.web.cern.ch/AccelConf/IPAC2015/papers/wepma024.pdf>.
- [43] Thibault Ferrand. Development of the LLRF system for a deterministic Bunch-to-Bucket transfer for FAIR. PhD thesis, Technical University Darmstadt.
- [44] Matthias Thieme, Wolfgang Panschow, and Stefan Rauch. SCU system goes productive. GSI Scientific Report, 2013. URL <http://repository.gsi.de/record/68061/files/FG-CS-07.pdf>.
- [45] Jiaoni Bai and Thibault Ferrand. Concept of the FAIR Bunch To Bucket Transfer System, 2016.
- [46] P Kainberger. PZS - SIS/ESR-Pulszentrale, 2003. URL <https://www-acc.gsi.de/data/documentation/eq-models/pzs/gm-pzs.pdf>.
- [47] U. Krause and Volker Schaa. Re-engineering of the GSI control system. 2001. URL <http://arxiv.org/abs/physics/0111060>.
- [48] J. Bai12, R. Bär, D. Beck, T. Ferrand13, M. Kreider, D. Ondreka, C. Prados, S. Rauch, W. Terpstra, and M. Zweig. First Idea on Bunch to Bucket Transfer for FAIR. 2014. URL http://epaper.kek.jp/PCaPAC2014/posters/fpo024_poster.pdf.
- [49] John R. Taylor. An introduction to error analysis: The study of uncertainty in physical measurements. Mill Valley, CA: Anonymous University Science Books, page 71ep, 1982.
- [50] Cesar Prados and Jiaoni Bai. Testing the WR Network of the FAIR General Machine Timing System, 2016.
- [51] Calculating Optical Fiber Latency, 2012. URL <http://www.m2optics.com/blog/bid/70587/Calculating-Optical-Fiber-Latency>.
- [52] Jana Roß. SIS18 Sektoren Technische Zeichnungen und Fotografien, January 2008.

BIBLIOGRAPHY

- [53] Blell Udo. Detailed specification of the SIS100 injection kicker magnets and their pulse power supplies. PSP 2.8.5.1, November 2014.
- [54] M. Steck, C. Dimopoulou, B. Franzke, O. Gorda, T. Katayama, F. Nolden, G. Schreiber, Germany D. Möhl, Switzerland R. Stassen, H. Stockhorst FZJ, and others. Demonstration of Longitudinal Stacking in the ESR with Barrier Buckets and Stochastic Cooling. page 140, Alushta, Ukraine, 2011. URL <http://accelconf.web.cern.ch/AccelConf/COOL2011/papers/proceed.pdf#page=150>.
- [55] F. Herfurth, A. Brauning-Demian, W. Enders, H. Danared, and others. The low energy storage ring CRYRING@ ESR. Proc. of COOL2013 (Murren, Switzerland), 2013. URL <https://accelconf.web.cern.ch/accelconf/COOL2013/papers/thpm1ha01.pdf>.

Glossary

accuracy	Deviation between the theoretically calculated start time of the synchronization window and the actual observed start time
B2B transfer master	Responsible for the data collection of two synchrotrons, the data calculation, the data redistribution and the B2B transfer status check
B2B target SCU	Collects the predicted phase of the target synchrotron and transfers it to the source synchrotron
B2B source SCU	Works as the B2B transfer master
batch	A train of bunches circulating along a synchrotron to be transferred to buckets
best estimate of alignment	Fine time for the alignment of two RF Reference Signals
bucket indication signal	Time indication of a dedicated bucket passing on the virtual rf cavity of the target synchrotron, when it is correct phase aligned with the rf system of the source synchrotron for the bunch-to-bucket injection
bucket pattern	Rules for the buckets to be filled
bucket area factor	Ratio of bucket size of a running bucket to a stationary bucket
bucket size	Area in longitudinal phase space plane enclosed by the bucket
bucket height	Maximum momentum deviation of the rf bucket

Glossary

bunch	Collection of particles captured within one rf bucket
bunch gap	Area without any bunches in a batch
Cavity DDS	Cavity DDS provides rf signal for cavities
circumference ratio	Ratio of the circumference for synchrotrons of different size
coarse synchronization	Bunches are transferred into buckets with the bunch-to-bucket center mismatch smaller than the upper bound
extraction kicker	Diverts a circulating beam to leave a synchrotron
fine synchronization	Bunches are transferred into correct buckets
frame transfer jitter	The time deviation between the transfer latencies of two consecutive frames
frame transfer latency	The time interval between the frame reception and sending
frame loss rate	The ratio of the number of the lost Ethernet frames to the number of the theoretic received frames of a tested port
Group DDS	DDS module that generates an phase measurement signal for a group of cavities
harmonic number	Integer ratio between the rf frequency and the revolution frequency
injection kicker	Merges one beam into a circulating beam in a synchrotron
kicker fall time	A period of time of kicker magnet to reduce to zero magnetic field
kicker flat-top	A period of time of kicker magnet with a stable magnetic field

Glossary

kicker rise time	A period of time for kicker magnet to reach a stable magnetic field
longitudinal emittance	Area occupied by a bunch in the longitudinal phase space plane
machine cycle	One complete operation cycle of a machine, i.e. injection, ramp up, flattop, ejection and ramp down
measurement uncertainty	A non-negative parameter characterizing the dispersion of the values attributed to a measured quantity
phase measurement signal	Harmonic or subharmonic signal generated by the Group DDS and transmitted to the individual rf station as a reference signal
probable range of alignment	Range within which the fine alignment lies because of the propagation of the uncertainty
revolution frequency ratio	Ratio of the revolution frequencies for synchrotrons of different size
running rf bucket	Rf system provides a region in the longitudinal phase space, within which all particles oscillate around the synchronous particle and stay together with energy gain/loss per turn
stationary rf bucket	Rf system provides a region in the longitudinal phase space, within which all particles oscillate around the synchronous particle and stay together without energy gain/loss per turn (short: bucket)
synchronization reference signal	Shared synchronous reference signal at each supply room (same frequency and in phase)
synchronization frequencies	An integral multiple of the derived rf frequency, which is the division of the revolution frequency. It is used for the phase alignment of two rf systems

Glossary

synchronous particle	A particle who always sees a constant rf phase at the rf cavity
synchrotron motion	Oscillation of asynchronous particles around the synchronous particle
T0 incidents	First positive zero-crossings of BuTiS C2 clocks after every BuTiS T0 edge
timing frame	A specific Ethernet frame with 110 byte frame length, which contains one timing message
Trigger SCU	Production of the trigger signal for kicker electronics
tune	Number of particle trajectory oscillations during one revolution in the ring (transverse and longitudinal)
virtual rf cavity	A virtual position around the ring, to which the phase measurement signal corresponds

Abbreviations

AGS	Alternating Gradient Synchrotron at BNL
API	Application Programming Interface
B2B	Bunch-to-bucket
BI	Beam Instrumentation
BNL	Brookhaven National Laboratory
CCS	Central Control System
CERN	Conseil Européen pour la Recherche Nucléaire
CM	Clock Master
CPU	Central Processing Unit
CR	Collector Ring at GSI
CSCO	Common Systems Control Systems
CSRe	Cooler Storage Ring experimental ring at IMP
CSRm	Cooler Storage Ring main ring at IMP
DDS	Direct Digital Synthesizer
DM	Data Master
DSP	Digital Signal Processor
ESR	Experimental Storage Ring at GSI
FAIR	Facility for Antiproton and Ion Research at GSI
FEC	Front End Controller

Abbreviations

Fermilab	Fermi National Accelerator Laboratory
FESA	Front-End software Architecture
FPGA	Field Programmable Gate Array
FRS	Fragment Separator
GCD	Greatest Common Divisor
GMT	General Machine Timing
GSI	GSI Helmholtzzentrum für Schwerionenforschung
GUI	Graphical User Interface
HESR	High Energy Storage Ring at GSI
HIRFL	Heavy Ion Research Facility at IMP
IMP	Institute of Modern Physics
J-PARC	Japan Proton Accelerator Complex
LEIR	Low Energy Ion Ring at CERN
LHC	Large Hadron Collider at CERN
LLRF	Low-level RF
LSA	LHC Software Architecture
MM	Management Master
MPS	Machine Protection System
MR	Main Ring at J-PARC
NESR	New Experimental Storage Ring at GSI
PAM	Phase Advance Measurement module
PAP	Phase Advance Prediction module
Pbar	Proton bar
PBV	Primary Beam High Voltage

Abbreviations

PBRF	Primary Beam Radio Frequency
PC	Personal Computer
PCM	Phase Correction Module
PS	Proton Synchrotron at CERN
PSB	Proton Synchrotron Booster at CERN
PSM	Phase Shift Module
RCS	Rapid Cycle Synchrotron at J-PARC
RESR	Recycled Experimental Storage Ring at GSI
RHIC	Relativistic Heavy Ion Collide at BNL
RIB	Rare Isotope Beams
SBES	Experimentierspeicherring ESR
SCU	Scalable Control Unit
SFC	Sector Focusing Cyclotron at IMP
SHE-P	SHE-Physik
SIS100	SchwerIonen Synchrotron (100 Tm magnetic rigidity) at GSI
SIS18	SchwerIonen Synchrotron (18 Tm magnetic rigidity) at GSI
SIS300	SchwerIonen Synchrotron (300 Tm magnetic rigidity) at GSI
SM	Settings Management
SPS	Super Proton Synchrotron at CERN
SR	Signal Reproduction module
SSC	Separated Sector Cyclotron at IMP
TD	Trigger Decision module

Abbreviations

TM	Timing Master
TOF	Time-Of-Flight
UNILAC	Universal Linear Accelerator at GSI
VLAN	Virtual LAN
WR	White Rabbit

Symbols

p	Particle momentum
R	Orbit radius
β	Relative speed to the speed of light
c	Speed of the light
γ	Relativistic factor, which measures the total particle energy, E , in units of the particle rest energy, E_0
E	Total particle energy
E_0	Particle rest energy
α_p	Momentum compaction factor
η	Phase-slip factor
q	Charge of a particle
α_b	Bucket area factor
ω_s	Angular synchrotron frequency
B	Magnetic field
ρ	Bending radius of a particle immersed in a magnetic field B
h^X	Harmonic number of a specific synchrotron
f_{syn}^X	Synchronization frequency
ε	Adiabaticity parameter
$Q_{x/y}$	Horizontal/vertical tune

Symbols

$Q'_{x/y}$	Horizontal/vertical chromaticity
$\Delta Q_{x/y}$	Horizontal/vertical tune shift
T_w	Length of the synchronization window
t_{bucket}	Bucket delay for a specific bucket pattern
t_{TOF}	Time-of-Flight between two synchrotrons
t_{v_ext}	Time corresponding to the distance between the virtual rf cavity and the extraction position of the source synchrotron
t_{v_inj}	Time corresponding to the distance between the virtual rf cavity and the injection position of the target synchrotron
t_{ext}	Extraction kicker delay
t_{inj}	Injection kicker delay
t_{diff_sync}	Target time difference between the synchronization frequencies of two synchrotrons in the format of time
$\Delta\varphi^X$	Measured phase deviation between the phase measurement signal and the synchronization reference signal of the synchrotron X by PAM module
T_{sample_PAM}	Measurement sampling period of the phase deviation measurement by the PAM module
ψ^X	Extrapolated phase advance between the phase measurement signal and the synchronization reference signal of the synchrotron X by PAP module
T_{sample_PAP}	Extrapolation sampling period of the phase extrapolation by the PAP module
ψ_0^X	Phase advance extrapolated by the PAP module at t_ψ^X of the X synchrotron.
t_ψ^X	Timestamp corresponding to the extrapolated phase advance ψ^X

Symbols

$f_{normalized}$	Normalized rf frequency modulation profile, preloaded from SM
f_{actual}	Actual rf frequency modulation profile, calculated by PSM
t_{delay}	Delay compensation for the TOF, all propagation delays, the kicker preparation time and the bucket delay
t_w	Start of the synchronization window, calculated by B2B source SCU
t_{v_emg}	Time corresponding to the distance between the virtual rf cavity and the emergency extraction position of SIS100
t_{emg}	Extraction kicker delay of SIS100 for the emergency kick
t_{align}	Best estimate of alignment of zero crossing points of phase measurement signals of source and target synchrotrons
δt_{align}	Uncertainty of the best estimate of alignment of zero crossing points of phase measurement signals of source and target synchrotrons
$\delta\psi^X$	Uncertainty of the extrapolated phase of the synchrotron X in the phase domain
δt_ψ^X	Uncertainty of the measured timestamp
t_{w_rect}	Rectified start of the synchronization window, calculated by B2B source SCU
δt_{w_rect}	Uncertainty of the start of the synchronization window, calculated by B2B source SCU
t_{gap}	Bunch gap
$d_{crt1R-crt2L}$	Distance between two crates of the SIS18 extraction kicker
$d_{crt1L-crt2R}$	Distance from the leftmost to the rightmost of the SIS18 extraction/SIS100 injection kicker

Symbols

$d_{crt1R-crt2R}$	Distance between the rightmost of the 1 st crate and the rightmost of the 2 nd crate of the SIS18 extraction kicker
t_{B2B}	Start time of the B2B transfer
ϕ_s	Synchronous phase
f_{rf}	Rf frequency
h	Harmonic number
f_{rev}	Revolution frequency
f_{syn}^{REF}	Frequency of the synchronization reference signal
f_{B2B}^X	Frequency of the specified phase measurement signal for the phase advance measurement
u	Longitudinal accelerating voltage at rf cavity
V_0	Amplitude of the rf voltage
m_0	Rest mass
C^X	Circumference of the extraction/injection orbit of a specific synchrotron
f_{rev}^X	or $f_{h=1}^X$. Revolution frequency of a specific synchrotron
f_{rf}^X	or $f_{h=cavity\,harmonic}^X$. Cavity rf frequency of a specific synchrotron
T	Duration of rf frequency modulation for the phase shift method
Y	Greatest common divisor
ϕ_{syn}^X	Initial phase of the synchronization frequency
$\Delta\phi_{rf}$	Phase difference between two cavity rf frequencies for the phase shift method, Bunch-to-bucket injection center mismatch within the synchronization window for the frequency beating method

Symbols

$\Delta\phi_{syn}$	Phase difference between two synchronization frequencies for the phase shift method, phase mismatch between two synchronization frequencies for the frequency beating method
Δf_{syn}	Rf frequency modulation on the synchronization frequency for the phase shift method, rf frequency detune on the synchronization frequency for the frequency beating method
Δf_{rf}	Rf frequency modulation on the cavity rf frequency for the phase shift method, rf frequency detune on the cavity rf frequency for the frequency beating method
T_{rev}^X	Period of the revolution period of machine X
T_{rf}^X	Period of the cavity rf frequency of machine X
f_{bucket}	Rf frequency of the bucket indication signal
k^X	Slope of the phase deviation between the synchronization reference signal and a dedicated phase measurement signal of the synchrotron X
$\Delta\phi_{shift}$	Required phase shift for the Group DDS with the synchronization frequency

Symbols

List of Figures

1.1	Illustration of a bunch-to-bucket transfer.	2
1.2	The structure of the dissertation.	6
2.1	The longitudinal focusing of particles by a rf voltage ($\eta > 0$).	10
2.2	The longitudinal motion of asynchronous particles in the longitudinal phase space plane ($\eta > 0$).	10
2.3	A stationary rf bucket.	12
2.4	A running rf bucket.	13
2.5	The bunch-to-bucket injection with a phase, energy or voltage error. .	14
2.6	The constant phase difference between two synchronization frequencies f_{syn}^l and f_{syn}^s when $\kappa = 5$, $h^s = 1$ and $h^l = 10$	17
2.7	The periodically variable phase difference between two slightly different synchronization frequencies f_{syn}^l and f_{syn}^s when $\kappa = 2$, $\lambda = -0.003$, $h^s = 2$ and $h^l = 4$	19
2.8	The periodically variable phase difference between two synchronization frequencies f_{syn}^l and f_{syn}^s when $m = 26$, $n = 10$, $\lambda = -0.003$, $h^s = 1$ and $h^l = 1$	20
2.9	An example for the phase shift method with a sinusoidal rf frequency modulation.	21
2.10	The illustration of the frequency beating method.	25
2.11	The schematic diagram of a kicker magnet.	26
2.12	The rise time, kicker flat-top and fall time of an extraction kicker. .	27
2.13	The rise time, kicker flat-top and fall time of an injection kicker for multiple batches injection.	28
3.1	phase measurement signal distribution system	32
3.2	Local Cavity Synchronization	33
4.1	The illustration of the B2B transfer from the SIS18 to the SIS100. .	36
4.2	The frequency of the bucket indication signal equals to the revolution freuqncy of the target synchrotron.	39
4.3	The frequency of the bucket indication signal equals to the synchronization freuqncy of the target synchrotron.	39
4.4	The procedure for the B2B transfer within one acceleration cycle. .	41
4.5	The realization of the phase deviation measurement at one synchrotron	43
4.6	The realization of the phase advance extrapolation at one synchrotron	45
4.7	Implementation of the Phase Advance Prediction Module in the B2B source SCU	45

LIST OF FIGURES

4.8	The synchronization of the extrapolated phase to the timestamp in one synchrotron	46
4.9	One example of the transfer path of the B2B timing frames in the WR network	47
4.10	The normalized frequency and phase modulation profile and the actual profiles	48
4.11	Implementation of the Phase Shift Module in the B2B source SCU . .	49
4.12	Implementation of the Phase Correction Module in the Trigger SCU .	51
4.13	The realization of the bucket label for the normal extraction and injection.	52
4.14	The realization of the bunch gap for the emergency extraction.	52
4.15	Implementation of the Trigger Decision module in the Trigger SCU .	53
4.16	The illustration of the kicker delay compensation when the bucket indication signal has the frequency of f_{syn}^{trg}	54
4.18	The current realization of the bunch-to-bucket transfer between the SIS18 and the ESR with the GSI control system.	56
4.17	The data flow of the B2B transfer system	59
5.1	Examples of rf frequency modulation.	61
5.2	First derivation of three cases.	62
5.3	Second derivation of three cases.	63
5.4	The phase shift modulation of three cases.	63
5.5	Average radial excursions of three cases.	64
5.6	Relative momentum shift of three cases.	65
5.7	Changes in synchronous phase of three cases.	66
5.8	Ratio of bucket areas of a running bucket to the stationary bucket of three cases.	66
5.9	Adiabaticity parameter of three cases.	67
5.10	Frequency detune during the SIS18 U^{28+} rf ramp.	69
5.11	The rectification of the start of the synchronization window.	74
5.12	The accuracy of the start of the synchronization window.	75
5.13	The WR network test setup.	77
5.14	Frame loss rate of the B2B Broadcast frames.	78
5.15	The average latency and jitter for B2B Broadcast frames.	79
5.16	The maximum latency and jitter for B2B Broadcast frames.	80
5.17	The average latency and jitter for B2B Unicast frames.	80
5.18	The maximum latency and jitter for B2B Unicast frames.	81
5.19	The schematic diagram of the kicker magnets in the 2 nd crate of the SIS18 extraction kicker.	82
5.20	A possible firing delay between kicker magnets in two crates of SIS18 extraction kicker.	83
5.21	The maximum firing delay between kicker magnets in two crates of SIS18 extraction kicker.	84
5.22	The minimum firing delay between kicker magnets in two crates of SIS18 extraction kicker.	84
5.23	SIS100 injection kicker.	85
5.24	Schematic of the test setup.	87
5.25	The front view of the test setup.	88

LIST OF FIGURES

5.26 Flow chart of the firmware for the B2B source SCU	89
5.27 Flow chart of the firmware for the B2B target SCU	90
5.28 Flow chart of the firmware for the B2B Trigger SCU	91
5.29 The time constraints of the B2B transfer system.	93
B.1 Timing frames transfer for the B2B transfer	118

LIST OF FIGURES

List of Tables

5.1	Acceptable range of the parameters accompanying with the frequency adjustment of SIS18	61
5.2	The maximum average radial excursion of three cases	64
5.3	The maximum relative momentum shift of three cases	65
5.4	The minimum bucket area factor of three cases	67
5.5	The maximum adiabaticity of three cases	67
5.6	Parameters accompanying with a 7 ms sinusoidal modulation for the SIS18 H^+ beam	69
5.7	Parameters accompanying with a 20 ms sinusoidal modulation for the SIS18 H^+ beam	70
5.8	Uncertainty of the phase alignment of all FAIR B2B use cases	73
5.9	B2B transfer requirements on the WR network	76
5.10	The connection between the traffic generator and WR switches	78
5.11	The average latency and jitter of the B2B Broadcast frames	79
5.12	The maximum latency and jitter of the B2B Broadcast frames	80
5.13	The result of the WR network test for the B2B transfer	81
5.14	The firing delay for SIS18 kicker magnets in two crates	85
5.15	The delay for firing SIS00 injection kicker	86
6.1	List of the FAIR B2B transfer use cases	96
6.2	Parameters related to the B2B transfer when the circumference ratio is an integer and the large synchrotron is the target	97
6.3	Parameters related to the B2B transfer when the circumference ratio is an integer and the small synchrotron is the target	98
6.4	Parameters related to the U^{28+} B2B transfer from the SIS18 to the SIS100 with the frequency beating method	98
6.5	Parameters related to the H^+ B2B transfer from the SIS18 to the SIS100 with the frequency beating method	99
6.6	Parameters related to the B2B transfer when the circumference ratio is close to an integer and the large synchrotron is the target	101
6.7	Parameters related to the B2B transfer when the circumference ratio is close to an integer and the small synchrotron is the target	101
6.8	Parameters related to the h=4 B2B transfer from the SIS18 to the ESR with the frequency beating method	102
6.9	Parameters related to the h=1 B2B transfer from the SIS18 to the ESR with the frequency beating method	102
6.10	Parameters related to the B2B transfer from the ESR to the CRYRING with the frequency beating method	103

6.11	Parameters related to the B2B transfer when the circumference ratio is far away from an integer and the large synchrotron is the target	104
6.12	Parameters related to the B2B transfer when the circumference ratio is far away from an integer and the small synchrotron is the target	105
6.13	Parameters related to the H^+ B2B transfer from the SIS100 to the CR with the frequency beating method	106
6.14	Parameters related to the RIB B2B transfer from the SIS100 to the CR with the frequency beating method	106
6.15	Parameters related to the B2B transfer from the CR to the HESR with the frequency beating method	107
6.16	Parameters related to the B2B transfer from the SIS18 to the ESR via a FRS with the frequency beating method	108
6.17	Summary of the formulas related to the B2B transfer when the large synchrotron is the target	110
6.18	Summary of the formulas related to the B2B transfer when the small synchrotron is the target and the revolution period is longer than the period of the synchronization frequency of the target synchrotron	111
6.19	Summary of the formulas related to the B2B transfer when the small synchrotron is the target and the revolution period is shorter than the period of the synchronization frequency of the target synchrotron	112
A.1	B2B timing frames	116
C.1	Parameters related to the B2B transfer from SIS18 to SIS100	119
C.2	Parameters related to the B2B transfer from SIS18 to ESR	120
C.3	Parameters related to the B2B transfer from SIS18 to ESR via FRS .	121
C.5	Parameters related to the B2B transfer from CR to HESR	123
C.6	Parameters related to the B2B transfer from SIS100 to CR	124
D.1	Parameters for the B2B transfer provided by SM	126
E.1	Parameters of kicker magnets	127

Publications

- 2015 J. Bai, T. Ferrand, D. Beck, R. Br, O. Kester, D. Ondreka, C. Prados, and W. Terpstra. BUNCH TO BUCKET TRANSFER SYSTEM FOR FAIR. *In Proc. of ICAL EPICS*, 2015
- T. Ferrand and J. Bai. SYSTEM DESIGN FOR A DETERMINISTIC BUNCH-TO-BUCKET TRANSFER. *In Proc. of IPAC*, 2015
- 2014 J. Bai, D. Beck, R. Br, D. Ondreka, T. Ferrand, M. Kreider, C. Prados, S. Rauch, W. Terpstra, and M. Zweig. FIRST IDEA ON BUNCH TO BUCKET TRANSFER FOR FAIR. *In Proc. of PCaPAC*, 2014
- M. Kreider, J. Bai, R. Br, D. Beck, A. Hahn, C. Prados, S. Rauch, W. W. Terpstra, and M. Zweig. Launching the FAIR timing system with CRYRING. *In Proc. of PCaPAC*, 2014
- T. Ferrand and J. Bai. System Simulation of Bunch-to-Bucket Transfer Between Synchrotrons. *GSI Scientific Report*, 2014
- 2013 Bai Jiao-Ni, Zeng Lei, Wang Biao, Li Peng, Li Fang, Xu Tao-Guang, and Li Zi-Gao. Modified read-out system of the beam phase measurement system for CSNS. *Chinese physics C*, 37(10):107004, 2013
- D. Beck, J. Adamczewski-Musch, J. Bai, R. Br, J. Frhauf, J. Hoffmann, M. Kreider, N. Kurz, C. Prados, S. Rauch, and others. Paving the Way for the General Machine Timing System. *GSI Scientific Report*, 2013
- Mathias Kreider, Jiaoni Bai, Dietrich Beck, Cesar Prados, Wesley Terpstra, Stefan Rauch, and Marcus Zweig. Receiver Nodes of the General Machine Timing System for FAIR and GSI
- 2012 Jiaoni Bai, Shuai Xiao, Taoguang Xu, and Lei Zeng. The Development of Timing Control System for RFQ. *In Proc. of LINAC*, 2012

Jiaoni Bai

Curriculum Vitae

"I am a slow walker, but I never stop walking." - Jiaoni Bai

Education

- 2013–Now **Ph.D of physics**, Goethe University, Frankfurt am Main, Germany, .
- 2010–2013 **Master of Engineering Study in Computer Technology**, Institute of High Energy Physics, Chinese Academy of Sciences, Peking, China, GPA – 8.0.
- 2006–2010 **Bachelor of Engineering Study in Medical Informatics Engineering**, Southern Medical University, Guangzhou, China, GPA – 9.0.

PhD Dissertation

- Title *Development of the timing system for the Bunch-to-Bucket transfer between the FAIR accelerators*
- Professor Prof. Oliver Kester
- Supervisors Dr. Dietrich Beck and Dr. David Ondreka
- Description
- Development of the Bunch-to-Bucket transfer system
 - C-programming of the soft CPU LatticeMico32
 - VHDL programming of Altera FPGAs
 - Measurement of the White Rabbit network performance

Master Thesis

- Title *The development of EPICS driver for customized VME hardwares*
- Supervisor Taoguang Xu
- Description
- Development of the software interface between EPICS and VME hardware
 - Development of the operator controlling and monitoring interfaces by MEDM hardware
 - VxWorks program for Motorola VME board MVME5100

Bachelor Thesis

- Title *The CCD performance test and analysis*

R"omergasse 10 – 64291 Darmstadt, Germany

✉ (49) 017682537175 • ☎ (49) 6159 71 3126

✉ baijiaoni1314@gmail.com

- Description
- Investigation of the influence factors for CCD
 - Test how these factors influence CCD

Awards

- 2012 Won "Scholarship of the head of the Institute of High Energy Physics, CAS" for master thesis
- 2007 Won second prize of "Mathematical Contest in Modeling in Southern Medical University"

Key skills

- Intermediate Network engineering, Bash shell script and Visual Basic programming
- Advanced VHDL program for Altera FPGAs, C, Accelerator technology and beam dynamics, VxWorks programming and EPICS

Computer literacy

- Basic Windows, Linux (Ubuntu/Debian), Microsoft Office and LaTeX applications
- Engineering Altera Quartus and Matlab applications
- Art design Photoshop and Corel VideoStudio application
- Web design Dreamweaver

Languages

- Mandarin Mother tongue Chinese
- English Good written and spoken
- German Goethe-Zertifikat B2

R"omergasse 10 – 64291 Darmstadt, Germany

✉ (49) 017682537175 • ☎ (49) 6159 71 3126
✉ baijiaoni1314@gmail.com